


12-2019

## Rotational Tuning of Transmembrane Helix Properties Based on the Precise Placements of Aromatic and Charged Residues

Matthew J. McKay  
*University of Arkansas, Fayetteville*

Follow this and additional works at: <https://scholarworks.uark.edu/etd>

 Part of the [Analytical Chemistry Commons](#), [Biochemistry Commons](#), and the [Biophysics Commons](#)

---

### Recommended Citation

McKay, Matthew J., "Rotational Tuning of Transmembrane Helix Properties Based on the Precise Placements of Aromatic and Charged Residues" (2019). *Theses and Dissertations*. 3421.  
<https://scholarworks.uark.edu/etd/3421>

This Dissertation is brought to you for free and open access by ScholarWorks@UARK. It has been accepted for inclusion in Theses and Dissertations by an authorized administrator of ScholarWorks@UARK. For more information, please contact [ccmiddle@uark.edu](mailto:ccmiddle@uark.edu).

Rotational Tuning of Transmembrane Helix Properties Based on the Precise  
Placements of Aromatic and Charged Residues

A dissertation submitted in partial fulfillment  
of the requirements for the degree of  
Doctor of Philosophy in Chemistry

by

Matthew McKay  
Ursinus College  
Bachelor of Science in Biochemistry & Molecular Biology, 2014

December 2019  
University of Arkansas

This dissertation is approved for recommendation to the Graduate Council.

---

Roger Koeppe II, Ph.D.  
Dissertation Director

---

Stefan Kilyanek, Ph.D.  
Committee Member

---

Wesley Stites, Ph.D.  
Committee Member

---

Susanne Striegler, Ph.D.  
Committee Member

---

Suresh Thallapuranam, Ph.D.  
Committee Member

## Abstract

Designed model transmembrane peptides and oriented  $^2\text{H}$  and  $^{15}\text{N}$  solid-state nuclear magnetic resonance (NMR) spectroscopy were used to analyze how simple sequence modifications can influence peptide structure, behavior and dynamics as well as for determining the pKa of glutamic acid at the membrane interface. The  $\text{GW}^{5,19}\text{ALP23}$  (acetyl-GGALW(LA)<sub>6</sub>LWLAGA-amide) peptide framework adopts a well-defined tilted orientation in lipid bilayers (DLPC, DMPC and DOPC) and undergoes low amounts of dynamic motion. The sequence was initially modified by moving the Trp residues outwards to positions 4 and 20. This new sequence  $\text{GW}^{4,20}\text{ALP23}$  (acetyl-GGAW(AL)<sub>7</sub>AWAGA-amide) displays high amounts of signal averaging of NMR observables caused by extensive dynamic motion about its average azimuthal rotation. The high dynamics are due to side chain competition induced by the opposing radial locations of the interfacial Trp(W) residues. The  $\text{GW}^{4,20}\text{ALP23}$  sequence was subsequently modified by introducing Arg(R) residues at either position 14 or 12. The R14 peptide adopts a well-defined tilt in lipid bilayers while completely arresting the high dynamics of the parent framework. In response, the C-terminal Trp causes partial unwinding of the core helix, while the N-terminal residues tighten into the core helix to compensate. R12 pulls the peptide to the membrane surface. A helix discontinuity is observed beginning at residue 11 as well as the formation of a partial N-terminal  $3_{10}$ -helix. Modifying the core sequence of  $\text{GW}^{4,20}\text{ALP23}$  with Leu residues at positions 5 and 19 does not significantly affect the high dynamics, yet causes the peptide to adopt the same tilt as the original  $\text{GW}^{5,19}\text{ALP23}$  sequence. Removing W4 and replacing it with two Phe residues at positions 4 and 5 not only reduces the dynamics but also causes C-terminal helix distortion. Moving away from helix dynamics,  $^2\text{H}$  NMR was used to determine the side chain pKa of an interfacial Glu residue in the  $\text{GW}^{5,19}\text{ALP23}$  framework will oriented in the three

lipid bilayers. The pKa increases with lipid bilayer thickness ranging from 4.3 to 11.0.

Together, these experiments with model membrane peptides and solid-state NMR can be used to help our understanding of the basic principles that govern protein-lipid interactions.

## **Acknowledgements**

I would first like to thank my family and friends for supporting me throughout this process. I especially want to thank my advisor, Dr. Roger Koeppel for all that he has done for me these last five years. His guidance and enthusiasm helped me culture my independence as a researcher and for that I will be forever grateful. I would also like to thank Dr. Denise Greathouse for her suggestions in both science and life as well as for her help whenever an instrument inevitably stopped working.

I want to say thank you to Ashley Henderson for showing me the ropes when I was brand new to the lab. I am grateful for her friendship – even her motherly advice. I am also thankful for my lab mate Fahmida Afrose who started in the lab with me. It's been a true pleasure getting to know you and being able to call you a friend. I also want to thank the many undergrads who have trickled in and out of the lab. They certainly kept our research interesting and fun.

## Table of Contents

<b>Chapter 1: Introduction .....</b>	<b>1</b>
1.1 References .....	5
<b>Chapter 2: Control of Transmembrane Helix Dynamics by Interfacial Tryptophan</b>	
<b>Residues .....</b>	<b>8</b>
2.1 Abstract.....	8
2.2 Introduction .....	9
2.3 Materials and Methods .....	13
2.4 Results .....	17
2.5 Discussion.....	25
2.6 Acknowledgements .....	32
2.7 References .....	32
2.8 Tables.....	37
2.9 Figures .....	43
2.10 Supporting Information .....	52
<b>Chapter 3: Breaking the Backbone: Central Arginine Residues Induce Membrane Exit and Helix Distortions Within a Dynamic Membrane Peptide .....</b>	<b>59</b>
3.1 Abstract.....	59
3.2 Introduction .....	60
3.3 Materials and Methods .....	62
3.4 Results .....	68

3.5 Discussion.....	73
3.6 Conclusion.....	79
3.7 Acknowledgements .....	79
3.8 References .....	80
3.9 Tables.....	85
3.10 Figures .....	88
3.10 Supplemental Figures .....	100
<b>Chapter 4: A Link Between Flanking Aromatic Residue Competition and Transmembrane Peptide Dynamics .....</b>	<b>104</b>
4.1 Abstract.....	104
4.2 Introduction .....	104
4.3 Materials and Methods .....	106
4.4 Results .....	108
4.5 Discussion.....	111
4.6 Conclusion.....	113
4.6 Acknowledgements .....	114
4.7 References .....	114
4.8 Tables.....	117
4.9 Figures .....	120
4.10 Supplemental Figures .....	127

<b>Chapter 5: Titration of Glutamic Acid at the Lipid Bilayer Interface .....</b>	<b>131</b>
5.1 Abstract.....	131
5.2 Introduction .....	131
5.3 Materials and Methods .....	132
5.4 Results .....	134
5.5 Discussion.....	134
4.6 Conclusion.....	136
5.6 Acknowledgements .....	136
5.7 References .....	137
5.8 Tables.....	139
5.9 Figures .....	141
5.10 Supplemental Figures .....	144
<b>Chapter 6: Conclusions .....</b>	<b>147</b>
<b>Appendix I: List of Current Publications.....</b>	<b>149</b>



## List of Published Papers

### Published Peer Review:

**Matthew J. McKay\***, Ashley N. Martfeld, Anna A. De Angelis, Stanley J. Opella, Denise V. Greathouse, and Roger E. Koeppe II. 2018. Control of transmembrane helix dynamics by interfacial tryptophan residues. *Biophysical Journal* 114(11):2617-2629. (**Chapter 2**)

**Matthew J. McKay\***, Riqiang Fu, Denise V. Greathouse, and Roger E. Koeppe II. 2019. Breaking the Backbone: Central Arginine Residues Induce  $\alpha$ -Helix Distortions Within a Dynamic Transmembrane Peptide. *Journal of Physical Chemistry B* DOI: 10.1021/acs.jpcb.9b06034. (**Chapter 3**)

## CHAPTER 1

### Introduction

Biological membranes are intricate environments enriched with various mixtures of lipids and membrane proteins alike. The interactions between proteins and lipids are important to understand as such relationships help govern membrane protein structure which ultimately determines their function in essential biological roles such as signal transduction and transport. Membrane spanning proteins must follow strict rules to meet the demands of the membrane while still being able to fold properly and carry out their biological functions.(1) For example, unfolded polypeptide chains cannot favorably integrate into the hydrophobic lipid bilayer interior due to the energy cost of partitioning exposed amide bonds.(2) Bilayer integration can be favored through hydrogen bond formation which is the driving force of  $\alpha$ -helix secondary structure formation found in the most common types of transmembrane domains. To help the folding process along, these protein domains consist primarily of hydrophobic amino acids; unfortunately, this often leads to experimental difficulties such as aggregation. Lipid contributions to folding are also not the only factor to consider. The system gets further complicated as transmembrane domains often contain numerous  $\alpha$ -helices bundled together, each helix orientation influenced by its relationship with its neighbor. Protein-lipid interactions are therefore only part of a complicated network of interactions that give membrane proteins their folded conformations and are not entirely well understood. Simple model systems can be employed to gain an understanding of the basic principles that undergird protein-lipid interactions while also circumventing many experimental difficulties associated with membrane proteins. A common approach is to characterize the behavior of single spanning transmembrane peptides incorporated within bilayers consisting of a set lipid species and thickness. Results

acquired from such studies typically mirror natural protein folding behavior and therefore these systems can be utilized to understand various secondary structure interactions in the context of both folding and unfolding often at single residue resolution.(3) Some of the earliest model peptides used to study peptide-lipid interactions, such as hydrophobic matching, were the WALP peptides which consisted of a hydrophobic core sequence of repeating Leu-Ala residues and multiple flanking Trp residues at either terminus.(4-6) The second generation WALP peptide framework, GW<sup>5,19</sup>ALP23 (acetyl-GGALW(LA)<sub>6</sub>LWLAGA-amide),(7) has been extensively used to study protein-lipid interactions including: interfacial anchoring properties of aromatic residues(8), transmembrane orientation stabilization provided by terminal  $\alpha$ -helix fraying(9, 10) and even elucidating amino acid pKa's at various depths of the bilayer.(11, 12) It contains only two flanking Trp residues in the sequence which allows it to adopt a well-defined tilted orientation in lipid bilayers and maintain a fairly static rotation with only a moderate degree of dynamic motion. It can be effectively used to show how simple changes in amino-acid sequence impact the peptide orientation, dynamics and structure, providing insight into how protein-lipid interactions influence the folding of much larger membrane protein species.

Oriented solid-state NMR can be effectively used to study the orientation, secondary structure and dynamics of model transmembrane peptides and simple membrane proteins in lipid bilayers. Samples typically consist of peptides incorporated into either oriented lipid bilayers on stacked glass plates which are mechanically aligned with the bilayer normal parallel or perpendicular to the magnetic field(6) or bicelles(13) which are lipid discs that self-orient perpendicular to the magnetic field. <sup>2</sup>H NMR is a particularly sensitive tool for determining the orientation and dynamics adopted by a transmembrane  $\alpha$ -helix. The core sequence of the GWALP23 family peptides contain multiple repeating alanine residues whose <sup>2</sup>H-labeled methyl side chain

orientations can be used to calculate the overall tilt and azimuthal rotation of the helix.(6) The helix backbone N-H bond geometry directly correlates to the overall peptide orientation and can be monitored using oriented  $^{15}\text{N}$  based separated local field NMR experiments.(14, 15) Both NMR methods are sensitive to the dynamic motion of the peptide, particularly the slippage about its average azimuthal rotation. The motionally averaged NMR observables ( $^2\text{H}$  quadrupolar splittings,  $^1\text{H}/^{15}\text{N}$  dipolar couplings,  $^{15}\text{N}$  chemical shifts) can be used to estimate the extent of oscillations the peptide undergoes about both its the average tilt and rotation.(16, 17)

The  $\text{GW}^{5,19}\text{ALP23}$  peptide contains two interfacial Trp residues on the same face of the  $\alpha$ -helix. Previous experiments have moved these Trp residues outwards to positions 3 and 21 or inwards to positions 7 and 17.(8) In Chapter 2, the Trp residues are moved outward to opposite faces of the helix at positions 4 and 20. The new peptide  $\text{GW}^{4,20}\text{ALP23}$  (acetyl-GGAW<sup>4</sup>(AL)<sub>7</sub>AW<sup>20</sup>AGA-amide) was characterized using both  $^2\text{H}$  and  $^{15}\text{N}$  static solid-state NMR experiments. Unlike the original well-behaved  $\text{GW}^{5,19}\text{ALP23}$  peptide, the new  $\text{GW}^{4,20}\text{ALP23}$  sequence undergoes extensive amounts of dynamic motion in particular about its azimuthal rotation caused by side chain competition between the flanking Trp residues at opposing radial locations of the helix.

This new  $\text{GW}^{4,20}\text{ALP23}$  framework was then used to study how simple sequence mutations can affect the overall peptide dynamics and orientation. Positively charged residues are essential for voltage sensing domains found in various channel proteins.(18) Arg residues were previously introduced into the  $\text{GW}^{5,19}\text{ALP23}$  sequence and caused the peptide to either remain transmembrane and exhibit low dynamics at position 14 or adopt multiple states, including a surface bound state, when placed at the center of the sequence at position 12.(19) In Chapter 3, Arg residues were separately introduced again at positions 14 and 12. The  $\text{R}^{14}\text{GW}^{4,20}\text{ALP23}$

peptide similarly remains transmembrane and exhibits very low dynamics (lower than the original GW<sup>5,19</sup>ALP23 sequence) as the peptide is essentially locked into place by the Arg side chain. The dominance of R14 also induces a partial C-terminal unwinding of the helix, while the N-terminal residues integrate into the core helix to compensate. The new W4,20 sequence with R12, R<sup>12</sup>GW<sup>4,20</sup>ALP23, adopts only a single state. The central Arg brings the peptide out of the membrane to the surface and breaks the helix in half forming a partial 3<sub>10</sub>-helix at the N-terminus confirmed by both <sup>2</sup>H and <sup>15</sup>N NMR experiments.

The GW<sup>4,20</sup>ALP23 sequence is not a complete isomer of GW<sup>5,19</sup>ALP23 as it lacks Leu residues that would neighbor each interfacial Trp residue. It was unknown what to what extent these Leu residues had on the dynamics, and if the Trp radial locations were the primary factor behind them. Therefore, in [Chapter 4](#), Leu is introduced into the sequence of GW<sup>4,20</sup>ALP23 at positions 5 and 19. This new L<sup>5,19</sup>GW<sup>4,20</sup>ALP23 sequence exhibits the same dynamic profile as the parent sequence, with only slightly lower degrees of rotational slippage. However, the introduction of the two Leu residues does cause the peptide to adopt the same tilt in the various lipid bilayers as its isomer, GW<sup>5,19</sup>ALP23. In order to prove the Trp residues are responsible for the dynamics, W4 and A5 were each replaced with a Phe(F) residue which is incapable of forming hydrogen bonds and would remove side chain competition. F<sup>4,5</sup>GW<sup>20</sup>ALP23 indeed lowers the dynamics to moderate values, however distortion is evident for the C-terminal portion of the helix as well as possible oligomerization. Together L<sup>5,19</sup>GW<sup>4,20</sup>ALP23 and F<sup>4,5</sup>GW<sup>20</sup>ALP23 prove the side chain competition caused by the radial Trp locations is the primary factor responsible for the extensive dynamic motion of the parent framework.

Transmembrane domains of proteins sometimes contain charged residues which are often conserved and essential for protein function. Solid-state <sup>2</sup>H NMR can also be used to determine

the titration points of ionizable residues within the sequences of model transmembrane peptides at various lipid bilayer depths. The transmembrane pKa's of residues such as His, Lys, and Arg have all been previously examined using the GW<sup>5,19</sup>ALP23 sequence.(11, 12, 20) Experiments attempting to determine the pKa of Glu predicted the titration point would occur at high pH levels or that the helix is indifferent to the charged state of the side chain.(21) In Chapter 5, the GW<sup>5,19</sup>ALP23 sequence was used to analyze the titration behavior of glutamic acid at position 4 residing at the membrane interface. Titration curves were successfully obtained in three different lipid bilayers (DLPC, DMPC and DOPC). The calculated pKa's show that the charged state of the interfacial Glu4 side chain has a lipid dependence and the pKa's increase with bilayer thickness, up to 11.0 in the thickest bilayer. This provides support for the high pKa values previously predicted(21) and agrees with the wide range of pKa's observed in nature (ranging from 3.5 to 14) that are dependent on the side chain's local environment.(22, 23)

## 1.1 References

1. McKay, M., F. Afrose, R. Koeppe, and D. Greathouse. 2018. Helix formation and stability in membranes. *Biochimica Et Biophysica Acta-Biomembranes* 1860(10):2108-2117.
2. Cymer, F., G. von Heijne, and S. H. White. 2015. Mechanisms of integral membrane protein insertion and folding. *Journal of Molecular Biology* 427(5):999-1022.
3. Choi, S., I. Guzei, L. Spencer, and S. Gellman. 2008. Crystallographic characterization of helical secondary structures in alpha/beta-peptides with 1 : 1 residue alternation. *Journal of the American Chemical Society* 130(20):6544-6550.
4. Killian, J. A., I. Salemink, M. R. R. dePlanque, G. Lindblom, R. E. Koeppe, and D. V. Greathouse. 1996. Induction of nonbilayer structures in diacylphosphatidylcholine model membranes by transmembrane alpha-helical peptides: importance of hydrophobic mismatch and proposed role of tryptophans. *Biochemistry* 35(3):1037-1045.
5. de Planque, M. R. R., J. A. W. Kruijtzter, R. M. J. Liskamp, D. Marsh, D. V. Greathouse, R. E. Koeppe, B. de Kruijff, and J. A. Killian. 1999. Different membrane anchoring positions of tryptophan and lysine in synthetic transmembrane alpha-helical peptides. *Journal of Biological Chemistry* 274(30):20839-20846.

6. van der Wel, P. C. A., E. Strandberg, J. A. Killian, and R. E. Koeppe. 2002. Geometry and intrinsic tilt of a tryptophan-anchored transmembrane alpha-helix determined by H-2 NMR. *Biophysical Journal* 83(3):1479-1488.
7. Vostrikov, V. V., C. V. Grant, A. E. Daily, S. J. Opella, and R. E. Koeppe, II. 2008. Comparison of "Polarization Inversion with Spin Exchange at Magic Angle" and "Geometric Analysis of Labeled Alanines" methods for transmembrane helix alignment. *Journal of the American Chemical Society* 130(38):12584.
8. Vostrikov, V., and R. Koeppe. 2011. Response of gwalp transmembrane peptides to changes in the tryptophan anchor positions. *Biochemistry* 50(35):7522-7535.
9. Mortazavi, A., V. Rajagopalan, K. A. Sparks, D. V. Greathouse, and R. E. Koeppe. 2016. Juxta-terminal helix unwinding as a stabilizing factor to modulate the dynamics of transmembrane helices. *Chembiochem* 17(6):462-465.
10. Afrose, F., M. McKay, A. Mortazavi, V. Kumar, D. Greathouse, and R. Koeppe. 2019. Transmembrane helix integrity versus fraying to expose hydrogen bonds at a membrane-water interface. *Biochemistry* 58(6):633-645.
11. Gleason, N., V. Vostrikov, D. Greathouse, and R. Koeppe. 2013. Buried lysine, but not arginine, titrates and alters transmembrane helix tilt. *Proceedings of the National Academy of Sciences of the United States of America* 110(5):1692-1695.
12. Martfeld, A., D. Greathouse, and R. Koeppe. 2016. Ionization properties of histidine residues in the lipid bilayer membrane environment. *Journal of Biological Chemistry* 291(36):19146-19156.
13. De Angelis, A., and S. Opella. 2007. Bicelle samples for solid-state NMR of membrane proteins. *Nature Protocols* 2(10):2332-2338.
14. Nevzorov, A. A., and S. J. Opella. 2007. Selective averaging for high-resolution solid-state NMR spectroscopy of aligned samples. *Journal of Magnetic Resonance* 185(1):59-70.
15. Wu, C., A. Ramamoorthy, and S. Opella. 1994. High-resolution heteronuclear dipolar solid-state NMR-spectroscopy. *Journal of Magnetic Resonance Series a* 109(2):270-272.
16. Strandberg, E., S. Esteban-Martin, J. Salgado, and A. S. Ulrich. 2009. Orientation and dynamics of peptides in membranes calculated from H-2-NMR data. *Biophysical Journal* 96(8):3223-3232.
17. Vostrikov, V., C. Grant, S. Opella, and R. Koeppe. 2011. On the combined analysis of H-2 and N-15/H-1 solid-state NMR data for determination of transmembrane peptide orientation and dynamics. *Biophysical Journal* 101(12):2939-2947.

18. Schwaiger, C., P. Bjelkmar, B. Hess, and E. Lindahl. 2011. 3(10)-helix conformation facilitates the transition of a voltage sensor S4 segment toward the down state. *Biophysical Journal* 100(6):1446-1454.
19. Vostrikov, V. V., B. A. Hall, D. V. Greathouse, R. E. Koeppe, and M. S. P. Sansom. 2010. Changes in transmembrane helix alignment by arginine residues revealed by solid-state NMR experiments and coarse-grained MD simulations. *Journal of the American Chemical Society* 132(16):5803-5811.
20. Thibado, J. K., A. N. Martfeld, D. V. Greathouse, and R. E. Koeppe. 2016. Influence of high pH and cholesterol on single arginine-containing transmembrane peptide helices. *Biochemistry* 55(45):6337-6343.
21. Rajagopalan, V., D. Greathouse, and R. Koeppe. 2017. Influence of glutamic acid residues and pH on the properties of transmembrane helices. *Biochimica Et Biophysica Acta-Biomembranes* 1859(3):484-492.
22. Isom, D., C. Castaneda, P. Velu, and B. Garcia-Moreno. 2010. Charges in the hydrophobic interior of proteins. *Proceedings of the National Academy of Sciences of the United States of America* 107(37):16096-16100.
23. Popovic, D., J. Quenneville, and A. Stuchebrukhov. 2005. DFT/electrostatic calculations of pK(a) values in cytochrome c oxidase. *Journal of Physical Chemistry B* 109(8):3616-3626.



## CHAPTER 2

### Control of Transmembrane Helix Dynamics by Interfacial Tryptophan Residues

Published originally in M. J. McKay, A. A. De Angelis, S. E. Opella, D.V. Greathouse and R.E. Koeppe 2nd. Control of transmembrane helix dynamics by interfacial tryptophan residues. *Biophys J.* 2018; 114:2617-2629. © 2018 Biophysical Society

#### 2.1 Abstract

Transmembrane protein domains often contain interfacial aromatic residues, which may play roles for the insertion and stability of membrane helices. Residues such as Trp or Tyr, therefore, are often found situated at the lipid-water interface. We have examined the extent to which the precise radial locations of interfacial Trp residues may influence peptide helix orientation and dynamics. To address these questions, we have modified the GW<sup>5,19</sup>ALP23 (acetyl-GGALW<sup>5</sup>(LA)<sub>6</sub>LW<sup>19</sup>LAGA-[ethanol]amide) model peptide framework to relocate the Trp residues. Peptide orientation and dynamics were analyzed by means of solid-state NMR spectroscopy to monitor specific <sup>2</sup>H and <sup>15</sup>N labeled residues. GW<sup>5,19</sup>ALP23 adopts a defined tilted orientation within lipid bilayer membranes with minimal evidence of motional averaging of NMR observables such as <sup>2</sup>H quadrupolar or <sup>15</sup>N-<sup>1</sup>H dipolar splittings. Here we examine how peptide dynamics are impacted by relocating the interfacial Trp (W) residues on both ends and opposing faces of the helix, for example by a 100° rotation on the helical wheel for positions 4 and 20. In contrast to GW<sup>5,19</sup>ALP23, the modified GW<sup>4,20</sup>ALP23 helix experiences more extensive motional averaging of the NMR observables in several lipid bilayers of different thickness. Individual and combined Gaussian analyses of the <sup>2</sup>H and <sup>15</sup>N NMR signals confirm that the extent of dynamic averaging, particularly rotational “slippage” about the helix axis, is strongly coupled to the radial distribution of the interfacial Trp residues as well as the bilayer

thickness. Additional  $^2\text{H}$  labels on alanines A3 and A21 reveal partial fraying of the helix ends. Even within the context of partial unwinding, the locations of particular Trp residues around the helix axis are prominent factors for determining transmembrane helix orientation and dynamics within the lipid membrane environment.

## **2.2 Introduction**

The lipid bilayers of cell membranes host a variety of membrane proteins for which essential protein-lipid interactions influence the management of biological function. Indeed, a better understanding of protein-lipid interactions will be crucial for more complete elucidation of the molecular control mechanisms that underlie cell signaling and other actions mediated by membrane proteins. Transmembrane domains of proteins are often anchored within their lipid environment by flanking aromatic or charged residues.(1) For example, four Trp (W) residues at positions 9, 11, 13, and 15 govern the folding and anchor the subunits of gramicidin A ion channels produced by *Bacillus brevis*, wherein the channel protein consists of two monomeric peptides that dimerize at the N-terminal in the lipid bilayer.(2) The subunit anchoring is a result of the Trp indole ring's affinity for the membrane interface and is also what prevents each subunit from crossing the bilayer.(3) Therefore, the peptide must be added to each opposing bilayer leaflet in order to form channels. Whereas tryptophans 9 and 11 in gA are essential for efficient channel formation, interestingly, replacing residues 13 and 15 in gA with Phe allows the peptides to cross the membrane in a putative double-stranded conformation and then form channels.(4, 5) The different outcomes for modified gA sequence isomers (having Phe 9, 11 as opposed to Phe 13, 15) is particularly intriguing in that the differing properties are caused by different relative locations of interfacial aromatic Trp and Phe residues.

Indeed, interfacial Trp residues are important for the function of a number of membrane proteins. For example, conserved Trp residues provide membrane anchoring and govern helix dynamics and association to form functional integrin  $\alpha\text{IIb}\beta\text{3}$  heterodimers (6), wherein it is noted that particular Trp residues at different helix locations interact with heterogeneous lipids and cannot necessarily be functionally replaced by Tyr or Phe. Additionally, the switching between the kinase and phosphatase activities of a bacterial thermo-sensor is linked to not only temperature, membrane thickness and the hydrophobic length of a helix, but also whether Trp or Phe occupies a particular location on the transmembrane helix (7). For larger and more complex membrane proteins, for example NADH:ubiquinone oxidoreductase which has multiple transmembrane helices with interfacial Trp and Tyr residues,(8) it becomes more difficult to characterize, individually or collectively, the local or global impact exerted by the aromatic residues. However, fundamental and broadly applicable insights may be obtained at the single-residue level from investigations of model peptide-lipid systems that incorporate defined molecular features. In particular, examinations of how individual interfacial residues affect the orientation and dynamic behavior of a transmembrane helix are feasible using model peptide systems. Within such model systems, direct sequence modifications can be made and compared, such that resulting changes in the peptide-lipid interaction can be investigated in detail. Varying the membrane composition, lipid acyl chain length or peptide helix length may offer additional insights into these types of interactions.(9, 10) To match the hydrophobic lengths of different lipids, variable numbers of repeating pairs of core helix-forming residues, such as leucine-alanine (LA)<sub>n</sub> repeats, may be used within a peptide's central helical sequence,(11) with aromatic or charged residues flanking each end of the principal helix.

The original WALP family peptides were based on a sequence that included four interfacial Trp residues, acetyl-GWW-(LA)<sub>n</sub>-LWWA-[ethanol]amide (Figure 1, Table 1).(11) These peptides proved useful for examining the fundamentals associated with membrane partitioning by interfacial tryptophan residues and the modulation of lipid phase behavior when the hydrophobic length of the peptide helix was shorter than the thickness of the lipid bilayer.(11) Although the original concept envisioned a transmembrane helix normal to the bilayer, the WALP peptides subsequently were discovered to adopt a defined tilted orientation within lipid bilayers, with “apparently” only a “minor” dependence on lipid acyl chain length.(12, 13) Indeed a non-zero tilt angle between the helix axis and the bilayer normal has by now been universally observed with many peptides and has been rationalized in terms of the favorable precession entropy that accompanies a finite tilt angle.(14) The minor apparent response to bilayer thickness subsequently was attributed to motional averaging of the solid-state NMR observables(15, 16), primarily in the form of rotational “slippage” about the helix axis.(16, 17) The motion furthermore has been correlated with the presence of four interfacial tryptophan residues, two at each end of the core sequence, potentially competing among themselves for preferential orientations at the lipid-water interface.(17-20) The pairs of tryptophan residues were mutated to other aromatic or charged residues(21, 22) in order to observe how different pairs of identical residues could impact the transmembrane peptide helix behavior.

It was eventually determined that a single tryptophan residue at each end of the core helix is sufficient to minimize aggregation, regulate a hydrophobic peptide helix within a lipid membrane, and define its orientation, as seen with GW<sup>5,19</sup>ALP23 (acetylGGALW-(LA)<sub>6</sub>-LWLAGA-amide).(23, 24) Furthermore, it was discovered that fraying of helix ends may be crucially important for stabilizing the defined transmembrane orientation.(25) The presence of

fewer tryptophans tends to diminish the motional averaging and increase the sensitivity of the peptide helix to changes in lipid bilayer thickness. Indeed GW<sup>5,19</sup>ALP23 is observed to adopt a well-defined tilt angle that scales with lipid bilayer thickness. (26) The limited averaging exhibited by transmembrane GW<sup>5,19</sup>ALP23 stands in stark contrast to the behavior of transmembrane WALP peptides.(27, 28)

The effects of repositioning individual Trp residues have been tested by following placements that were shifted by  $\pm 200^\circ$  from positions 5,19 to positions 3, 21 (outward) or positions 7, 17 (inward), thereby increasing or decreasing the length of the hydrophobic core and the Trp-Trp distance along the helix axis, while maintaining an analogous radial separation of the flanking tryptophans on one face of the helix.(27) GW<sup>3,21</sup>ALP23 adopts a similar tilt distribution to that of GW<sup>5,19</sup>ALP23 within various lipid bilayer membranes, with low to moderate levels of motional averaging, whereas GW<sup>7,17</sup>ALP23 orients with smaller average tilt angles due to its shorter hydrophobic core helix.

Bearing in mind the extensive differences in motional averaging observed with different numbers of interfacial Trp residues, a principal aim of the research described here is to examine the influence of individual Trp residue radial locations on the transmembrane helix properties when two Trp residues are present, one at each end of the core helix. To this end, we moved W5 and W19 of GW<sup>5,19</sup>ALP23 each  $100^\circ$  outward to positions 4 and 20. As a consequence, the radial separation of the two aromatic residues changed from  $-40^\circ$  to  $+160^\circ$ . Whereas W5 and W19 are located on the same helix face, W4 and W20 are located on opposite faces of the helix, raising new questions: How will these Trp residue placements affect the peptide dynamics? What role might helix terminal unwinding play now that fewer residues are available for fraying beyond each aromatic residue? Answering such questions will provide a framework to better understand

how the interactions between transmembrane domains and their lipid environment are governed by specific residues within their sequences.

## 2.3 Materials and Methods

### <sup>2</sup>H Labeled Peptide Synthesis

The sequence of the host peptide GW<sup>5,19</sup>ALP23 was altered by changing tryptophans 5 and 19 to alanines, while changing leucines 4 and 20 to tryptophans, to yield the sequence for GW<sup>4,20</sup>ALP23 (Table 1). Peptides were synthesized using solid-phase FastMoc® chemistry on a 0.1 mmol scale as previously described (18) using a model 433A Applied Biosciences synthesizer by Life Technologies (Foster City, CA). *L*-alanine-d<sub>4</sub> was purchased from Cambridge Isotope Laboratories (Andover, MA) and modified to Fmoc-*L*-alanine-d<sub>4</sub> as previously described. (29) Successful synthesis of Fmoc-*L*-alanine-d<sub>4</sub> was verified by <sup>1</sup>H NMR. Each peptide was labeled with two Ala-d<sub>4</sub> residues in different isotope abundances. Peptides were purified using reversed-phase HPLC with an octyl silica column (Zorbax Rx-C8, 9.4 × 250 mm, 5 μm particle size; Agilent Technologies, Santa Clara, CA) and with a gradient of 92-96% methanol (with 0.1% trifluoroacetic acid) over 32 minutes. Peptide purity of > 95% and molar mass were confirmed by means of reversed-phase HPLC and MALDI mass spectrometry, respectively, as indicated in the Supporting Information (Figures S1 and S2).

To confirm peptide alpha helicity, circular dichroism(CD) samples were prepared by combining 62.5 nM peptide with 3.75 μM lipid (1/60). Mixtures were initially dissolved in methanol/chloroform; the solvents were removed with a stream of N<sub>2</sub> gas. The peptide/lipid films were further dried under vacuum for 48 h, hydrated to the final concentrations noted above, and then sonicated to form lipid vesicles with incorporated peptide. Each experiment consisted of 15 scans which were recorded with a Jasco (Easton, MD) J-1500 CD/fluorescence

spectropolarimeter at 22 °C, using a 1 mm cell path length, 1.0 nm bandwidth, 0.1 nm slit, and a scan speed of 20 nm/min.

#### Solid-State $^2\text{H}$ NMR Spectroscopy

For mechanically aligned samples, peptides were incorporated into lipid bilayers as previously described,(12) with a peptide/lipid molar ratio of 1:60 using DLPC, DMPC, or DOPC from Avanti Polar Lipids (Alabaster, AL) and a final hydration of 45% w/w using deuterium-depleted water from Cambridge Isotope Laboratories. Bilayer alignment in the liquid-crystalline samples was confirmed by  $^{31}\text{P}$  NMR using a Bruker (Billerica, MA) Avance 300 spectrometer with broadband  $^1\text{H}$  decoupling. Sample orientations at both  $\beta=0^\circ$  (bilayer normal parallel to the magnetic field) and  $\beta=90^\circ$  were tested. A quadrupole echo pulse sequence was utilized with full phase cycling,(30) at 50 °C at both sample orientations. Quadrupole echo delay was 4.5  $\mu\text{s}$  and the recycle delay was 90 ms. Between 0.7 and 1.5 million scans were acquired for each  $^2\text{H}$  NMR experiment and spectra were processed with 150 Hz line broadening.

For experiments where magnetically aligned bicelle samples containing  $^2\text{H}$ -labeled peptides were examined, the samples were prepared as described below.

#### Solid-State $^{15}\text{N}$ NMR Spectroscopy

Magnetically aligned bicelle samples (1:105, peptide/total lipid) were prepared by combining 61  $\mu\text{mol}$  DMPC, 19  $\mu\text{mol}$  ether-DHPC ( $q = 3.2$ , long lipid/short lipid) from Avanti Polar Lipids (Alabaster, AL) and 0.76  $\mu\text{mol}$  peptide. Peptide and DMPC were mixed, dried down under nitrogen flow, and then placed under vacuum for 48 hours to remove residual organic solvent. Separate aliquots of ether linked-DHPC were dried down in the same manner. The peptide/DMPC mixture and the ether linked-DHPC were hydrated separately with 100  $\mu\text{L}$  and 75  $\mu\text{L}$  of  $^2\text{H}$ -depleted water for a minimum of 4 hours with intermittent vortexing. The ether linked-

DHPC was then added to the peptide/DMPC mixture and the combined sample was subjected to multiple freeze-thaw cycles, alternating the temperature between 0 °C and 42 °C with gentle intermittent vortexing until the sample remained clear at 0 °C. While still cold, the sample liquid was transferred to a 5 mm NMR tube (New Era Enterprises, Vineland, NJ) and sealed.

For  $^{15}\text{N}$ -detected separated local field experiments,  $\text{GW}^{4,20}\text{ALP23}$  was synthesized with five  $^{15}\text{N}$  labeled residues at positions 13-17. Fmoc-*L*-Ala- $^{15}\text{N}$  and Fmoc-*L*-Leu- $^{15}\text{N}$  were purchased from Cambridge Isotope Laboratories.  $^{15}\text{N}$  chemical shifts and  $^{15}\text{N}/^1\text{H}$  dipolar coupling signals were recorded using a 700 MHz Bruker Avance spectrometer with a Magnex magnet and room temperature shims. A home-built “low-E”  $^{15}\text{N}/^1\text{H}$  double resonance probe with a modified Alderman–Grant (MAGC) 5 mm coil was used to minimize sample heating.(31) The  $\text{GW}^{4,20}\text{ALP23}$  sample in DMPC/ether linked-DHPC bicelles was equilibrated in the magnetic field at 42 °C (just below the critical temperature for DMPC/DHoPC bicelle structural transformation at  $q = 3.2$ ) for 30 min before initiating the NMR measurements. Previously, we have found that the peptide order parameter in plated samples remains essentially constant from 40 °C to 60 °C; optimal spectral resolution is observed at 50 °C.(17, 32) To confirm this feature, in Figure S3,  $^2\text{H}$  NMR spectra for a plated DMPC sample at 42 °C versus 50 °C show only ~0.1 kHz difference in quadrupolar splittings after 800,000 acquisitions. Agreeing with previous results, better spectral resolution is observed for plate samples at 50 °C as opposed to the lower temperature. SAMPI-4 (33) separated local field spectra were recorded with 256 scans, 64  $t_1$  increments, and a recycle delay of 6.5 s. The  $t_1$  evolution was preceded by a 1 ms CP-MOIST cross polarization (34), which compensates for power mismatch. The  $^1\text{H}$  irradiation at all times was 46.3 kHz, and composite pulse SPINAL-16 was applied for  $^1\text{H}$  heteronuclear decoupling during the 10 ms acquisition



time.(35, 36) The  $^1\text{H}$  carrier frequency of  $\sim 9$  ppm is optimal for transmembrane helices in perpendicular magnetically oriented bilayers.(37)

The  $^{15}\text{N}$  NMR data sets were processed and displayed using the programs NMRPipe/NMRDraw (38) and Sparky (39), using a dipolar coupling scaling factor of 0.61 for SAMPI-4 evolution.(33)

The chemical shifts were externally referenced to  $^{15}\text{N}$ -labeled solid ammonium sulfate, set to 26.8 ppm, corresponding to the signal from liquid ammonia at 0 ppm.(40) The  $^{15}\text{N}$  data for  $\text{W}^{2,22}\text{W}^{5,19}\text{ALP23}$  and  $\text{GW}^{5,19}\text{ALP23}$  (Table 1) previously had been previously processed with line broadening and with zero filling applied to both dimensions, and with apodization via a  $36^\circ$  shifted sine-squared bell function applied to the indirect dimension with a first point scaling factor of 0.5.(17, 18) To account for truncation of data in both data sets (primarily in  $t_1$ ) the  $\text{W}^{2,22}\text{W}^{5,19}\text{ALP23}$  and  $\text{GW}^{5,19}\text{ALP23}$   $^{15}\text{N}$  data presented in this study were reprocessed by omitting line broadening and instead applying linear prediction, zero filling and a  $36^\circ$  shifted sine-squared bell function without first point adjustment to both dimensions.

### Data Analysis

Preferred peptide helical orientations were assessed by several independent or combined analytical methods. The patterns for the recorded  $^2\text{H}$  quadrupolar splittings were evaluated by a geometric analysis of labeled alanines (“GALA”) as previously described.(12) The semistatic GALA method is based on three adjustable parameters: the apparent azimuthal rotation (or tilt direction)  $\rho_0$  with respect to the alpha carbon of Gly1, the apparent average tilt  $\tau_0$  of the helix axis relative to the bilayer normal, and a principal order parameter  $S_{zz}$ . The whole body dynamics of the peptide can be described by analyzing the oscillations about the helix  $\tau_0$  or  $\rho_0$ ; Gaussian treatments of  $^2\text{H}$  quadrupolar splittings,  $^{15}\text{N}$  chemical shifts, and  $^{15}\text{N}/^1\text{H}$  dipolar couplings were employed to further analyze the dynamics, following the method of

Vostrikov.(17) The Gaussian analysis of helix dynamics relies on four adjustable parameters:  $\rho_0$ ,  $\tau_0$ , a distribution  $\sigma\rho$  (rotational “slippage”), and a distribution  $\sigma\tau$  (helix “wobble”). For this particular study, the Gaussian calculations were performed as previously described,(17) over the ranges of 0-30° for  $\sigma\tau$ , 0-200° for  $\sigma\rho$ , 0-90° for  $\tau_0$ , and 0-359° for  $\rho_0$  in 1° increments. For comparative purposes, the  $^2\text{H}$  quadrupolar splittings, and the  $^{15}\text{N}$  chemical shifts with  $^{15}\text{N}/^1\text{H}$  dipolar couplings, were subjected to individual Gaussian analyses ( $^2\text{H}$  “only” or  $^{15}\text{N}$  “only”), as well as to combined analysis of the full data sets.

## 2.4 Results

Model transmembrane peptides such as  $\text{GW}^{5,19}\text{ALP23}$  and its analogues exhibit  $\alpha$ -helical secondary structure in lipid-bilayer membranes. The high stability of the repeating Leu-Ala core helix is manifested in the increased strength of backbone hydrogen bonds within a hydrophobic lipid environment.(41, 42) Relocating the Trp residues in  $\text{GW}^{5,19}\text{ALP23}$  to positions 4 and 20, as in  $\text{GW}^{4,20}\text{ALP23}$ , increases the length of the hydrophobic core sequence from  $(\text{LA})_6\text{L}$  (13 residues) to  $\text{A}(\text{LA})_7$  (15 residues). To characterize the secondary structure, CD spectra were recorded at 22 °C for  $\text{GW}^{4,20}\text{ALP23}$  incorporated within DLPC, DMPC and DOPC vesicles with a P/L ratio of 1:60 (Figure 2). Indeed, an  $\alpha$ -helical folding motif is confirmed in each lipid bilayer sample by the spectral minima observed at 208 nm and 222 nm. The relative ellipticity ratio ( $\epsilon_{222}/\epsilon_{208}$ ) is greater than 0.91 in each lipid. (When DOPC is the host lipid, the spectral noise observed below 200 nm is due to absorbance of UV radiation by the double bonds present in the acyl chains of DOPC.)

Solid-state NMR techniques can be utilized to determine the extent of a helix and the average peptide and lipid orientations and dynamics within lipid bilayers. The  $^{31}\text{P}$  NMR spectra confirmed the presence of oriented lipids within the mechanically aligned bilayers and

magnetically aligned bicelle samples. The peptide-lipid bilayer samples (1:60, peptide:lipid) were set so that the membrane normal was either perpendicular ( $\beta = 90^\circ$ ) or parallel ( $\beta = 0^\circ$ ) to the applied magnetic field (Figure 3A). For the  $\beta = 90^\circ$  spectra, a single peak was typically observed near -16 ppm; for the  $\beta = 0^\circ$  spectra, a major peak was observed near +30 ppm, with a minor peak at -16 ppm indicating small amounts of unoriented lipid. Peptide-bicelle samples (1:80, peptide:DMPC; or 1:105, peptide:(DMPC+DHoPC),  $q=3.2$ ) were observed to align properly giving  $\beta = 90^\circ$  with respect to the applied magnetic field (Figure 3B). In Figure 3B, the major  $^{31}\text{P}$  peak results from the DMPC head groups in the bicelles, and the minor peak is from the ether linked-DHPC head groups of the shorter lipids.

Insights into the orientation and dynamics of the GW<sup>4,20</sup>ALP23 transmembrane helix were gained from  $^{15}\text{N}$  and  $^2\text{H}$  solid-state NMR experiments. The  $^{15}\text{N}$  NMR spectrum of GW<sup>4,20</sup>ALP23 in DMPC/DHoPC bicelles reveals five  $^{15}\text{N}$  amide resonances, two of which overlap (Figure 4B). The  $^{15}\text{N}$  chemical shift frequencies span the narrow range between 82 and 90 ppm (Table 2), providing evidence of substantial motional averaging. Additional assignments (shown in Figure 4A) indicate that the  $^{15}\text{N}$  resonances from leucines 14 and 16 overlap in Figure 4B. The two-dimensional  $^{15}\text{N}$ -detected SAMPI4 spectra reveal a “PISA” wheel composed of the five signals corresponding to the five  $^{15}\text{N}$ -labeled core residues 13-17 (Figure 4A). In similar fashion to the  $^{15}\text{N}$  chemical shifts, the  $^{15}\text{N}/^1\text{H}$  splittings also lie within a narrow range (3.1-3.6 kHz) (Table 2 and Figure 4A). The signals in Figure 4A were assigned by comparisons with  $^2\text{H}$  NMR data and a subsequent combined analysis (see below). Position L16 produced an “aberrant” dipolar coupling value that moved the peak somewhat “inside” the PISA wheel, probably also reflecting dynamic averaging; because of the peak location in figure 4A, the L16 data points were not used in the analysis described below. The averaging observed for the  $^{15}\text{N}$  signals suggests that the

GW<sup>4,20</sup>ALP23 helix may experience extensive motion about its apparent average orientation in a bicelle environment.

Additional solid-state NMR experiments, including <sup>2</sup>H NMR measurements, can be used to analyze further the nature of helical peptides in oriented lipid bilayer membranes. To this end, <sup>2</sup>H-labeled alanine residues were incorporated into the core helix of GW<sup>4,20</sup>ALP23 and solid-state NMR was used to monitor the peptide's behavior in aligned lipid bilayers of increasing thickness (DLPC < DMPC < DOPC). For these spectra, mechanically aligned bilayer samples produce solid-state NMR observables that are similar to those from magnetically aligned bicelle samples.(17) GW<sup>5,19</sup>ALP23 was previously observed to adopt well-defined orientations relative to bilayer thickness(23, 26), and similar responses were seen when the interfacial tryptophan residues were relocated by ± two sequence positions to effectively increase or decrease the length of the Leu-Ala core sequence.(27) The helix of GW<sup>4,20</sup>ALP23 (Figure 5) behaves differently.

Each <sup>2</sup>H-labeled core alanine residue in GW<sup>4,20</sup>ALP23 yields a unique deuterium quadrupolar splitting when the lipid-peptide samples are aligned with  $\beta = 90^\circ$  (Figure 5) or  $\beta = 0^\circ$  (Figure S4). The variations among the core Ala-CD<sub>3</sub>  $\Delta\nu_q$  magnitudes (Figure 5, Table 3) indicate that GW<sup>4,20</sup>ALP23 is tilted away from the bilayer normal, since each value would be the same if the peptide helix were parallel to the membrane normal.(12) The  $\Delta\nu_q$  magnitudes for the core labels are observed, nevertheless, to span a frequency range from about 0.5 kHz to 16.0 kHz in all three lipids. The range is indeed narrow when compared to that of the parent transmembrane GW<sup>5,19</sup>ALP23 helix, for which the core alanines display <sup>2</sup>H  $|\Delta\nu_q|$  values ranging from 1.0 kHz to 27 kHz.(26) The large extent of motional averaging of the <sup>2</sup>H  $\Delta\nu_q$  values for GW<sup>4,20</sup>ALP23 correlates with the narrow ranges of resonance frequencies and dipolar splittings observed in the

<sup>15</sup>N-based experiments (Figure 4), again suggesting the presence of additional motions in the GW<sup>4,20</sup>ALP23 helix; these may involve “wobble” about the helix tilt angle or “slippage” around the helix axis.(17, 19, 28, 43)

Overlaying the <sup>15</sup>N PISA wheel of GW<sup>5,19</sup>ALP23 (Figure 6A) onto the spectrum of GW<sup>4,20</sup>ALP23 (Figure 6B) puts the extent of motional averaging into a visual context. The <sup>15</sup>N backbone signals (black contours) for GW<sup>4,20</sup>ALP23 are cluster to one side of the wheel produced by GW<sup>5,19</sup>ALP23 (red contours, black ring). The <sup>15</sup>N resonances of GW<sup>4,20</sup>ALP23 converge around essentially the same location as the extensively averaged signals from the corresponding labels in residues 13-17 in W<sup>2,22</sup>W<sup>5,19</sup>ALP23 (blue contours). Neither set of peptide <sup>15</sup>N resonances converges towards the value calculated for  $\tau_0 = 0^\circ$  (4.1 kHz, 79.3 ppm) and instead remain within the larger GW<sup>5,19</sup>ALP23 PISA wheel, which implies that the PISA signal convergence and <sup>2</sup>H signal averaging are likely due to dynamics.(17) (We note that the data set presented here for W<sup>2,22</sup>W<sup>5,19</sup>ALP23 has been reprocessed to isolate previously unresolved peaks; see Methods.) The PISA wheel signal convergence suggests that the GW<sup>4,20</sup>ALP23 helix undergoes extensive motional averaging in DMPC bicelles.

Several methods were employed to deduce the average helix orientation and quantify the dynamics of GW<sup>4,20</sup>ALP23. Notably, the availability of eight core alanine data points enabled a full Gaussian analysis (see (17) and (28)) for GW<sup>4,20</sup>ALP23 using the <sup>2</sup>H quadrupolar splitting magnitudes  $|\Delta\nu_q|$  observed for the core helix alanine residues spanning sequence positions 5-19 in bilayers of DLPC, DMPC and DOPC (Table 4). The Gaussian analysis generates estimates for peptide dynamics by considering the widths of distributions ( $\sigma_\tau$  and  $\sigma_\rho$ ) about the helix’s average tilt ( $\tau_0$ ) and azimuthal rotation ( $\rho_0$ ). A full Gaussian treatment requires four adjustable parameters ( $\tau_0$ ,  $\sigma_\tau$ ,  $\rho_0$ ,  $\sigma_\rho$ ) while holding a principal order parameter  $S_{zz}$  to a fixed value,

typically 0.88 as an estimate for the overall isotropic motion of the peptide with respect to its average orientation.(16) A modified Gaussian analysis (13, 19) can provide a suitable alternative approach when there are insufficient data points available to treat the four variables independently. While also setting  $S_{zz}$  to 0.88, this modified calculation requires only three adjustable parameters ( $\tau_0$ ,  $\rho_0$ ,  $\sigma_\rho$ ), as  $\sigma_\tau$  has been found to be a less important descriptor (28) that can be assigned a small finite value. (19)

For comparison with  $GW^{4,20}ALP23$ , a modified Gaussian analysis was performed for  $GW^{5,19}ALP23$  to represent low dynamic averaging and  $Y^{4,5}GW^{19}ALP23$  to represent high dynamic averaging.(18) Each of the latter helices contains only six core alanine data points. The fitted  $\sigma_\rho$  values that emerge from the full Gaussian treatment of the eight core alanines for  $GW^{4,20}ALP23$  exceed  $80^\circ$  in both DLPC and DOPC bilayers (Table 4). These results are comparable to those calculated for  $Y^{4,5}GW^{19}ALP23$  ( $> 70^\circ$ ). The large  $\sigma_\rho$  values are consistent with rotational “slippage” about the helix axis of the peptide’s average orientation, leading to the motional averaging observed in the  $^{15}N$  NMR as well as the  $^2H$  NMR data. The behavior of the  $GW^{4,20}ALP23$  helix in DOPC and DLPC bilayers differs substantially from the reduced dynamics calculated for  $GW^{5,19}ALP23$  in the same lipids. Indeed, the  $\sigma_\rho$  values for the parent  $GW^{5,19}ALP23$  helix are less than  $50^\circ$  in all three lipids. Surprisingly, the estimated  $\sigma_\rho$  value for  $GW^{4,20}ALP23$  in DMPC is much lower ( $51^\circ$ ) than its corresponding  $\sigma_\rho$  values in DLPC and DOPC (Table 4). This lower  $\sigma_\rho$  for  $GW^{4,20}ALP23$  in DMPC bilayers is similar to that observed for  $GW^{5,19}ALP23$  in DMPC and DOPC. The reason for this unusual lipid dependence of  $\sigma_\rho$  for  $GW^{4,20}ALP23$  remains to be determined. However, we note that the gel-fluid phase transition temperature of  $23^\circ C$  for DMPC is higher than those of the other lipids used in the experiments.,

and this result in DMPC contrasts with that for Y<sup>4,5</sup>GW<sup>19</sup>ALP23, which is highly dynamic in all three lipids.

The results of the Gaussian analysis were compared to those from a semi-static GALA analysis, which uses a grid search to find the lowest RMSD for fitting the <sup>2</sup>H alanine  $|\Delta v_q|$  values based on three adjustable parameters:  $\tau_0$ ,  $\rho_0$ , and  $S_{zz}$ . The GALA curves previously calculated for GW<sup>5,19</sup>ALP23 are shown for comparison in figure 7A (26). For this peptide helix, similar results emerge from the GALA and Gaussian analyses, even though the values of  $\tau_0$  are slightly lower for the GALA method, regardless of the lipid environment (Table 4). Importantly, the dependence of  $\tau_0$  upon the bilayer thickness is maintained in both methods of analysis. The trends for the GALA (or Gaussian) derived values of  $\tau_0$  for GW<sup>5,19</sup>ALP23 are that  $\tau_0$  decreases from about 20.7° (or 23°) in DLPC to 11.7° (or 13°) in DMPC and to 6.0° (or 9°) in DOPC (Table 4). Thus, it is evident that the helix tilt decreases as the lipid bilayer thickness increases. In contrast, when the tryptophans are relocated to positions 4 and 20, increased motional averaging obscures the trend, such that the peptide helix no longer exhibits a clear relationship between an apparent  $\tau_0$  and the bilayer thickness (Figure 7B). Instead, according to the GALA analysis, the GW<sup>4,20</sup>ALP23 helix “appears” to adopt a relatively small  $\tau_0$  value in all three lipids ( $\leq 6.0^\circ$ ). The low  $\tau_0$  angles in DLPC and DOPC do not match the tilts obtained in the full Gaussian analysis (which would be expected in the case of a peptide undergoing dynamic averaging as the GALA does not consider the oscillating motions about  $\rho_0$  and  $\tau_0$ ), yet in DMPC the  $\tau_0$  values from both methods of analysis are remarkably similar.

Dynamic averaging is manifest in several ways (see Figure 8). For example, large values of  $\sigma_\rho$  in the Gaussian analysis indicate extensive rotational averaging about the helix axis, as is evident for the Y<sup>4,5</sup>GW<sup>19</sup>ALP23 helix in all three lipids, and for the GW<sup>4,20</sup>ALP23 helix in DLPC and

DOPC (Table 4). The fitted “apparent” values of  $\rho_0$  also reflect the dynamic properties. When  $\sigma_\rho$  is less than about  $50^\circ$ , the  $\rho_0$  values tend to be rigorously consistent in all three lipid membranes, as is seen for GW<sup>5,19</sup>ALP23 in Figure 7A. By contrast, when  $\sigma_\rho$  is very large, then the apparent  $\rho_0$  values vary widely, as is seen for GW<sup>4,20</sup>ALP23 in Figure 7B and has been similarly observed for Y<sup>4,5</sup>GW<sup>19</sup>ALP23.<sup>(18)</sup> Interestingly, when  $\sigma_\rho$  is large, the extensive dynamics about the peptide’s helix axis has been indicated by consensus from a number of different analytical treatments of not only experimental data but also populations from molecular simulations (13, 15, 26, 42). Indeed, the accompanying  $\rho_0$  predictions from the GALA and Gaussian methods tend to agree (Table 4), even though the  $\tau_0$  predictions from the GALA method are systematically smaller by  $5^\circ$ - $10^\circ$ . Extensive motional averaging in the form of rotational slippage can essentially mask the realistic  $\tau_0$  values, as has been observed previously.<sup>(15, 44)</sup>

Besides the  $^2\text{H}$  NMR data, the  $^{15}\text{N}$  chemical shifts and  $^{15}\text{N}/^1\text{H}$  dipolar couplings can be used to characterize peptide dynamics with the Gaussian treatment. Indeed, we have compared Gaussian analyses of GW<sup>4,20</sup>ALP23 in bicelles of DMPC/DHoPC (based on  $^{15}\text{N}$  NMR data) with results from mechanically aligned DMPC bilayer samples. Notably, the  $^{15}\text{N}$  NMR data sets for the bicelles suggest a value of  $\rho_0$  that differs by about  $25^\circ$  from the consistent predictions from both the GALA and Gaussian analyses of the  $^2\text{H}$  NMR data for the same helix in mechanically aligned DMPC bilayers (Table 5). The different analytical outcomes for  $\rho_0$  may indicate that the properties of the GW<sup>4,20</sup>ALP23 helix are somewhat different between the lipid environments provided by the bicelle and bilayer samples. We note also that somewhat larger values of  $\tau_0$  and  $\sigma_\rho$  are calculated from the analysis of the helix properties in bicelles (Table 5). To investigate further, we prepared  $^2\text{H}$ -labeled samples of the GW<sup>4,20</sup>ALP23 helix in DMPC/DHoPC bicelles.



The measured  $^2\text{H } |\Delta\nu_q|$  values are quite similar for the alanine methyl groups of the core helix, but somewhat different for the terminal alanines 3 and 21 (Figures 9 and S5, Table 3). The semi-static analysis furthermore generates similar GALA curves for the core helix in DMPC bilayers and DMPC/DHoPC bicelles (Figure 9), with a similar value of  $\tau_0$  ( $3.7^\circ$ ), and a value of  $\rho_0$  ( $339^\circ$ ) that differs by about  $10^\circ$  (Figure 9) from that found for the helix in DMPC bilayers. A Gaussian treatment applied to the bicelle  $^2\text{H}$  NMR data also predicts a similar  $10^\circ$  difference in  $\rho_0$ , while fitting  $\tau_0$  to  $9.0^\circ$  and  $\sigma_\rho$  to  $64^\circ$  (Table 5). The observed  $\sigma_\rho$  of  $64^\circ$  and the  $5^\circ$  difference in  $\tau_0$  between the semi-static and full Gaussian analyses would suggest somewhat more extensive dynamics for the GW<sup>4,20</sup>ALP23 helix in bicelles. These variations contrast with the dynamic analysis of the mechanically oriented DMPC samples, for which similar results emerge from the GALA and Gaussian methods.

To further clarify the helix properties in bilayer and bicelle samples, we performed a combined Gaussian analysis (17) using the  $^{15}\text{N}$  chemical shifts and  $^{15}\text{N}/^1\text{H}$  dipolar couplings for bicelle samples, along with the  $^2\text{H } |\Delta\nu_q|$  data recorded for either bicelles or oriented samples. The combined analysis (using 17 data points) for GW<sup>4,20</sup>ALP23 in DMPC bilayers (with  $^{15}\text{N}$  bicelle data) predicts a similar tilt and rotation to that of the bilayer  $^2\text{H}$  Gaussian data set alone, and a lower  $\sigma_\rho$  of about  $42^\circ$  (Table 5). An additional combined analysis using the  $^2\text{H}$  and  $^{15}\text{N}$  bicelle data for GW<sup>4,20</sup>ALP23 (also 17 data points) reveals a similar tilt  $\tau_0$  value ( $6^\circ$ ) as the analysis of the smaller  $^2\text{H}$  data set alone (8 data points; Table 4). When comparing the bicelle and bilayer results, using either the  $^2\text{H}$  data alone or all available data points in the combined analysis (Table 5), the prediction for  $\rho_0$  seems to differ by about  $10^\circ$  between bicelle and oriented samples, and  $\sigma_\rho$  is calculated to be about  $20^\circ$  higher for the helix in bicelles ( $62^\circ$  versus  $42^\circ$  for bilayers). It is

possible that the minor variations with respect to helix azimuthal rotation result from differences between bicelle and lipid bilayer curvature and lipid composition (see Discussion).

To illustrate the key links between helix dynamics and Trp radial locations, the RMSD fits for the Gaussian and GALA analyses as a function of  $\tau_0$  vs  $\rho_0$  for GW<sup>4,20</sup>ALP23 and GW<sup>5,19</sup>ALP23 in DMPC/DHoPC bicelles are shown and compared in Figure S6. Both the GALA and Gaussian methods generate an acceptable solution area for GW<sup>5,19</sup>ALP23 and agree on both  $\tau_0$  and  $\rho_0$ .

The GALA analysis of GW<sup>4,20</sup>ALP23 reveals a larger range of solutions with comparable probabilities for the peptide helix adopting orientations over a range of  $\rho_0$  values at low values of  $\tau_0$ . The Gaussian refines this distribution about  $\rho_0$  somewhat, yet the similarly low average values for  $\tau_0$  are predicted. Furthermore, examination of the fits for  $\sigma_\tau$  and  $\sigma_\rho$  (see Figure S6, top) reveals that GW<sup>4,20</sup>ALP23 generates the lowest rmsd values at relatively high values of  $\sigma_\tau$  (~17°) and moderate values of  $\sigma_\rho$ , indicating much more extensive motional averaging when the Trp radial locations are moved +/- 100°, from sequence positions (5, 19) to (4, 20).

## 2.5 Discussion

The interfacial tryptophan residues present in many membrane proteins merit detailed investigations because of their profound effects on the structure and dynamics of trans-membrane helices, the dominant structural element of the helical class of membrane proteins. GWALP-like peptides serve as effective models for the roles of interfacial tryptophan residues that are tractable experimental systems whose sequences can be readily altered, enabling them to provide insights into how membrane proteins are situated and moving within lipid membrane environments.

The positioning of each particular tryptophan residue at the lipid-water interface may adjust the alignment of the parent helix in order to minimize hydrophobic mismatch between peptide length

and lipid thickness (45) and may also maximize favorable interactions with the lipid head groups. This type of “anchoring” behavior, along with possible “fraying” of the helix termini,(25) is responsible for the relatively modest dynamic averaging and the well-defined helix tilt of GW<sup>5,19</sup>ALP23, a tilt that indeed increases systematically while lipid thickness decreases.(26) When multiple tryptophan residues are present, as seen in the WALP peptides,(11-13) nevertheless, competition may occur between nearby aromatic residues as each one seeks an optimal position at the interface. Such a molecular “tug of war” could contribute to the extensive motional averaging of the transmembrane helix that is observed.(15, 44) The helix motion is particularly evident as rotational averaging of the axis of the tilted helix.(15, 17, 43) It should be noted that this phenomenon is not restricted to tryptophan residues. While the replacement of W5 by Y5 in Y<sup>5</sup>GW<sup>19</sup>ALP23 resulted in peptide dynamics similar to the original GW<sup>5,19</sup>ALP23, an additional Tyr residue in Y<sup>4,5</sup>GW<sup>19</sup>ALP23,(18) nevertheless, led to additional motional averaging, reminiscent of the properties of the WALP and other peptides that have more than two interfacial Trp residues. The extent of averaging was much more modest when Y4 and Y5 were replaced with F4 and F5, likely due to an absence of hydrogen bonding ability of the phenyl rings of F4 and F5 and consequently a lower tendency to “seek” interactions with the lipid head groups.(19) Replacing these two aromatic side chains by methyl groups in A<sup>4,5</sup>GW<sup>19</sup>ALP23 surprisingly also resulted in a stabilized transmembrane helix experiencing low dynamic averaging.(25) The complete lack of any side chain with hydrogen bonding potential near the N-terminal, in both F<sup>4,5</sup>GW<sup>19</sup>ALP23 and A<sup>4,5</sup>GW<sup>19</sup>ALP23, raised questions concerning how a well-defined tilted transmembrane helix orientation could be stabilized and maintained. The unfolding of helix termini may suggest an answer; exposure of backbone groups caused by the unwinding of 3-4 residues at the N- and/or C-termini could serve to stabilize each peptide

helix in a preferred transmembrane orientation and minimize the local motions.(25) The potential link between helix fraying and orientational stability of a helix in a phospholipid bilayer environment may provide a bridge between the studies of model systems, such as the WALP and GWALP peptides, and membrane proteins with multiple transmembrane helices.

In the present studies, we again find that the helix termini are partially unwound as seen with the anomalous quadrupolar splittings of residues 3 and 21 in Figures 7C and 9. Partial helix unraveling characterized by such a pattern has also been observed in the absence of a terminal Trp residues in A<sup>4,5</sup>GW<sup>19</sup>ALP23 (25) and therefore, the quadrupolar splittings of alanines 3 and 21 are not a result of any interference with an adjacent Trp. Even with partial unwinding present at the helix termini, relocation of the juxta-terminal tryptophan residues from positions W5 and W19 in GW<sup>5,19</sup>ALP23 to W4 and W20 is sufficient to introduce additional motion into the system. Indeed, GW<sup>4,20</sup>ALP23 experiences comparable dynamic averaging to that of Y<sup>4,5</sup>GW<sup>19</sup>ALP23,(18) with high values of  $\sigma_p$  observed in both DLPC and DOPC bilayers. This extensive azimuthal averaging about the helix axis is also responsible for the apparent mismatch of  $\tau_0$  values between the semi-static and Gaussian analyses. One factor that may influence the azimuthal averaging is the radial positioning of particular interfacial tryptophan residues, which more specifically are located on opposite sides of the GW<sup>4,20</sup>ALP23 alpha helix. This arrangement is similar to that of W2 and W22 found within the highly dynamic peptides W<sup>2,22</sup>W<sup>5,19</sup>ALP23 and W<sup>2,3,21,22</sup>ALP23 (Figure 1). While competition between tryptophan residues oriented on opposite helix faces could play a major role in determining the helix dynamics, it is not the only factor to consider. For example, compared to GW<sup>5,19</sup>ALP23, GW<sup>4,20</sup>ALP23 lacks leucine residues on either side of the terminal tryptophans, such that W4 and W20 have Ala neighbors instead of Leu neighbors, and this may influence the dynamics.

GW<sup>4,20</sup>ALP23 additionally contains a longer hydrophobic core than that of GW<sup>5,19</sup>ALP23, consisting of two additional residues. The length of the hydrophobic core varies for each face of the helix. After considering both the core length and the competition between W4 and W20, a high “slippage” about the helix axis is likely the most facile way in which the peptide can compensate and minimize hydrophobic mismatch. Therefore, the extensive motional averaging of GW<sup>4,20</sup>ALP23 observed in DLPC and DOPC bilayers is not surprising. However, the lack of additional motion when the helix is incorporated into DMPC bilayers is unexpected. Notably, GW<sup>4,20</sup>ALP23 is seemingly well-behaved with only modest dynamics about the helix average rotation in DMPC bilayers. The core helix adopts a small tilt angle  $\tau_0$  of 3°-5° as determined by both the GALA and Gaussian analysis methods, while maintaining a  $\sigma_p$  of about 50°, a value which is comparable to that observed for GW<sup>5,19</sup>ALP23 in DMPC, DLPC and DOPC bilayers (Table 4). This behavior of GW<sup>4,20</sup>ALP23 is different from that of Y<sup>4,5</sup>GW<sup>19</sup>ALP23, which retains its high level of dynamics about the helical axis in all three lipids. Additionally, in DMPC bilayers, the lowest rmsd values are fitted to higher values of  $\sigma_\tau$  which suggests that the helical wobble may have an impact. DLPC and DOPC bilayers have hydrophobic thicknesses (excluding head group region) of 20.8 Å and ~ 26 Å respectively at 50 °C(46, 47), and may match the hydrophobic length of GW<sup>4,20</sup>ALP23 less well than does DMPC. A DMPC bilayer of 24.8 Å (at 50 °C)(46) is of similar thickness to the inter-tryptophan distance of 24 Å for the 16 residues in the  $\alpha$ -helix between W4 and W20 in GW<sup>4,20</sup>ALP23. It is plausible, therefore, that DMPC may be an optimal environment for GW<sup>4,20</sup>ALP23 to adopt a “stabilized” orientation with wobbling about the membrane normal over a low tilt angle without the need for additional motions about the peptides average rotation to further minimize hydrophobic mismatch. The substantial unwinding of the helix at residues 3 and 21 (Figure 7) confirms a

maximum length for the core helix. The behavior of  $\text{GW}^{4,20}\text{ALP23}$  in DMPC/DHPC bicelles, while arguably somewhat more dynamic, further supports these concepts.

Data points for peptides in DMPC/DHPC bicelles and DMPC bilayers have been used interchangeably in the past due to the almost indistinguishable results when the sample types are compared using either the semi-static or Gaussian analyses. (17) While the quadrupolar wave plots generated by both analyses are similar (Figure 9), we find that  $\text{GW}^{4,20}\text{ALP23}$  nevertheless is consistently found to adopt a slightly different preferred rotation corresponding to a  $10^\circ$  difference in  $\rho_0$  in bicelles compared to DMPC bilayer samples. The Gaussian analysis agrees with this difference in rotation, and furthermore finds a higher rotational distribution reflected by  $\sigma_\rho$  for the peptide within a bicelle environment. The topology of the mixed lipids found in bicelles is somewhat different from that of DMPC bilayers and may play a role in the different rotational minimum and higher level of dynamic averaging that is observed for the helix in bicelles. A bicelle's discoid shape is composed of a long-chained DMPC lipid bilayer surrounded by a curved edge formed by a short-chained DHPC lipid assembly which protects the longer lipids from the surrounding solvent.(48) Hydration is also somewhat higher for bicelle samples and thus can increase the membrane fluidity. The  $\sigma_\rho$  calculated for  $\text{GW}^{4,20}\text{ALP23}$  in bicelle samples is in between the value calculated in DMPC bilayers and the extensive motion calculated for both DLPC and DOPC bilayers. The size of the  $^{15}\text{N}$  PISA wheel (Figure 6) agrees with the presence of additional motional averaging for the peptide in bicelles, as the signals partially collapse toward a single locus, a behavior also exhibited by the signals from the highly dynamic  $\text{W}^{2,22}\text{W}^{5,19}\text{ALP23}$  helix (Figure 6). One possibility is that the more fluid bicelle environment may impact the  $\text{GW}^{4,20}\text{ALP23}$  helix so as to induce more extensive rotational oscillations (larger  $\sigma_\rho$ ) to compensate. The edges of the bicelle where the DMPC lipids meet the

shorter DHPC lipids may also impact the helix properties, which would be seen as a system average. For example, an averaging between central and outer populations of the peptide would influence the NMR spectra. We also note that the  $\tau_0$  calculated by the combined Gaussian analysis of the complete bicelle data set does not deviate from the semi-static analysis, while  $\sigma_\rho$  remains relatively high. The overall results suggest somewhat increased dynamics about the peptide's average rotation for GW<sup>4,20</sup>ALP23 in bicelles versus bilayer samples.

Previously, it was reported that transmembrane peptides with low  $\tau_0$  usually can be fitted with multiple solutions (17) and that by increasing the number of observed <sup>2</sup>H or <sup>15</sup>N restraints, the array of possible solutions could be significantly decreased. The large pool of data points and interesting dynamics of the GW<sup>4,20</sup>ALP23 system provide an opportunity to examine how a full Gaussian analysis, using only <sup>2</sup>H  $|\Delta\nu_q|$  values, compares to a combined Gaussian analysis which incorporates both the <sup>2</sup>H and <sup>15</sup>N data sets. For peptides such as GW<sup>5,19</sup>ALP23, the six data points available from the CD<sub>3</sub> side chains of the six <sup>2</sup>H-labeled core alanine residues are not sufficient for reliable solutions for the four variables involved in a full Gaussian analysis. (If quadrupolar splittings can be observed from some of the backbone C<sub>α</sub> deuterons of the labeled alanines, the resulting larger data set can sometimes suffice for a full Gaussian analysis.(49)) In the absence of additional data points, a three-parameter modified Gaussian analysis proves to be useful. The modified analysis may be implemented by setting  $\sigma_\tau$  to a small finite value and varying  $\sigma_\rho$ ,  $\rho_0$ , and  $\tau_0$ .(13, 19) For well-behaved peptides that adopt a relatively large  $\tau_0$  in lipid bilayers, such as GW<sup>5,19</sup>ALP23, the limited data set is less of an issue, as the solutions calculated by the modified analysis tend to agree with a semi-static GALA treatment and predict similar dynamics (see Table 6). The limitations of the modified Gaussian calculation can be highlighted when examining all eight <sup>2</sup>H data points from the core alanines of GW<sup>4,20</sup>ALP23 in DMPC

bilayers and comparing these results to those of the full Gaussian calculation over the same data set. The solutions calculated by the modified Gaussian analysis may overestimate the peptide dynamics, predicting somewhat higher values for both  $\tau_0$  and  $\sigma_p$  with similar RMSD values (Table 6). The full Gaussian calculation for GW<sup>4,20</sup>ALP23 in DMPC narrows the solution range to lower values of  $\tau_0$  and  $\sigma_p$ , and provides a value of 20° for  $\sigma_\tau$ , while also giving a better RMSD fit. Therefore, in this case, minor limitations to the modified Gaussian analysis are revealed, and the advantage of eight data points allows access to the full calculation and a narrower range of solutions for GW<sup>4,20</sup>ALP23. Notably, the  $\rho_0$  and  $\sigma_p$  values obtained from the combined Gaussian analyses, utilizing bicelle data alone or bilayer <sup>2</sup>H data and bicelle <sup>15</sup>N data, agree with the dynamic properties predicted by full Gaussian analysis (Table 5) and suggest a lower extent of slippage about the helix axis in DMPC bilayer samples compared to bicelles. While the combined analysis does not resolve the minor discrepancies in  $\rho_0$  and  $\sigma_p$  observed between the bilayer and bicelle samples, its overall agreement with the full Gaussian calculation further indicates the advantages of a larger experimental data set when dealing with dynamic transmembrane peptide systems such as GW<sup>4,20</sup>ALP23.

The radial locations of particular Trp residues about the helix principal axis influence transmembrane helix dynamics. We have performed multiple analyses incorporating <sup>2</sup>H NMR and <sup>15</sup>N NMR data from solid-state NMR experiments to determine the effects of relocating interfacial tryptophan residues 5 and 19 outward and to opposing faces of the GW<sup>5,19</sup>ALP23 framework to positions 4 and 20. The extent of motion around the peptide helix axis then becomes quite high in both DLPC and DOPC bilayers and intermediate in DMPC/DHPC bicelles, while remaining moderate in DMPC bilayers. An added benefit of having eight core alanine residues available for <sup>2</sup>H labeling in the GW<sup>4,20</sup>ALP23 framework is the opportunity to



perform calculations that reveal the complex behavior of this transmembrane helix. In summary, the numbers and precise locations of tryptophan residues are both important determinants of the helix dynamics.

## 2.6 Acknowledgements

This work was supported in part by NSF MCB grant 1713242, and by the Arkansas Biosciences Institute. The peptide, NMR and mass spectrometry facilities at the University of Arkansas are supported in part by NIH grants GM103429 and GM103450. The Biotechnology Research Center for NMR Molecular Imaging of Proteins at the University of California, San Diego is supported by NIH grant P41 EB002031, and research on membrane associated peptides and proteins was supported by NIH grant R35 GM122501.

## 2.7 References

1. Yau, W. M., W. C. Wimley, K. Gawrisch, and S. H. White. 1998. The preference of tryptophan for membrane interfaces. *Biochemistry* 37(42):14713-14718.
2. Koeppe, R. E., and O. S. Andersen. 1996. Engineering the gramicidin channel. *Ann. Rev. Biophys. Biomol. Struct.* 25:231-258.
3. Oconnell, A. M., R. E. Koeppe, and O. S. Andersen. 1990. Kinetics of gramicidin channel formation in lipid bilayers - transmembrane monomer association. *Science* 250(4985):1256-1259.
4. Gu, H., K. Lum, J. H. Kim, D. V. Greathouse, O. S. Andersen, and R. E. Koeppe. 2011. The membrane interface dictates different anchor roles for “inner pair” and “outer pair” tryptophan indole rings in gramicidin A channels. *Biochemistry* 50(22):4855-4866.
5. McKay, M. J., F. Afrose, R. E. Koeppe, and D. V. Greathouse. 2018. Helix formation and stability in membranes. *Biochimica et Biophysica Acta (BBA) - Biomembranes*.
6. Andersen, O. S., and R. E. Koeppe, II. 2007. Bilayer thickness and membrane protein function: An energetic perspective. *Ann. Rev. Biophys. Biomol. Struct.* 36:107-130.
7. Thibado, J. K., A. N. Martfeld, D. V. Greathouse, and R. E. Koeppe. 2016. Influence of high pH and cholesterol on single arginine-containing transmembrane peptide helices. *Biochemistry* 55(45):6337-6343.

8. Killian, J. A., I. Salemink, M. R. R. dePlanque, G. Lindblom, R. E. Koeppe, and D. V. Greathouse. 1996. Induction of nonbilayer structures in diacylphosphatidylcholine model membranes by transmembrane alpha-helical peptides: Importance of hydrophobic mismatch and proposed role of tryptophans. *Biochemistry* 35(3):1037-1045.
9. van der Wel, P., E. Strandberg, J. Killian, and R. Koeppe. 2002. Geometry and intrinsic tilt of a tryptophan-anchored transmembrane alpha-helix determined by H-2 NMR. *Biophysical Journal* 83(3):1479-1488.
10. Strandberg, E., S. Özdirekcan, D. T. S. Rijkers, P. C. A. van der Wel, R. E. Koeppe, R. M. J. Liskamp, and J. A. Killian. 2004. Tilt angles of transmembrane model peptides in oriented and non-oriented lipid bilayers as determined by H-2 solid-state NMR. *Biophys. J.* 86(6):3709-3721.
11. Lee, J., and W. Im. 2008. Transmembrane helix tilting: Insights from calculating the potential of mean force. *Physical Review Letters* 100(1).
12. Oezdirekcan, S., C. Etchebest, J. A. Killian, and P. F. J. Fuchs. 2007. On the orientation of a designed transmembrane peptide: Toward the right tilt angle? *Journal of the American Chemical Society* 129(49):15174-15181.
13. Strandberg, E., S. Esteban-Martin, J. Salgado, and A. S. Ulrich. 2009. Orientation and dynamics of peptides in membranes calculated from H-2-NMR data. *Biophysical Journal* 96(8):3223-3232.
14. Vostrikov, V., C. Grant, S. Opella, and R. Koeppe. 2011. On the combined analysis of H-2 and N-15/H-1 solid-state NMR data for determination of transmembrane peptide orientation and dynamics. *Biophysical Journal* 101(12):2939-2947.
15. Gleason, N., V. Vostrikov, D. Greathouse, C. Grant, S. Opella, and R. Koeppe. 2012. Tyrosine replacing tryptophan as an anchor in GWALP peptides. *Biochemistry* 51(10):2044-2053.
16. Sparks, K., N. Gleason, R. Gist, R. Langston, D. Greathouse, and R. Koeppe. 2014. Comparisons of interfacial Phe, Tyr, and Trp residues as determinants of orientation and dynamics for GWALP transmembrane peptides. *Biochemistry* 53(22):3637-3645.
17. de Planque, M. R. R., B. B. Bonev, J. A. A. Demmers, D. V. Greathouse, R. E. Koeppe, F. Separovic, A. Watts, and J. A. Killian. 2003. Interfacial anchor properties of tryptophan residues in transmembrane peptides can dominate over hydrophobic matching effects in peptide-lipid interactions. *Biochemistry* 42(18):5341-5348.
18. de Planque, M. R. R., J. A. W. Kruijtzter, R. M. J. Liskamp, D. Marsh, D. V. Greathouse, R. E. Koeppe, B. de Kruijff, and J. A. Killian. 1999. Different membrane anchoring positions of tryptophan and lysine in synthetic transmembrane alpha-helical peptides. *J. Biol. Chem.* 274(30):20839-20846.

19. de Planque, M. R. R., J. W. P. Boots, D. T. S. Rijkers, R. M. J. Liskamp, D. V. Greathouse, and J. A. Killian. 2002. The effects of hydrophobic mismatch between phosphatidylcholine bilayers and transmembrane alpha-helical peptides depend on the nature of interfacially exposed aromatic and charged residues. *Biochemistry* 41(26):8396-8404.
20. Vostrikov, V. V., C. V. Grant, A. E. Daily, S. J. Opella, and R. E. Koeppe, II. 2008. Comparison of "Polarization Inversion with Spin Exchange at Magic Angle" and "Geometric Analysis of Labeled Alanines" methods for transmembrane helix alignment. *J. Am. Chem. Soc.* 130(38):12584-+.
21. Vostrikov, V. V., B. A. Hall, D. V. Greathouse, R. E. Koeppe, and M. S. P. Sansom. 2010. Changes in transmembrane helix alignment by arginine residues revealed by solid-state NMR experiments and coarse-grained MD simulations. *J. Am. Chem. Soc.* 132(16):5803-5811.
22. Mortazavi, A., V. Rajagopalan, K. A. Sparks, D. V. Greathouse, and R. E. Koeppe. 2016. Juxta-terminal helix unwinding as a stabilizing factor to modulate the dynamics of transmembrane helices. *Chembiochem* 17(6):462-465.
23. Vostrikov, V., A. Daily, D. Greathouse, and R. Koeppe. 2010. Charged or aromatic anchor residue dependence of transmembrane peptide tilt. *Journal of Biological Chemistry* 285(41):31723-31730.
24. Vostrikov, V., and R. Koeppe. 2011. Response of GWALP Transmembrane peptides to changes in the tryptophan anchor positions. *Biochemistry* 50(35):7522-7535.
25. Strandberg, E., S. Esteban-Martin, A. Ulrich, and J. Salgado. 2012. Hydrophobic mismatch of mobile transmembrane helices: Merging theory and experiments. *Biochimica Et Biophysica Acta-Biomembranes* 1818(5):1242-1249.
26. Thomas, R., V. Vostrikov, D. Greathouse, and R. Koeppe. 2009. Influence of proline upon the folding and geometry of the WALP19 transmembrane peptide. *Biochemistry* 48(50):11883-11891.
27. Davis, J., K. Jeffrey, M. Bloom, M. Valic, and T. Higgs. 1976. Quadrupolar echo deuteron magnetic-resonance spectroscopy in ordered hydrocarbon chains. *Chemical Physics Letters* 42(2):390-394.
28. Grant, C., Y. Yang, M. Glibowicka, C. Wu, S. Park, C. Deber, and S. Opella. 2009. A Modified Alderman-Grant Coil makes possible an efficient cross-coil probe for high field solid-state NMR of lossy biological samples. *Journal of Magnetic Resonance* 201(1):87-92.

29. van der Wel, P. C. A., N. D. Reed, D. V. Greathouse, and R. E. Koeppe. 2007. Orientation and motion of tryptophan interfacial anchors in membrane-spanning peptides. *Biochemistry* 46(25):7514-7524.
30. Nevzorov, A., and S. Opella. 2007. Selective averaging for high-resolution solid-state NMR spectroscopy of aligned samples. *Journal of Magnetic Resonance* 185(1):59-70.
31. Levitt, M., D. Suter, and R. Ernst. 1986. Spin dynamics and thermodynamics in solid-state NMR cross polarization. *Journal of Chemical Physics* 84(8):4243-4255.
32. Fung, B., A. Khitrin, and K. Ermolaev. 2000. An improved broadband decoupling sequence for liquid crystals and solids. *J. Magn. Reson.* 142(1):97-101.
33. Sinha, N., C. Grant, K. Rotondi, L. Feduik-Rotondi, L. Gierasch, and S. Opella. 2005. Peptides and the development of double- and triple-resonance solid-state NMR of aligned samples. *Journal of Peptide Research* 65(6):605-620.
34. De Angelis, A., S. Howell, A. Nevzorov, and S. Opella. 2006. Structure determination of a membrane protein with two trans-membrane helices in aligned phospholipid bicelles by solid-state NMR spectroscopy. *Journal of the American Chemical Society* 128(37):12256-12267.
35. Delaglio, F., S. Grzesiek, G. Vuister, G. Zhu, J. Pfeifer, and A. Bax. 1995. NMRPIPE - a multidimensional spectral processing system based on unix pipes. *Journal of Biomolecular NMR* 6(3):277-293.
36. Goddard, T. D., and D. G. Kneller. SPARKY 3. University of California, San Francisco.
37. Wishart, D., C. Bigam, J. Yao, F. Abildgaard, H. Dyson, E. Oldfield, J. Markley, and B. Sykes. 1995. H-1, C-13 and N-15 chemical-shift referencing in biomolecular NMR. *Journal of Biomolecular NMR* 6(2):135-140.
38. Esteban-Martin, S., E. Strandberg, J. Salgado, and A. Ulrich. 2010. Solid state NMR analysis of peptides in membranes: Influence of dynamics and labeling scheme. *BBA-Biomembranes* 1798(2):252-257.
39. Esteban-Martin, S., and J. Salgado. 2007. Self-assembling of peptide/membrane complexes by atomistic molecular dynamics simulations. *Biophys. J.* 92(3):903-912.
40. Killian, J., and T. Nyholm. 2006. Peptides in lipid bilayers: the power of simple models. *Current Opinion in Structural Biology* 16(4):473-479.
41. Kucerka, N., M. P. Nieh, and J. Katsaras. 2011. Fluid phase lipid areas and bilayer thicknesses of commonly used phosphatidylcholines as a function of temperature. *BBA-Biomembranes* 1808(11):2761-2771.

42. Pan, J., S. Tristram-Nagle, N. Kucerka, and J. F. Nagle. 2008. Temperature dependence of structure, bending rigidity, and bilayer interactions of dioleoylphosphatidylcholine bilayers. *Biophys. J.* 94(1):117-124.
43. Sanders, C., and R. Prosser. 1998. Bicelles: a model membrane system for all seasons? *Struct. With Folding & Design* 6(10):1227-1234.
44. Vostrikov, V., B. Hall, M. Sansom, and R. Koeppe. 2012. Accommodation of a central arginine in a transmembrane peptide by changing the placement of anchor residues. *Journal of Physical Chemistry B* 116(43):12980-12990.

## 2.8 Tables

*TABLE 1 Sequences of GW<sup>5,19</sup>ALP23 and High Dynamic Averaging GWALP-Like Peptides*

Name	Sequence	Reference
GW <sup>5,19</sup> ALP23	acetyl-GGALW <sup>5</sup> LALALALALALALW <sup>19</sup> LAGA-amide	(15)
W <sup>2,22</sup> W <sup>5,19</sup> ALP23	acetyl-GW <sup>2</sup> ALW <sup>5</sup> LALALALALALALW <sup>19</sup> LAW <sup>22</sup> A-amide	(4)
W <sup>2,3,21,22</sup> ALP23	acetyl-GW <sup>2</sup> W <sup>3</sup> LALALALALALALALALW <sup>21</sup> W <sup>22</sup> A-amide	(28)
Y <sup>4,5</sup> GW <sup>19</sup> ALP23	acetyl-GGAY <sup>4</sup> Y <sup>5</sup> LALALALALALALW <sup>19</sup> LAGA-amide	(11)
GW <sup>4,20</sup> ALP23	acetyl-GGAW <sup>4</sup> ALALALALALALALAW <sup>20</sup> AGA-amide	This work

TABLE 2  $^{15}\text{N}$  chemical shifts and  $^1\text{H}$ - $^{15}\text{N}$  dipolar Splittings for  $\text{GW}^{4,20}\text{ALP23}$  in DMPC/DHPC Bicelles

DMPC/DHPC	Position				
	13	14	15	16	17
$^{15}\text{N}$ Chemical Shift (ppm)	88.4	84.1	82.4	84.5	89.7
$^1\text{H}$ - $^{15}\text{N}$ Coupling (kHz)	3.53	3.15	3.55	3.33*	3.38

\*The aberrant  $^1\text{H}$ - $^{15}\text{N}$  coupling for residue 16 was omitted from future data analyses.

TABLE 3 *Quadrupolar Splitting Magnitudes ( $|\Delta\nu_q|$ , in kHz) for Labeled Alanine CD<sub>3</sub> Groups in GW<sup>4,20</sup>ALP23<sup>a</sup>*

Lipid(s)	Alanine CD <sub>3</sub> Position/ $\Delta\nu_q$ (kHz)									
	3	5	7	9	11	13	15	17	19	21
DLPC	15.7	2.1	14.0	1.4	14.6	0.8	12.2	1.8	8.2	0.1
DMPC	14.5	6.6	10.3	4.1	9.9	1.8	10.3	1.6	9.0	1.0
DOPC	13.1	10.2	5.3	10.4	4.2	9.4	6.8	2.9	6.2	3.3
DMPC/DH(o)PC	12.8	5.4	11.0	3.0	9.2	1.9	11.2	1.9	8.2	6.4

<sup>a</sup> *Quadrupolar splittings are reported for samples oriented with  $\beta = 0^\circ$  and are twice the magnitude observed when  $\beta = 90^\circ$ . The core alanine residues 5, 7, 9, 11, 13, 15, 17 and 19 sit between W4 and W20 in the sequence, whereas the juxta-terminal alanines 3 and 21 are near the ends. The DMPC/DH(o)PC lipid mixture indicates bicelle samples with  $q = 3.2$ .*



TABLE 4 Comparison of Orientations and Dynamics Calculated by GALA and Gaussian Analyses Using Ala-CD<sub>3</sub>  $|\Delta\nu_q|$  magnitudes of GWALP23 Family Peptides<sup>a</sup>

Analysis	DLPC				DMPC				DOPC			
	$\tau_0$	$\rho_0$	$\sigma\rho$	RMSD (kHz)	$\tau_0$	$\rho_0$	$\sigma\rho$	RMSD (kHz)	$\tau_0$	$\rho_0$	$\sigma\rho$	RMSD (kHz)
CD <sub>3</sub> Gauss.	$\tau_0$	$\rho_0$	$\sigma\rho$	RMSD (kHz)	$\tau_0$	$\rho_0$	$\sigma\rho$	RMSD (kHz)	$\tau_0$	$\rho_0$	$\sigma\rho$	RMSD (kHz)
W <sup>4,20</sup>	16°	321°	85°	0.49	5.0°	347°	51°	0.68	9.0°	129°	122°	0.78 <sup>c</sup>
Y <sup>4,5</sup> <sup>b</sup>	14°	259°	>90°	1.7	15°	321°	124°	0.63	6.0°	344°	72°	0.9
W <sup>5,19</sup> <sup>b</sup>	23°	304°	33°	0.70	13°	308°	44°	1.1	9.0°	321°	48°	0.7
GALA	$\tau_0$	$\rho_0$	S <sub>zz</sub>	RMSD (kHz)	$\tau_0$	$\rho_0$	S <sub>zz</sub>	RMSD (kHz)	$\tau_0$	$\rho_0$	S <sub>zz</sub>	RMSD (kHz)
W <sup>4,20</sup>	6.0°	322°	0.72	0.70	3.3°	349°	0.71	0.85	1.7°	133°	0.81	0.80 <sup>c</sup>
Y <sup>4,5</sup>	5.0°	260°	0.66	1.6	3.0°	323°	0.77	0.60	3.0°	359°	0.82	1.1
W <sup>5,19</sup>	20.7°	305°	0.71	0.66	11.7°	311°	0.86	0.90	6.0°	323°	0.87	0.6

<sup>a</sup> The abbreviations refer to peptides based on the locations of selected aromatic residues, W<sup>4,20</sup> in GW<sup>4,20</sup>ALP23, Y<sup>4,5</sup> in Y<sup>4,5</sup>GW<sup>19</sup>ALP23 and W<sup>5,19</sup> in GW<sup>5,19</sup>ALP23. See also Table 1.

<sup>b</sup> For the six core Ala-CD<sub>3</sub> data points of GW<sup>5,19</sup>ALP23 and Y<sup>4,5</sup>GW<sup>19</sup>ALP23, a modified three-variable Gaussian treatment was used as described by (28) while constraining  $\sigma$  to 5°. (19) For the eight core Ala-CD<sub>3</sub> data points of GW<sup>4,20</sup>ALP23, a full Gaussian analysis was used, and the resulting  $\sigma$  values were 15°, 20° and 5° in DLPC, DMPC and DOPC, respectively.

<sup>c</sup> For GW<sup>4,20</sup>ALP23 in DOPC, the <sup>2</sup>H  $|\Delta\nu_q|$  value for position 17 was left out of the analysis, as it deviates from the calculated GALA curve (see Figure 7C).

TABLE 5 Comparison of  $GW^{4,20}ALP23$  in DMPC Oriented Samples and DMPC/DHPC Bicelle Dynamics

Analysis	DMPC Bilayers				DMPC/DH(o)PC Bicelles			
	$^1H\text{-}^{15}N/^{15}N$ Gaussian*					$\tau_0$	$\rho_0$	$\sigma\rho$
					14°	321°	80°	0.59
CD <sub>3</sub> Gaussian**	$\tau_0$	$\rho_0$	$\sigma\rho$	RMSD (kHz)	$\tau_0$	$\rho_0$	$\sigma\rho$	RMSD (kHz)
	5.0°	347°	51°	0.68	9.0°	338°	64°	0.82
Combined Gaussian	$\tau_0$	$\rho_0$	$\sigma\rho$	RMSD (kHz)	$\tau_0$	$\rho_0$	$\sigma\rho$	RMSD (kHz)
	4.0°	344°	42°	0.85 <sup>a</sup>	6.0°	337°	62°	1.00 <sup>b</sup>

\*Nine data points consisting of five  $^{15}N$  chemical shifts and four  $^1H\text{-}^{15}N$  dipolar splittings.

\*\*Eight data points from the core alanine side chain CD<sub>3</sub> quadrupolar splittings.

<sup>a</sup> Combined Gaussian Analysis was performed using  $^1H\text{-}^{15}N$  dipolar splittings and  $^{15}N$  chemical shifts obtained from  $^{15}N$  labeled DMPC/DHPC bicelle samples (9 data points), with  $^2H$  data from bilayers (8 data points). The resulting  $\sigma$  value was 16°.

<sup>b</sup> Combined Gaussian Analysis was performed using all bicelle data (17 data points). The resulting  $\sigma$  value was 17°.

TABLE 6 Comparison of Full vs Modified Gaussian Analyses of GWALP23 Family Peptides in DMPC Bilayers Using  $^2\text{H}$ -Quadrupolar Splittings

Modified <sup>a</sup>	GW <sup>4,20</sup> ALP23 (8 Data Points)				GW <sup>5,19</sup> ALP23 (6 Data Points)			
(fixed) $\sigma\tau$	$\tau_0$	$\rho_0$	$\sigma\rho$	RMSD (kHz)	$\tau_0$	$\rho_0$	$\sigma\rho$	RMSD (kHz)
5°	21°	346°	148°	0.98	13°	308°	44°	1.1
10°	19°	346°	138°	0.98	13°	308°	42°	1.2
15°	4.0°	344°	42°	0.96	16°	307°	51°	1.6
20°	5.0°	348°	51°	0.68	18°	306°	51°	2.3
Full <sup>b</sup>	$\tau_0$	$\rho_0$	$\sigma\rho$	RMSD (kHz)				
	5.0°	347°	51°	0.68				

<sup>a</sup> A modified three-variable Gaussian treatment was used as described by (28) while constraining  $\sigma\tau$  to finite values. (19)

<sup>b</sup> For GW<sup>4,20</sup>ALP23, a full Gaussian analysis was used, and the resulting  $\sigma\tau$  value was 20°.

## 2.9 Figures

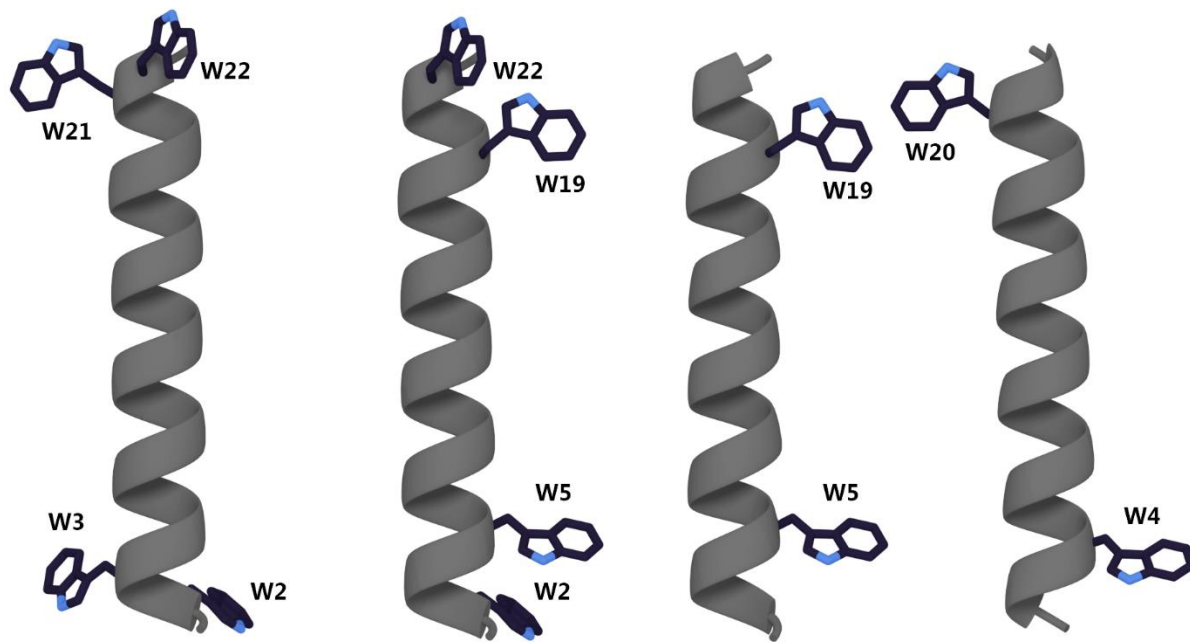


*FIGURE 1* Molecular models of GWALP-like peptides. From left to right:  $W^{2,3,21,22}$ ALP23,  $W^{2,22}W^{5,19}$ ALP23,  $GW^{5,19}$ ALP23, and  $GW^{4,20}$ ALP23. For amino acid sequences, see Table 1. The model for  $GW^{4,20}$ ALP23 was rotated 90°.

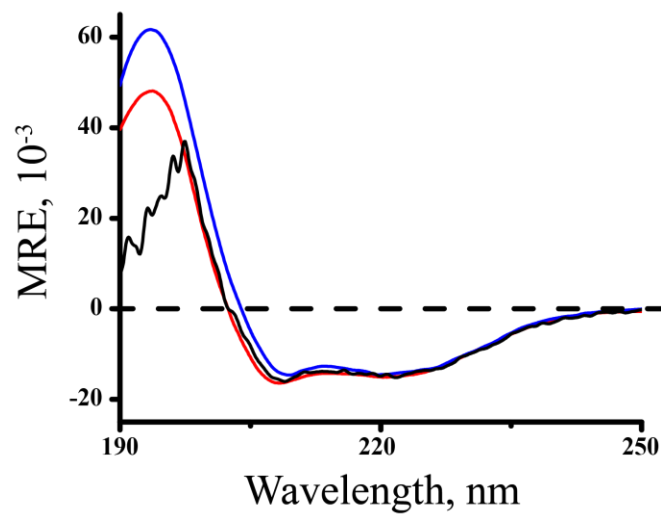


*FIGURE 2* Circular dichroism spectra for GW<sup>4,20</sup>ALP23 in DLPC(red), DMPC(blue), and DOPC(black) vesicles.

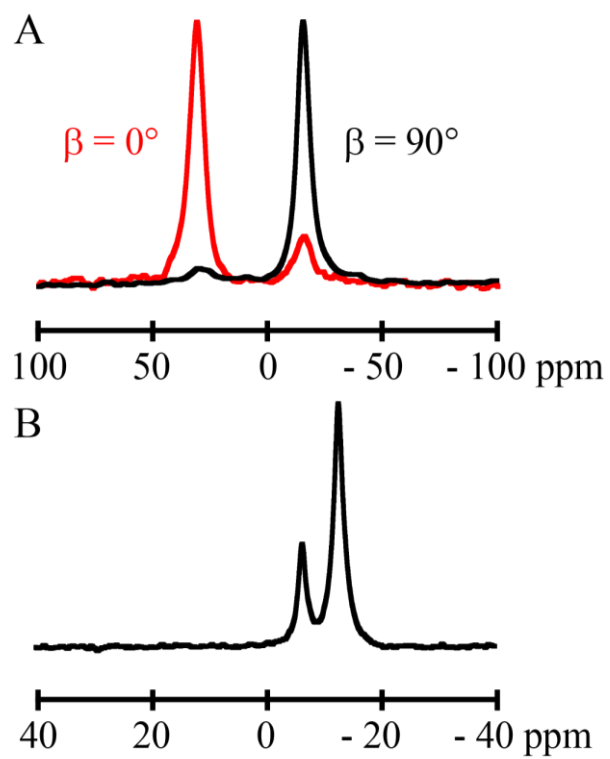


*FIGURE 3*  $^{31}\text{P}$ -NMR spectra for  $\text{GW}^{4,20}\text{ALP23}$  in (A) oriented DMPC bilayers and (B) DMPC/DHPC bicelles.

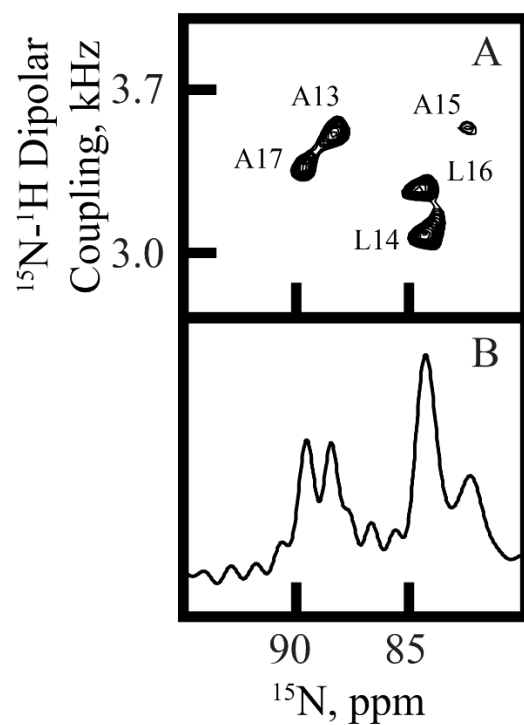


*FIGURE 4 Separated local field PISEMA spectra. A.  $^{15}\text{N}/^1\text{H}$  separated local field spectrum for  $\text{GW}^{4,20}\text{ALP23}$ . The sample is oriented in DMPC/DHPC bicelles and contains  $^{15}\text{N}$ -labeled residues 13-17 (assigned as depicted). B. 1D  $^{15}\text{N}$  NMR spectrum for  $\text{GW}^{4,20}\text{ALP23}$ .*

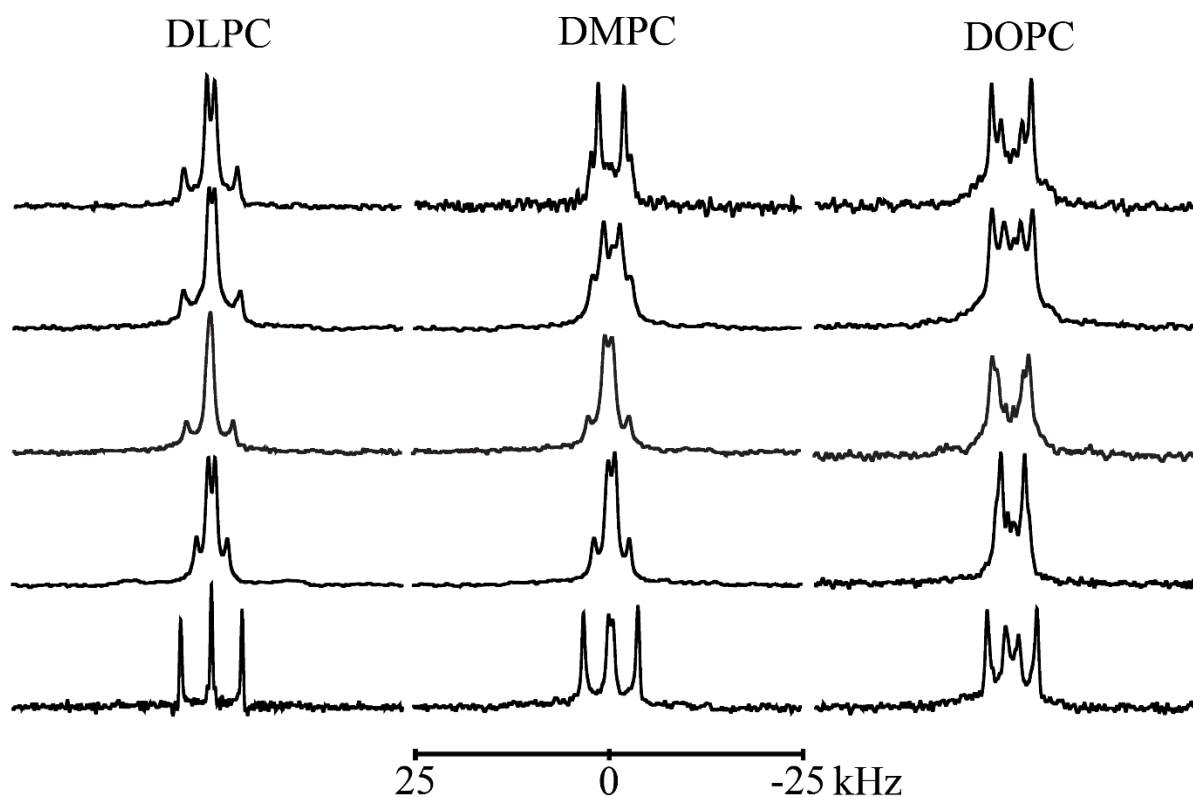
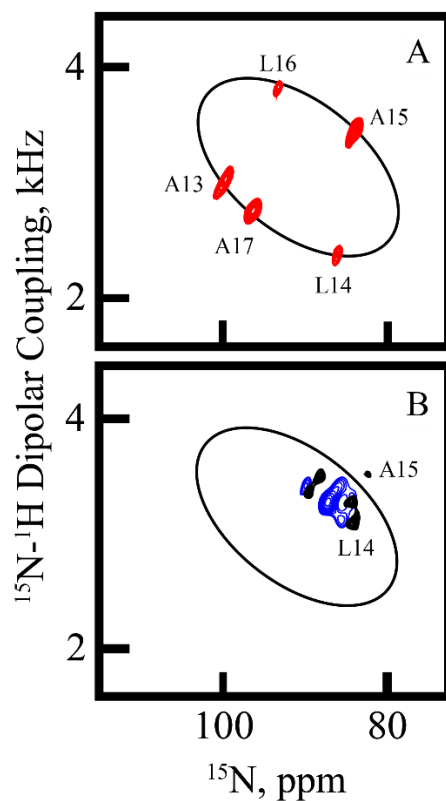


FIGURE 5 Deuterium quadrupolar splittings for  $GW^{4.20}ALP23$  in oriented DLPC, DMPC, and DOPC bilayers for samples oriented with  $\beta=90^\circ$ . The  $^2H$  labeled alanine identities are, from top to bottom, (5, 7); (9, 11); (13, 15); (17, 19); and (3, 21); with the first alanine of each pair 100% deuterated, and the second alanine 50% deuterated.





*FIGURE 6 Helix dynamics illustrated by separated local field PISEMA spectra. A. Data and PISA wheel for  $\text{GW}^{5,19}\text{ALP23}$ . B. The PISA wheel from A is repeated along with data showing full dynamic averaging for  $W^{2,22}W^{5,19}\text{ALP23}$  (blue contours) and for  $\text{GW}^{4,20}\text{ALP23}$  (black contours). Each sample is oriented in DMPC/DHPC bicelles and  $^{15}\text{N}$ -labeled in residues 13-17 (assigned as indicated). The spectra for  $\text{GW}^{5,19}\text{ALP23}$  and  $W^{2,22}W^{5,19}\text{ALP23}$  were recorded previously.(17, 18)*

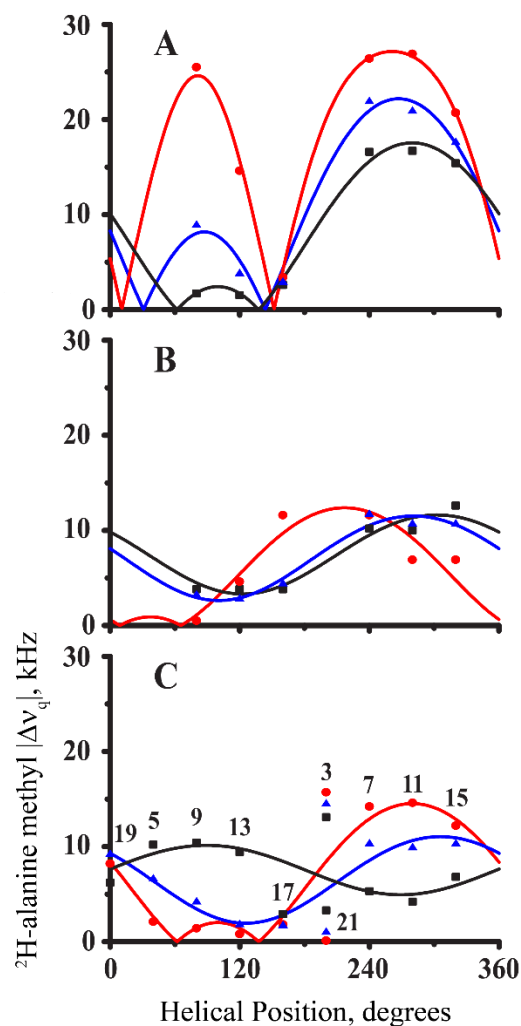
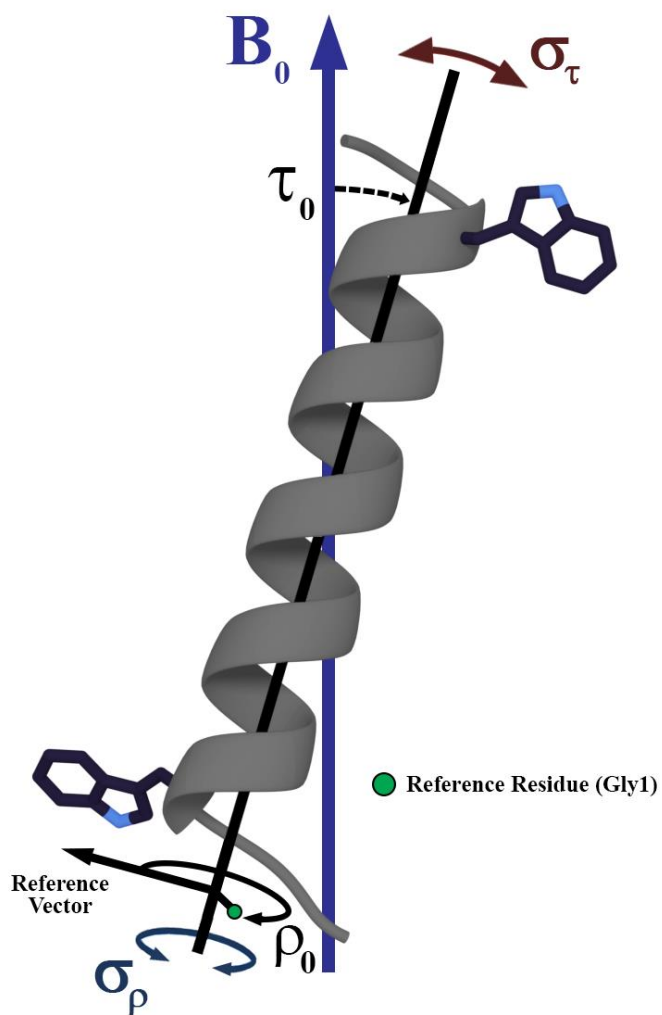


FIGURE 7 “Apparent” GALA quadrupolar wave plots for transmembrane peptide helices in DLPC (red circles), DMPC (blue triangles) or DOPC (black squares) oriented bilayer membranes: (A)  $GW^{5,19}ALP23$ , (B)  $Y^{4,5}GW^{19}ALP23$ , (C)  $GW^{4,20}ALP23$ . Panel C denotes the positions of the deuterium-labeled alanine residues. Only panel A reflects correctly the variation of the helix tilt  $\tau_0$  and the constant helix azimuthal rotation  $\rho_0$  in the different bilayers. The amplitudes and phases of the waves in panels B and C reflect excessive dynamic averaging of the  $^2H$  quadrupoles. See text for details. See also Table 4.



*FIGURE 8 Model to describe transmembrane peptide motions and dynamics with respect to the bilayer normal  $B_0$ . The apparent average helix tilt and rotation are denoted by  $\tau_0$  and  $\rho_0$  respectively and the oscillations about these orientations are shown as the helical "wobble" ( $\sigma_\tau$ ) and rotational "slippage" ( $\sigma_\rho$ ).*

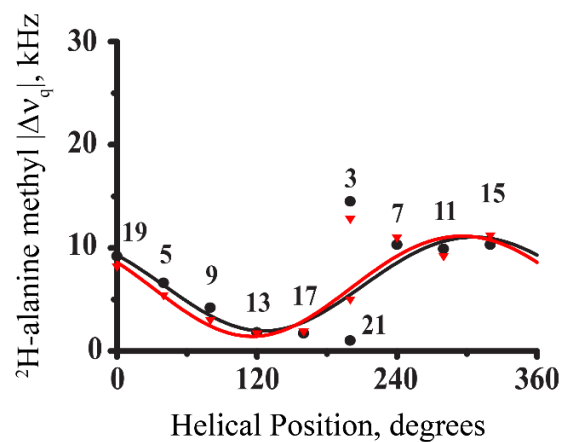


FIGURE 9 Comparison of the “apparent” GALA quadrupolar wave plots for  $\text{GW}^{4.20}\text{LP23}$  in DMPC oriented bilayers (black circles) and DMPC/DHPC bicelles (red triangles). Positions 3 and 21 were left out of both analyses.

## 2.10 Supporting Information

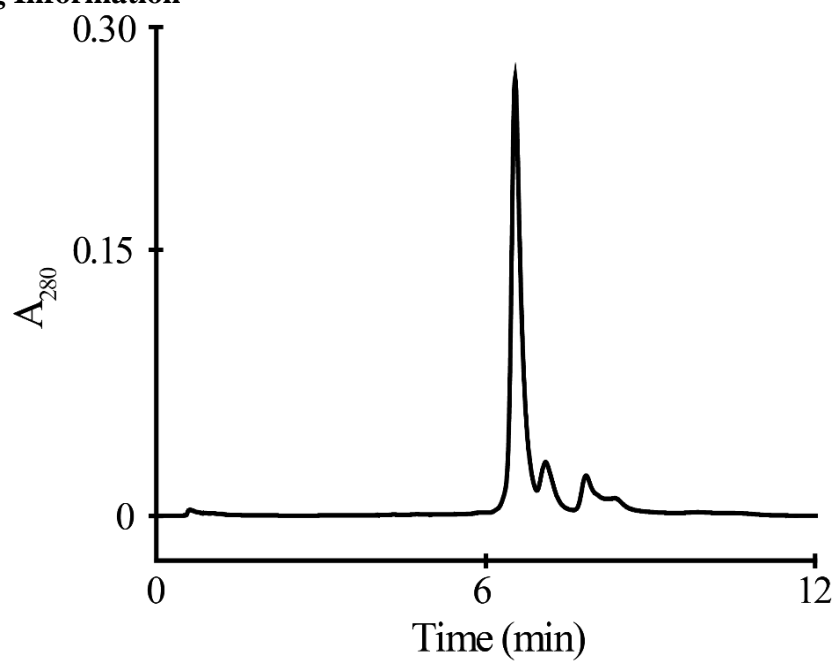
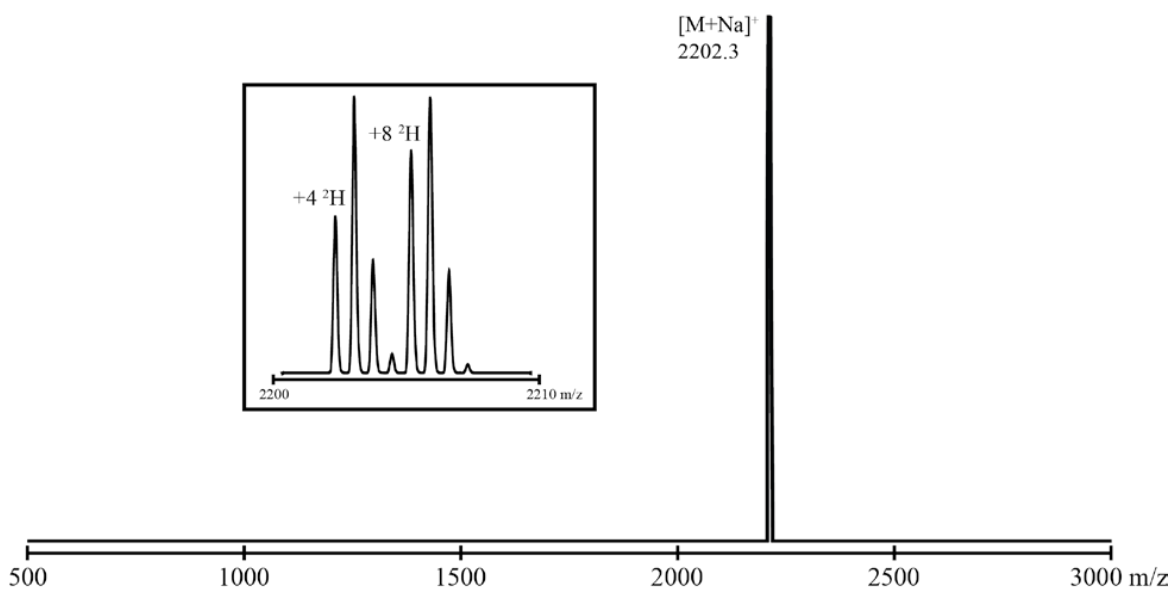
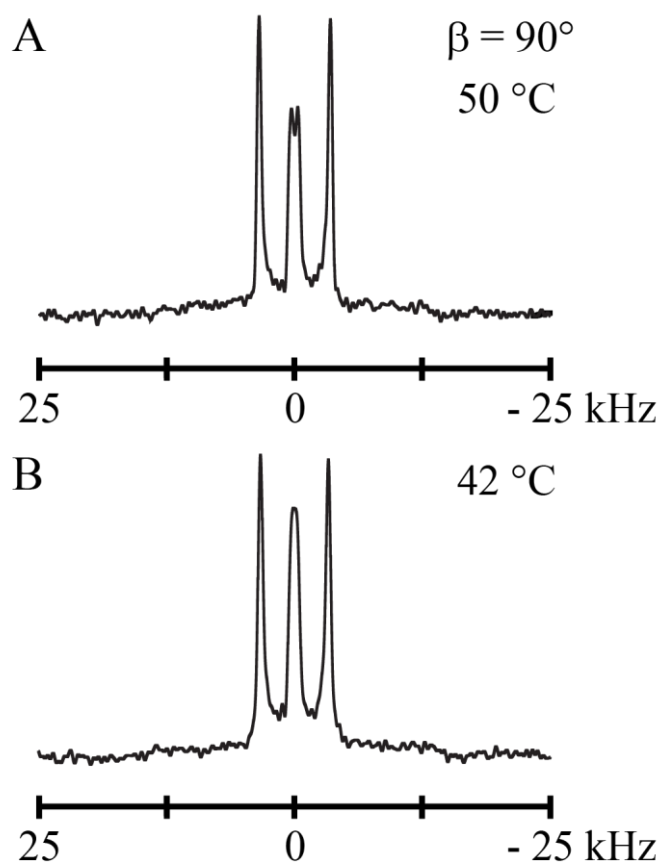


FIGURE S1 Reversed phase HPLC elution profile to confirm purification of  $GW^{4,20}ALP23$ .



*FIGURE S2 MALDI-TOF mass spectrum confirming the synthesis and purification of  $GW^{4,20}ALP23$ . The expected monoisotopic mass is 2176.6 daltons. The expected mass of the undeuterated peptide with  $Na^+$  is 1198 daltons. The observed mass is 2202.3 with  $Na^+$  and 4 deuterons, and 2206.3 with  $Na^+$  and 8 deuterons.*



*FIGURE S3. Deuterium ( $^2\text{H}$ ) NMR spectra for labeled  $\text{GW}^{4,20}\text{ALP23}$  in oriented DMPC bilayers at  $\beta=90^\circ$  measured at (A) 50 °C and (B) 42 °C.  $^2\text{H}$  labeled alanine positions are 3 and 21 and were labeled with 100% and 50% abundances respectively.*

GW<sup>4,20</sup>ALP23,  $\beta = 0^\circ$

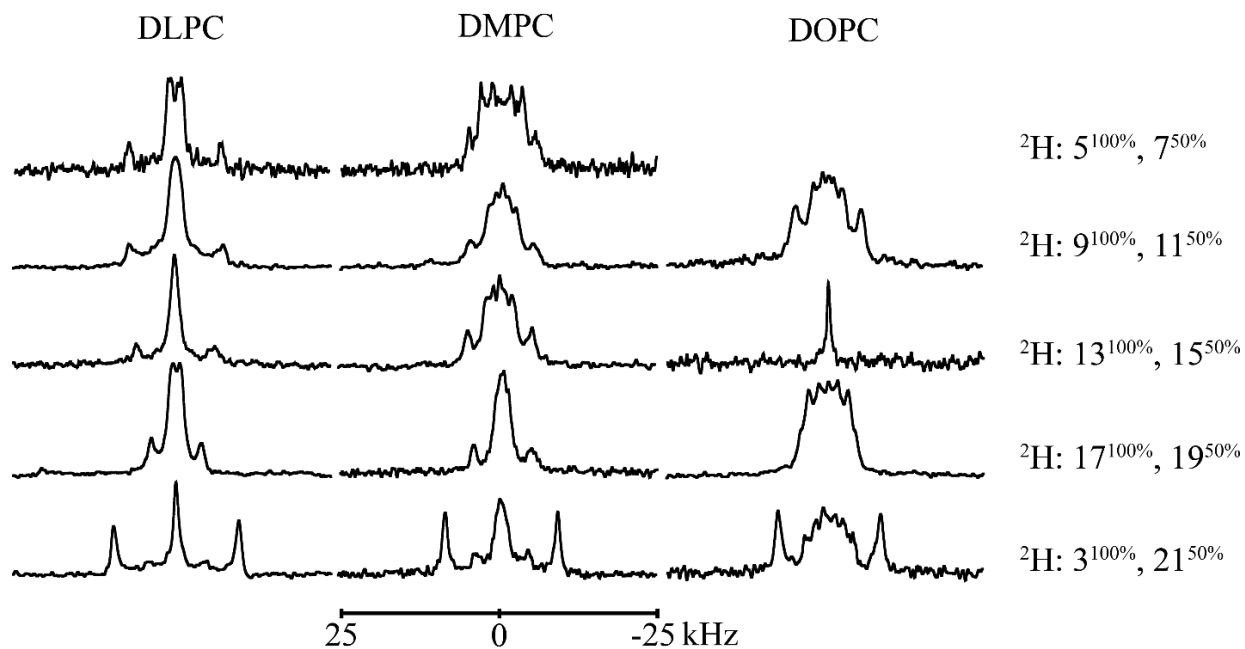


FIGURE S4 Deuterium (<sup>2</sup>H) NMR spectra for labeled GW<sup>4,20</sup>ALP23 in oriented DLPC, DMPC, and DOPC bilayers at  $\beta=0^\circ$  measured at 50 °C. <sup>2</sup>H labeled alanine positions are depicted on the right.



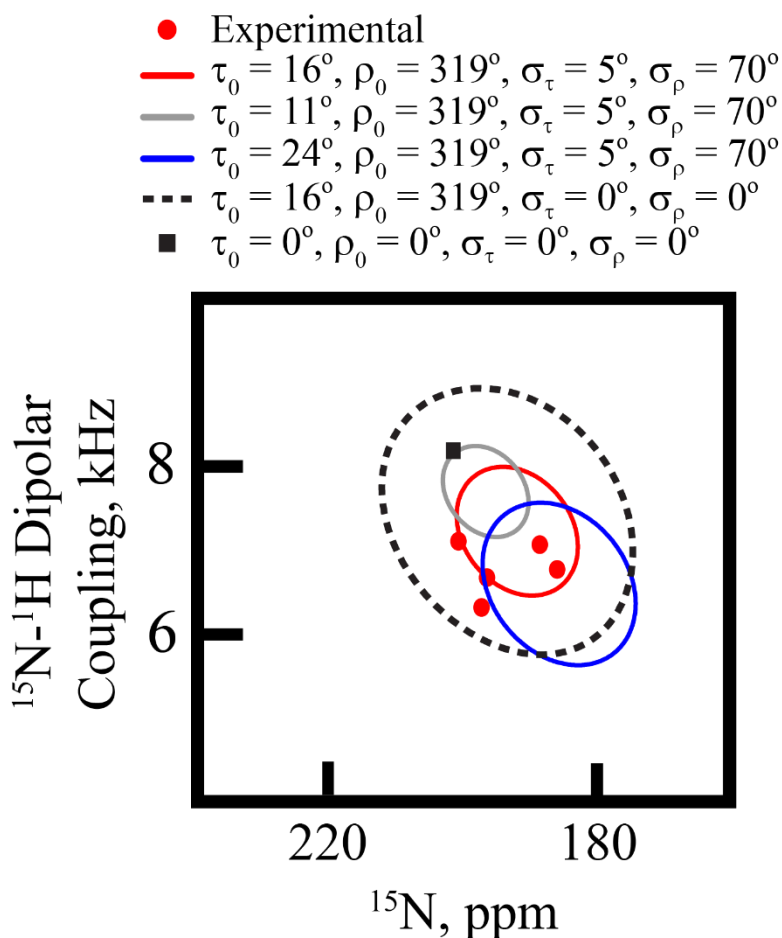


FIGURE S5 Illustration of PISA wheels (for sample orientation  $\beta = 0^\circ$ ) that fit and do not fit the data for GW<sup>4,20</sup>ALP23, labeled with  $^{15}\text{N}$  in residues 13-17, in oriented bicelles of DMPC/DHoPC (ether). The red PISA wheels are approximate fits to the red data points, with helix tilt values of  $15^\circ$ ,  $16^\circ$  and  $17^\circ$ ; and moderate motion represented by  $\sigma_\tau$  of  $5^\circ$  and  $\sigma_\rho$  of  $70^\circ$ . Larger or smaller values of the tilt angle (blue and gray wheels) do not fit the data. An ellipse with a correct tilt angle but no motional averaging ( - - - ) also does not fit. For a helix with zero tilt, the data points would collapse to the black square. Note that the red wheel sizes are much smaller and the motional averaging much more extensive than observed with GW<sup>5,19</sup>ALP23 (see figure 6 of the main article).

GW<sup>4,20</sup>ALP23, DMPC/DH(o)PC Bicelles

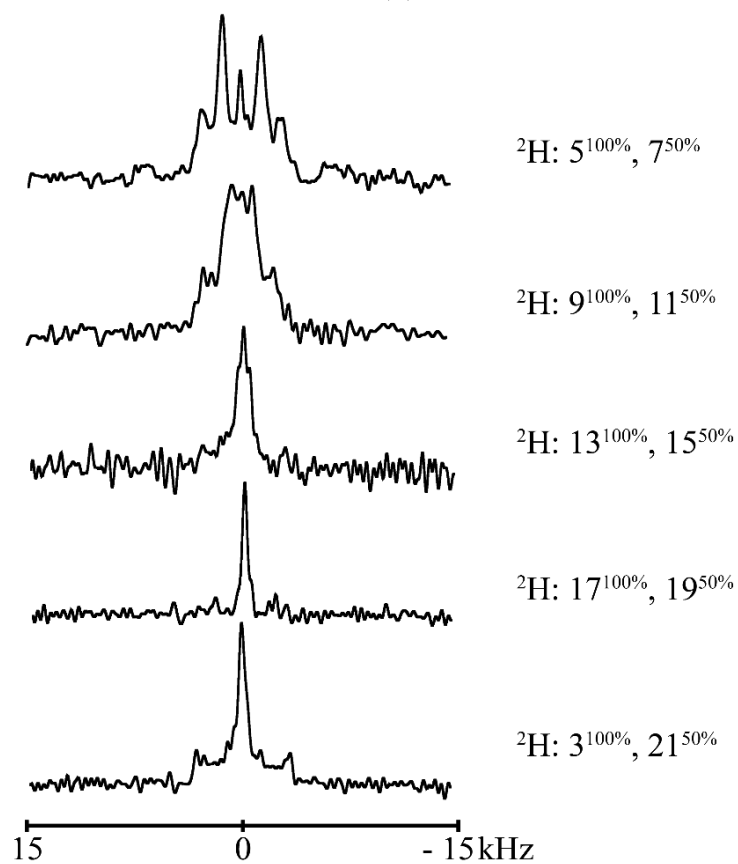


FIGURE S6 Deuterium (<sup>2</sup>H) NMR spectra for labeled GW<sup>4,20</sup>ALP23 in oriented DMPC/DHPC bicelles measured at 42 °C. <sup>2</sup>H labeled alanine positions are depicted on the right.

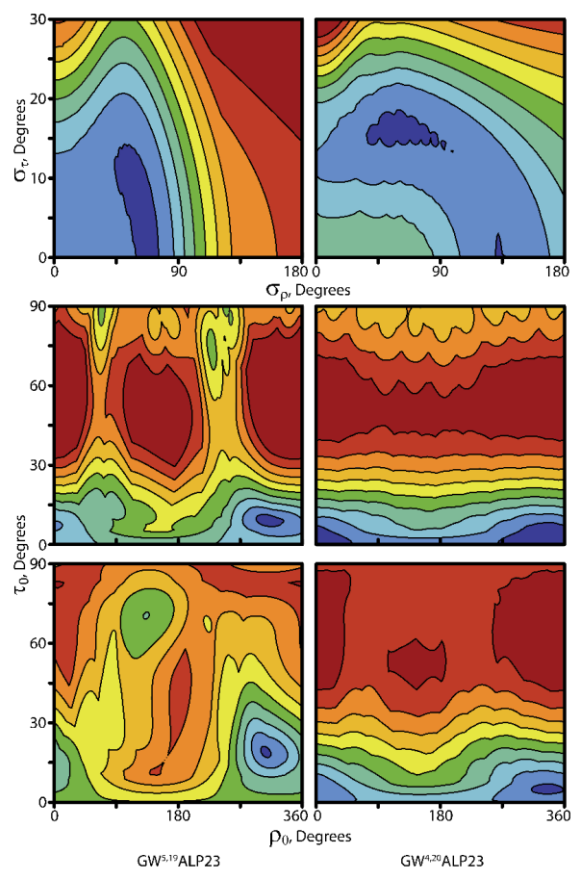


FIGURE S7. Rmsd contour plots for of GW<sup>5.19</sup>ALP23 and GW<sup>4.20</sup>ALP23 in DMPC/DHPC bicelles using <sup>15</sup>N + <sup>2</sup>H data combined (Gaussian analysis) or <sup>2</sup>H data alone (GALA analysis). Contour levels are drawn using 10 contours starting at 0 kHz (blue) to the highest value (red). (Top) Gaussian distributions of tilt  $\tau_0$  and rotation  $\rho_0$  (rmsd max left: 4.0 kHz; right: 3.9 kHz). (Middle) Average tilt and rotation from the GALA analysis (rmsd max left: 27.8.0 kHz; right: 25.6 kHz). (Bottom) Average tilt and rotation from the Gaussian analysis (rmsd max left: 9.0 kHz; right: 13.9 kHz).

## CHAPTER 3

### Breaking the Backbone: Central Arginine Residues Induce Membrane Exit and Helix Distortions Within a Dynamic Membrane Peptide

#### 3.1 Abstract

Transmembrane domains of membrane proteins sometimes contain conserved charged or ionizable residues which may be essential for protein function and regulation. This work examines the molecular interactions of single Arg residues within a highly dynamic transmembrane peptide helix. To this end, we have modified the GW<sup>4,20</sup>ALP23 (acetyl-GGAW<sup>4</sup>(AL)<sub>7</sub>AW<sup>20</sup>AGA-amide) model peptide framework to incorporate Arg residues near the center of the peptide. Peptide helix formation, orientation and dynamics were analyzed by means of solid-state NMR spectroscopy to monitor specific <sup>2</sup>H- or <sup>15</sup>N-labeled residues. GW<sup>4,20</sup>ALP23 itself adopts a tilted orientation within lipid bilayer membranes. Nevertheless, the GW<sup>4,20</sup>ALP23 helix exhibits moderate to high dynamic averaging of NMR observables, such as <sup>2</sup>H quadrupolar splittings or <sup>15</sup>N-<sup>1</sup>H dipolar couplings, due to competition between the interfacial Trp residues on opposing helix faces. Here we examine how the helix dynamics are impacted by the introduction of a single Arg residue at position 12 or 14. Residue R14 restricts the helix to low dynamic averaging and a well-defined tilt that varies inversely with the lipid bilayer thickness. To compensate for the dominance of R14, the competing Trp residues cause partial unwinding of the helix at the C-terminal. By contrast, R<sup>12</sup>GW<sup>4,20</sup>ALP23 exits the DOPC bilayer to an interfacial surface-bound location. Interestingly, multiple orientations are exhibited by a single residue, Ala-9. Quadrupolar splittings generated by <sup>2</sup>H-labeled residues A3, A5, A7 and A9 do not fit to the  $\alpha$ -helical quadrupolar wave plot defined by residues A11, A13, A15, A17, A19 and A21. The discontinuity at residue A9 implicates a helical swivel distortion and an

apparent  $3_{10}$ -helix involving the N-terminal residues preceding A11. These molecular features suggest that while arginine residues are prominent factors controlling transmembrane helix dynamics, the influence of interfacial tryptophan residues cannot be ignored.

### **3.2 Introduction**

Lipid-bilayer membranes define regions of high dielectric gradient. Indeed, by contrast with a lipid membrane surface, the nonpolar interior environment created by the acyl chains of a lipid bilayer is not readily hospitable for ionizable amino acid residues in membrane proteins.

Nevertheless, the transmembrane domains of proteins sometimes contain noteworthy polar or charged residues which may be conserved and essential for protein function and regulation of cellular activity. For example, arginine residues play major roles in membrane voltage sensing domains of voltage-gated ion channels.(1,2) The characteristic “snorkeling” effect that allows positively charged side chains of arginine or lysine residues to “reach” and interact with the lipid/membrane interface helps to keep the remaining nonpolar transmembrane domain within the hydrophobic membrane.(3,4) In this regard, mutations that introduce polar and charged residues within transmembrane domains may have disastrous consequences affecting protein structure, function, and stability.

Due to numerous experimental challenges with large membrane proteins, simplified model systems can be useful for understanding the physical chemistry of the lipid interactions of ionizable protein side chains. The membrane-spanning peptide GW<sup>5,19</sup>ALP23 (acetyl-GGALW<sup>5</sup>(LA)<sub>6</sub>LW<sup>19</sup>LAGA-amide)(5), for example, has been useful for defining the titration properties of membrane-imbedded ionizable Arg, Lys, His and Glu residues.(6-8) GW<sup>5,19</sup>ALP23 is advantageous because its robust helix adopts a well-defined orientation within lipid bilayers, wherein the helix tilt is dependent on membrane acyl chain length. Within this framework,

specific arginine substitutions introduce new and interesting interactions between the peptide helix and its lipid environment.(9) Arg at position 14, for example, changes the tilt, forces a large helix rotation and prefers to “snorkel,” moving its side chain guanidium group into the bilayer lipid head-group region. Molecular dynamics simulations additionally predict that the helix movement is accompanied by local membrane thinning.(9) By contrast, Arg placed at the dead-center of the GW<sup>5,19</sup>ALP23 helix, at position 12, causes the helix to adopt multiple states. In DOPC membranes, both coarse-grained molecular simulations and solid-state NMR experiments predict the presence of three major states.(9) Two states retain a transmembrane helix with the arginine side chain “snorkeling” either “up” or “down” toward the polar lipid head groups. The third state is entirely different, with the complete helix exiting the lipid bilayer to adopt an interfacial orientation, perpendicular to the membrane normal. Modest amounts of cholesterol, about 10 mol %, in the DOPC membrane force essentially the entire R<sup>12</sup>GW<sup>5,19</sup>ALP23 population into this interfacial state.(10) The multi-state features and membrane-exit property of R<sup>12</sup>GW<sup>5,19</sup>ALP23 are likely dictated by a Trp “cage” surrounding the R12 guanidium group, which effectively is trapped between the two aromatic side chains and restricted from favorable interactions with the bilayer head groups. Moving the Trp residues outward, to positions 3 and 21, increases the size of this cage and effectively frees the Arg side chain (at both positions 12 and 14) to permit a stable transmembrane orientation.(11) Recently, we developed a highly dynamic peptide framework by relocating the Trp residues of GW<sup>5,19</sup>ALP23 outward by only one sequence position on each side. With the Trp residues in positions 4 and 20, the large indole side chains then reside on opposite faces (Figure 1) of the  $\alpha$ -helix of acetyl-GGAW<sup>4</sup>(AL)<sub>7</sub>AW<sup>20</sup>AGA-amide.(12) The GW<sup>4,20</sup>ALP23 helix experiences moderate to high motional averaging of solid-state NMR observables such as <sup>2</sup>H quadrupolar

splittings,  $^1\text{H}$ - $^{15}\text{N}$  dipolar couplings and  $^{15}\text{N}$  chemical shifts. The excess dynamic averaging, much more than observed for GW<sup>5,19</sup>ALP23, is caused primarily by additional rotation about the helix axis. The observed azimuthal slippage attributed tentatively to a competition between the two Trp indole rings for preferential locations at the bilayer interface. An added benefit of the GW<sup>4,20</sup>ALP23 sequence (Table 1) is the availability of two additional Ala residues for deuterium labeling, such that more  $^2\text{H}$  are available for analysis of the  $\alpha$ -helical structural perturbations. We take advantage of these features to examine the influence of single arginine substitutions in GW<sup>4,20</sup>ALP23 (Table 1).

Here, we present the unique outcomes that results from introducing a central Arg residue into the dynamic GW<sup>4,20</sup>ALP23 framework at either position 12 or 14. Arginine at either position is situated on a different helix face from those of either Trp residue (Figures 1-2). Thus, neither R12 nor R14 in GW<sup>4,20</sup>ALP23 is likely to fall within a Trp “cage.” Nevertheless, the results will indicate that the R12 and R14 substitutions confer quite different modulations of the helix properties, with R12 not only driving the helix to the surface of DOPC membranes but also distorting the structure of the surface-bound helix.

### 3.3 Materials and Methods

Fmoc-amino acids with protected side chains were purchased from Novabiochem (San Diego, CA). The tryptophan and arginine side chains were protected with *t*-butoxycarbonyl and 2,2,4,6,7-pentamethyldihydrobenzofuran-5-sulfonyl protecting groups, respectively.

Commercial fmoc-L-alanine- $^{15}\text{N}$  and fmoc-L-leucine- $^{15}\text{N}$  were purchased from Cambridge Isotope Laboratories (Andover, MA). Commercial L-alanine- $d_4$  was also purchased from Cambridge Isotope Laboratories (Andover, MA) and was modified with an Fmoc group on a 100 mg scale as described.<sup>(13)</sup> Fmoc-L-alanine- $d_4$  was recrystallized from 20 mL ethyl

acetate:hexane 80:20 and successful synthesis was confirmed using  $^1\text{H}$  NMR. DLPC, DMPC, and DOPC lipids were purchased from Avanti Polar Lipids (Alabaster, Alabama). Other solvents and chemicals were the highest grade available.

### Peptide Synthesis

Peptides  $\text{R}^{12}\text{GW}^{4,20}\text{ALP23}$  and  $\text{R}^{14}\text{GW}^{4,20}\text{ALP23}$  (see Table 1) were synthesized on a 0.1 mmol scale using solid-phase FastMoc® chemistry(7) on a model 433A Applied Biosystems peptide synthesizer (Life Technologies, Foster City, CA). In most cases, two ala- $\text{d}_4$  residues were incorporated into each peptide in different isotopic abundances. In certain cases where spectral assignments remained ambiguous, a single  $^2\text{H}$ -labeled alanine residue was used instead.  $^{15}\text{N}$ -labeled peptides were also synthesized, containing two or three  $^{15}\text{N}$ -labeled Ala or Leu residues. The peptides were purified on a Zorbax 300SB-C3 column (9.4 x 250 mm, 5- $\mu\text{m}$  particle size; Agilent Technologies, Santa Clara, CA) with a gradient of 86-90% methanol (with 0.1% trifluoroacetic acid) over 11 min ( $\text{R}^{12}\text{GW}^{4,20}\text{ALP23}$ ) or 13 min ( $\text{R}^{14}\text{GW}^{4,20}\text{ALP23}$ ). Analytical HPLC and MALDI mass spectrometry were used to confirm peptide purity and identity (See Figure S1).

### Circular Dichroism Experiments

Circular dichroism (CD) spectroscopy samples were prepared to analyze peptide helicity by using a 1:60 peptide:lipid mixture (62.5 nmol peptide and 3.75  $\mu\text{mol}$  lipid). To create lipid vesicles, the samples were sonicated at 22  $^\circ\text{C}$ . The samples were analyzed using a Jasco (Easton, MD) J-1500 CD/Fluorescence spectropolarimeter with a 1 mm cell path, 1.0 nm bandwidth, 0.1 mm slit, and a scan speed of 20 nm/min, with averaging of 10 scans.

### $^2\text{H}$ Solid-State NMR Experiments



Mechanically aligned solid-state NMR samples were prepared as described previously(7) with a peptide/lipid ratio of 1:60 (1.33  $\mu\text{mol}$  /80  $\mu\text{mol}$ ) and 45% hydration (w/w) using deuterium-depleted water from Cambridge Isotope Laboratories (Andover, MA). Bilayer alignment was confirmed using  $^{31}\text{P}$  NMR on a Bruker (Billerica, MA) Avance 300 spectrometer with broadband  $^1\text{H}$  decoupling, with samples oriented at both  $\beta = 90^\circ$  (bilayer normal perpendicular to the magnetic field) and  $\beta = 0^\circ$  (see Figure S2). Solid-state  $^2\text{H}$  NMR experiments were performed with a solid quadrupolar echo pulse sequence at 50  $^\circ\text{C}$  using a Bruker Avance 300 spectrometer at both sample orientations. The pulse sequence included a pulse time of 3.0  $\mu\text{s}$ , an echo delay of 105  $\mu\text{s}$ , and a recycle delay of 120 ms. Each  $^2\text{H}$  NMR experiment acquired between 0.8 and 1.5 million scans.

#### $^{15}\text{N}$ - $^1\text{H}$ / $^{15}\text{N}$ Solid-State NMR Experiments

Static solid-state NMR samples were prepared as described previously(7) using glass slides with dimensions measuring 5.7 x 10 mm NO. 000 purchased from Matsunami Glass (Bellingham, WA) and glass cells with dimensions measuring 5.4 x 7.4 x 18 mm purchased from New Era Enterprises (Vineland, NJ). Samples contained 1.33  $\mu\text{mol}$  peptide and 80  $\mu\text{mol}$  lipid (1:60) and were hydrated to 45% (w/w) using deuterium depleted water.

SAMPI4 (14) separated local field spectra were recorded on a Bruker Avance NEO 600 MHz NMR spectrometer with Larmor frequencies of 600.13 and 60.81 MHz for  $^1\text{H}$  and  $^{15}\text{N}$ , respectively, using a low electrical field static 1H-X probe with a flat coil configuration(15) with 1600 scans, 32 t1 increments, and a recycle delay of 4.0 s at 50  $^\circ\text{C}$ . The t1 evolution was preceded by CP-MOIST cross-polarization(16) with a contact time of 810  $\mu\text{s}$ , during which the radio-frequency (RF) spin-lock amplitude of 50 kHz was applied for both  $^1\text{H}$  and  $^{15}\text{N}$  channels. The SPINAL-64(17) decoupling sequence with the  $^1\text{H}$  RF amplitude of 62.5 kHz was applied for

$^1\text{H}$  heteronuclear decoupling during the 15 ms acquisition time.(17) The  $^1\text{H}$  carrier frequency of 9 ppm was used and is optimal for transmembrane helices in oriented bilayers. The  $^{15}\text{N}$  NMR data were processed and displayed using NMRPipe/NMRDraw(18) and Sparky(19) and adjusted using the theoretical dipolar coupling scaling factor for SAMPI4 evolution.(14) The chemical shifts were externally referenced to  $^{15}\text{N}$ -labeled solid ammonium sulfate, set to 26.8 ppm, corresponding to the signal from liquid ammonia at 0 ppm.(20)

### Data Analysis

Analysis of the  $^2\text{H}$  NMR spectra was performed using the semi-static geometric analysis of labeled alanines (GALA) as described previously by van der Wel *et al* 2002.(21) The deuterium quadrupolar splittings of the alanine methyl groups ( $\Delta\nu_q$ ) are dependent on the macroscopic sample orientation as seen in eq 1 below.

$$\Delta\nu_q = \text{QCC} \times S_{zz} \times \left[ \frac{1}{2}(3\cos^2\theta - 1) \right] \times \left[ \frac{1}{2}(3\cos^2\beta - 1) \right] \times \left\langle \frac{1}{2}(3\cos^2\gamma - 1) \right\rangle \quad (1)$$

Known constants within this equation include the angle between the membrane normal and the applied magnetic field ( $\beta$ ) =  $90^\circ$  or  $0^\circ$ , the quadrupolar coupling constant for an aliphatic C-D bond (QCC) = 168 kHz, and the tetrahedral bond angle of the  $\text{CD}_3$  group ( $\gamma$ ) =  $109.5^\circ$  which results in a 1/3 reduction of the coupling constant due to the fast rotation of the methyl group. This leaves the principal order parameter  $S_{zz}$ , which serves as an estimate for peptide motion, and  $\theta$ , the angle between the magnetic field and the  $\text{C}_\alpha\text{-C}_\beta$  bond of the alanine side chain, as variables. The  $\theta$  angle, in turn, is dependent on the average peptide orientation as seen in eq 2 below.

$$\theta = \varepsilon_{\parallel} [\cos \tau_0 - \sin \tau_0 \times \cos (\rho_0 + \varepsilon_{\perp} + \varphi) \times \tan \varepsilon_{\parallel}] \quad (2)$$

The angles defining the local side chain orientation with respect to the  $\text{C}_\alpha\text{-C}_\beta$  bond ( $\varepsilon_{\parallel}$ ) and a plane perpendicular to the helix direction ( $\varepsilon_{\perp}$ ) are fixed to  $59.4^\circ$  and  $-43.3^\circ$  respectively, as

determined previously.(21) The angle  $\varphi$  is the angle between a reference point (here  $C_\alpha$  of Gly1)(21) and  $C_\alpha$  of the deuterium labeled residue in the peptide.

The GALA method, therefore, considers an  $\alpha$ -helical geometry and three adjustable parameters: the apparent tilt  $\tau_0$  of the helix axis with respect to the bilayer normal, the helix azimuthal rotation  $\rho_0$  and the order parameter  $S_{zz}$  (eq1 and eq 2).(21) The GALA calculation finds the lowest RMSD fit between the experimental  $\Delta\nu_q$ 's and those calculated for the peptide helix as it samples available orientations with respect to the bilayer normal and the reference point for  $\varphi$ . Deviations from  $\alpha$ -helical geometry result in either a uniformly high global RMSD or individual data points deviating from the GALA quadrupolar wave.(8) For our analysis, we searched ranges of  $\tau_0$  (0 - 90°) and  $\rho_0$  (0 - 359°), each incremented by steps of 1°, and  $S_{zz}$  (0 - 1.0) by steps of 0.1.

To modify the GALA calculation to match the  $^2\text{H}$  NMR data to a  $3_{10}$ -helix instead of an  $\alpha$ -helix, the calculation for the angle  $\varphi$  was changed by modifying  $\eta$ , the helical wheel separation between the residue in question ( $n$ ) and the previous residue ( $n - 1$ ) in equation 3 below. For a canonical  $\alpha$ -helix  $\eta = 100^\circ$ , and for a canonical  $3_{10}$ -helix  $\eta = 120^\circ$ .

$$\varphi = (n - 1) \times \eta + 360 \quad (3)$$

A canonical  $3_{10}$ -helix with  $\eta = 120^\circ$  would result in every third Ala residue generating, predictably, the same  $^2\text{H}$ -methyl quadrupolar splitting, which was not observed in this study. The value of  $\eta = 120^\circ$  also is unreasonable because of side chain repulsion between residue  $n$  and residue  $(n+3)$ . Instead, average  $3_{10}$ -helix torsion angles ( $-71^\circ$ ,  $-18^\circ$  for  $\phi$ ,  $\psi$ ) found in nature were used resulting in  $\eta = 112.5^\circ$ .(22) This value of  $\eta$  also results in  $\varepsilon_{||}$  of  $61^\circ$  and  $\varepsilon_{\perp}$  of  $-38^\circ$  required for equation 2 above. The angles  $\varepsilon_{||}$  and  $\varepsilon_{\perp}$  were calculated using a combination of UCSF Chimera and Blender (open-source 3D graphics software).(23-24)

The availability of eight core alanine residues in GW<sup>4,20</sup>ALP23 is especially useful when studying peptides that exhibit increased dynamic motion.(12,25) The large data pool allows for a more demanding Gaussian analysis to be utilized over <sup>2</sup>H quadrupolar splittings individually or combined with <sup>15</sup>N chemical shifts and <sup>15</sup>N/<sup>1</sup>H dipolar couplings, as derived from model 6 of Strandberg et al, 2009.(26) This model of helix dynamics considers a Gaussian distribution of helix tilt  $\tau$  and rotation  $\rho$  angles centered at the angles  $\tau_0$  and  $\rho_0$  with widths as the oscillations about them,  $\sigma_\tau$  (helix wobble) and  $\sigma_\rho$  (rotational slippage) respectively. The calculation performs a grid search over the variables  $\tau_0$ ,  $\rho_0$  and their standard deviations  $\sigma_\tau$  and  $\sigma_\rho$ , while fixing a principal order parameter  $S_{zz}$  to either 1.0 (no isotropic motion) or 0.88 as an estimate for the isotropic internal motion of a transmembrane peptide, or another value. Our analysis was performed by varying, in 1° increments,  $\tau_0$  from 0° to 90°,  $\rho_0$  from 0° to 359°,  $\sigma_\tau$  from 0° to 30° and  $\sigma_\rho$  from 0° to 200°. In cases of a limited availability of data points, a modified Gaussian calculation was used instead by restraining  $\sigma_\tau$  to a small finite value and varying the remaining three parameters as above. The in-house program estimates the helical geometry based on a polyalanine  $\alpha$ -helix model. Modifying the torsion angles within the model allows the data to be fit to a tighter 3<sub>10</sub>-helix. The  $\alpha$ -helix torsion angles for  $\phi$  and  $\psi$  (-64° and -40°)(27) were modified to -71° and -18°, respectively, to represent a 3<sub>10</sub>-helix, based on the mean torsion angles found within naturally occurring 3<sub>10</sub>-helices.(22)

In cases of helix distortion, the peptide kink angle ( $\kappa$ ) can be calculated using equation 4 below with the rotation ( $\rho$ ) and tilt ( $\tau$ ) relative to either the C-terminal or N-terminal segment of the peptide helix.(28)

$$\cos \kappa = \sin(\tau_N) \sin(\tau_C) \cos(\Delta\rho) + \cos(\tau_N) \cos(\tau_C) \quad (4)$$

### 3.4 Results

The parent peptide helix of GW<sup>4,20</sup>ALP23 exhibits extensive dynamic averaging in lipid-bilayer membranes.(12) The present experiments reveal the influence of introducing a single charged Arg residue into this highly dynamic helical framework at position 14 or position 12 of the 23-residue sequence.

#### R<sup>14</sup>GW<sup>4,20</sup>ALP23

Solid-state NMR techniques have proven useful for determining the extent of a transmembrane peptide's helicity(29) and furthermore the helix average orientation and dynamics within its lipid environment. A key result is that the presence of R14 lowers dramatically the extent of motional averaging. The reduced motion is evident from the wide range of <sup>2</sup>H quadrupolar splittings, from 1 kHz to 33 kHz, observed for the collection of Ala methyl side chains in R<sup>14</sup>GW<sup>4,20</sup>ALP23 (Figure 3, Figure S3, Table 2), compared to the narrow range of 1 kHz to 16 kHz when R14 is absent in GW<sup>4,20</sup>ALP23.(12) For reference, a moderately dynamic peptide such as GW<sup>5,19</sup>ALP23 produces core alanine <sup>2</sup>H quadrupolar splittings that span a range of about 1 kHz to 27 kHz.(30) Therefore, the presence of R14 indeed decreases the high extent of motional averaging of the <sup>2</sup>H NMR signals from the host peptide helix.

The helix orientations can be compared using the semi-static GALA method to analyze the patterns of alanine methyl <sup>2</sup>H quadrupolar splittings.(21) Indeed, the GALA quadrupolar wave-plots (Figure 4A) reveal a rather constant helix azimuthal rotation  $\rho_0$  of  $\sim 224^\circ$  (Table 3) for R<sup>14</sup>GW<sup>4,20</sup>ALP23 in DLPC, DMPC and DOPC bilayer membranes. An essentially constant preferred value of  $\rho_0$ , independent of the bilayer thickness, is indicative and even diagnostic of low dynamic averaging.(30-31) Hand in hand with the low dynamic averaging, the tilt  $\tau_0$  of the R<sup>14</sup>GW<sup>4,20</sup>ALP23 helix decreases systematically as the lipid bilayer thickness increases ( $\tau_0$  being

21°, 17°, 14° in DLPC, DMPC, DOPC; respectively). This behavior contrasts sharply with that of GW<sup>4,20</sup>ALP23, which shows extensive variation for  $\rho_0$  and no correlation for  $\tau_0$  with the lipid environment (Figure 4C). The arginine residue R14 has served to stabilize the membrane-incorporated helix in a preferred orientation.

The quadrupolar wave plots for R<sup>14</sup>GW<sup>4,20</sup>ALP23 are nicely similar to those of R<sup>14</sup>GW<sup>5,19</sup>ALP23, illustrating similar helix tilt angles and a difference of only 25° in the azimuthal rotation  $\rho_0$  about the helix axis (Figure 4 A,B). While it is apparent that the location of the Arg residue dominates the tilt in both peptides, the small difference in rotation is due to differences in the locations of the interfacial tryptophans, W<sup>4,20</sup> as opposed to W<sup>5,19</sup>.

Interestingly, residues A19 and A21 of R<sup>14</sup>GW<sup>4,20</sup>ALP23 fall off their respective curves for the core helix in all three lipids, whereas A3 fits in all three cases (Figure 4A). These features imply more extensive fraying of the helix at the C-terminal as opposed to the N-terminal.(8, 32) The circular dichroism spectra (Figure 5A) show a difference in the peptide's  $\epsilon_{222}$  to  $\epsilon_{208}$  ratio in DOPC and DMPC vesicles compared to DLPC and TFE (0.71 vs 0.8), which may be due to small changes in helix backbone structure or differing side-chain torsion angles for the indole rings.(33)

A Gaussian analysis of the <sup>2</sup>H quadrupolar splittings(26, 31, 34) provides further insight into the dynamics of the R<sup>14</sup>GW<sup>4,20</sup>ALP23 helix, in particular the lowering of the rotational slippage about the helix axis ( $\sigma_\rho$ ). As seen in Table 3, with R14 present,  $\sigma_\rho$  drops from a large value to less than 25° in all three lipids. These values are not only significantly less than those of GW<sup>4,20</sup>ALP23, but are also lower than those observed for the parent GW<sup>5,19</sup>ALP23 helix. Indeed, a single arginine residue generally dictates a preferred helix rotation  $\rho_0$  and lowers the width of the distribution  $\sigma_\rho$  about  $\rho_0$ .(25) The strikingly low extent of rotational slippage

exhibited by R<sup>14</sup>GW<sup>4,20</sup>ALP23 implies that the mere presence of R14 is enough to restrict the host peptide helix to minimal amounts of motional averaging.

### R<sup>12</sup>GW<sup>4,20</sup>ALP23

In the framework of GW<sup>5,19</sup>ALP23, an introduction of R12 leads to multiple states for the helix.<sup>(9)</sup> In similar fashion, in the framework of GW<sup>4,20</sup>ALP23, at least one residue, A9, exhibits two states (Figure 6; see also Figure S4). Do the two different quadrupolar splittings of 11.4 kHz and 27.4 kHz (Table 2) for residue A9 in R<sup>12</sup>GW<sup>4,20</sup>ALP23 reflect global changes for the entire molecule or local structural plasticity near residue A9? We note in this case that local variations are more likely because only residue A9, and possibly A11, exhibits multiple <sup>2</sup>H NMR peaks (Figure 6). (Only one state can easily be resolved for A11; see discussion.) This contrasts with the behavior of R<sup>12</sup>GW<sup>5,19</sup>ALP23 which shows three states for the global helix in DOPC and generates multiple <sup>2</sup>H NMR peaks for every Ala residue.<sup>(9)</sup> The range of observed <sup>2</sup>H-Ala quadrupolar splittings (0.5 to 37 kHz; see Table 2) also is higher for R<sup>12</sup>GW<sup>4,20</sup>ALP23 than for R<sup>12</sup>GW<sup>5,19</sup>ALP23.

To fit describe the orientation of the R<sup>12</sup>GW<sup>4,20</sup>ALP23 helix, a GALA or Gaussian fit (Table 4) describes a surface-bound  $\alpha$ -helix for the C-terminal of the core sequence from residue A9(a) through A19. This  $\alpha$ -helical segment is oriented with  $\tau_0$  of about 86° with respect to the bilayer normal, rotated such that  $\rho_0 = 33^\circ$ , and fits with an RMSD of 1.25 kHz (Table 4) on the surface of a DOPC bilayer. Notably, the alternate configuration for alanine-9 (spectrally indicated by the <sup>2</sup>H NMR  $|\Delta v_q|$  for A9(b); Figure 6 and Table 2) and the sole configurations for alanines 3, 5, and 7 do not fit the  $\alpha$ -helix defined by the C-terminal segment (Figure 7A). Instead, the N-terminal segment fits a suitably analyzed <sub>310</sub>-helix on the DOPC membrane surface.

While uncommon in typical transmembrane domains, the arginine rich voltage sensing domains of channel proteins are sometimes observed to contain  $3_{10}$ -helix motifs;(35-37) see Discussion. Modifying the GALA and Gaussian calculations to fit the N-terminal portion of the peptide to a tighter  $3_{10}$ -helix yields interesting results that provide further insight. The canonical Pauling  $3_{10}$ -helix with exactly 3.0 residues/turn(38) would not fit the experimental data, since every third residue would occupy the same position on a helical wheel and would therefore generate the same  $^2\text{H}$  quadrupolar splitting, which is not the case here. In line with our observations, nevertheless, the average helical wheel residue separation in  $3_{10}$ -helices observed in nature is not  $120^\circ$  but rather is roughly  $112.5^\circ$ , which corresponds to about 3.2 residues/turn. We therefore used values of  $112^\circ$ - $114^\circ$  for the radial separation to model the solid-state NMR data for the N-terminal as a  $3_{10}$ -helix.(22, 39) When applied to the  $^2\text{H}$  quadrupolar splittings (Table 2), or in combination with the  $^{15}\text{N}$  data (see below), the best Gaussian and GALA fits predict a surface bound N-terminal  $3_{10}$ -helical segment with  $112.5^\circ$  as the average residue radial separation, oriented with  $\tau_0$  of  $85^\circ$ - $88^\circ$ ,  $\rho_0$  around  $350^\circ$  and RMSD values between 0.5 and 0.9 kHz (Table 4). These N-terminal average tilt angles above  $85^\circ$  calculated for the tighter  $3_{10}$ -helix are strikingly similar to the predicted surface orientation of the C-terminal  $\alpha$ -helix. The discontinuity at residue A9, nevertheless, indicates an unwinding denoted by the  $30^\circ$ - $40^\circ$  difference in azimuthal rotation about the axes of the  $\alpha$ - and  $3_{10}$ -helices (Table 4; Figure 7). Notably, the  $^2\text{H}$  NMR observables can only fit the C-terminal residues to an  $\alpha$ -helix and the N-terminal residues to a tighter helix such as a  $3_{10}$ -helix. For the N-terminal  $^2\text{H}$  data, a modified Gaussian calculation(29) was incorporated in order to obtain an estimate of the dynamics if fitted to a  $3_{10}$ -helix. In this case, both  $\sigma\rho$  and  $\sigma\tau$  would be moderate (table 4). Therefore, a tighter



helix, such as a  $3_{10}$ -helix, with likely varying torsion angles,(22, 39) is a probable structure for the N-terminal portion of R<sup>12</sup>GW<sup>4,20</sup>ALP23 on the DOPC membrane surface.

The <sup>15</sup>N NMR spectra also indicate the surface orientation and the discontinuity at residue A9 for the R<sup>12</sup>GW<sup>4,20</sup>ALP23 helix. The <sup>2</sup>H and <sup>15</sup>N solid-state NMR experiments therefore agree. For example, the spectra obtained from the SAMPI4 experiments (Figure 8) have <sup>15</sup>N chemical shifts between 95 and 70 ppm as well as dipolar couplings between 4 and 6 kHz, which indicate a surface bound orientation,(40) perpendicular to the membrane normal, in contrast to the spectrum for a transmembrane helix (figure 8A). Residue A9 once again shows resonance doubling. Furthermore, the dipolar wave plot depicted in figure 9 shows a discontinuity in frequency and amplitude of the dipolar wave at residue A9, as the patterns N-terminal and C-terminal to residue A9 are distinctly different, with a much larger amplitude for the wave C-terminal to alanine 9.

Supporting the <sup>15</sup>N dipolar wave, the expanded region of the two-dimensional SAMPI4 spectrum (Figure 8B) shows separate elliptical patterns for the C-terminal and N-terminal segments. The <sup>15</sup>N polarity index slant angle (“PISA”) pattern in Figure 8B predicts a tilt  $\tau_0$  of 89° and a  $\rho_0$  of 42° for the C-terminal residues (Table 4), in agreement with the <sup>2</sup>H NMR data. The small difference of 10° in the estimate for  $\rho_0$  (Table 4) is likely due to the lower sensitivity of the SAMPI4 experiment, compared to the <sup>2</sup>H experiment, to the helix azimuthal rotation. Once again, the <sup>15</sup>N chemical shift range for the N-terminal residues indicates a surface-bound orientation for this portion of the helix (Figure 8).(41-42)

Gaussian analyses reported in table 4 indicate that the <sup>15</sup>N NMR observables “could” fit the N- and C-terminal segments, with different  $\rho_0$  values, to  $\alpha$ -helical or  $3_{10}$ -helical segments on the DOPC membrane surface. The ambiguity for the <sup>15</sup>N experiment is expected due to the similar

locations of 90° tilted peptide  $3_{10}$ -helix and  $\alpha$ -helix PISA wheels.(39) Nevertheless, the  $^2\text{H}$  quadrupolar splittings can fit the C-terminal residues only to an  $\alpha$ -helix, and the N-terminal residues only to a  $3_{10}$ -helix (see above). Additionally, only a  $3_{10}$ -helix fits the  $^{15}\text{N}$  data for the N-terminal if the extent of rotational slippage ( $\sigma\rho$ ) is moderate ( $\sigma\rho$  of 39 - 44°) instead of very high. A hypothetically higher  $\sigma\rho$  would in turn lead to more signal averaging and “would” make feasible an N-terminal  $\alpha$ -helix, with similar PISA wheel size as the blue wheel in figure 8B. Altogether, nevertheless, the  $^{15}\text{N}$  and  $^2\text{H}$  NMR observables agree concerning the surface location for R<sup>12</sup>GW<sup>4,20</sup>ALP23, the rotational discontinuity of 30°-40° at residue A9, the C-terminal  $\alpha$ -helix motif and the N-terminal  $3_{10}$ -helix motif (Table 4).

### 3.5 Discussion

Arginine dominates the GWALP23 peptide helix dynamics and behavior in a manner dependent on its location within the sequence relative to those of the juxta-terminal interfacial Trp residues. In the original GW<sup>5,19</sup>ALP23 peptide, the presence of R14 on the opposite face of the helix from that occupied by the two Trp residues (Figure 2) allows the peptide to remain transmembrane in bilayers of DOPC, yet with a 10° increase in tilt and 80° change in helix azimuthal rotation.(9) By contrast, R12, more centrally located and effectively “trapped” within a Trp “cage” defined by W5 and W19, leads to multiple states for the helix, including two competing transmembrane orientations and one at the surface of DOPC bilayers.(9) The multi-state behavior can be “rescued” by moving the tryptophans outward to positions 3 and 21.(11) In the context of W3 and W21, arginine R12 as well as R14 can be accommodated in a suitably tilted transmembrane helix.(11) Toleration of R12 with W3 and W21 as opposed to W5 and W19 has been attributed to the guanidium group occupying a different helix face and no longer needing to compete with the Trp residues for favorable interactions at the interface. Interestingly, R14 also is

accommodated with W3 and W21, perhaps because the Trp “cage” is effectively larger than that defined by W5 and W19.

For the present investigation, the structural context for W4 and W20 on the helix framework is entirely different. From this perspective, neither position 12 nor position 14 is located on a helix face containing a Trp residue. Therefore, while the two former cases (W<sup>5,19</sup> and W<sup>3,21</sup>) have addressed primarily the possibility that Trp could restrict water access to a central Arg side chain, the W<sup>4,20</sup> sequence removes this side chain competition and introduces instead a new factor, high dynamic motion for the parent helix when no arginine is present. Indeed, the helix of GW<sup>4,20</sup>ALP23 undergoes extensive motional averaging in the form of rotational slippage about the helix axis in order to compensate for apparently competing radial locations of the Trp residues and a rotation-dependent hydrophobic mismatch.<sup>(12)</sup> The inclusion of Arg at either position 12 or 14 within this sequence severely limits the excessive dynamic averaging and in each case leads to helix structural distortions, previously unobserved in the former GW<sup>5,19</sup>ALP23 framework.

Importantly, the Arg side chain carries a positive charge under all conditions.<sup>(10, 43)</sup> The finding is verified by numerous experimental and computational results.<sup>(10, 44-47)</sup> Indeed, the solution pK<sub>a</sub> for Arg has been revised upward to a value of 13.8,<sup>(43)</sup> and recent experiments showed that R<sup>14</sup>GW<sup>5,19</sup>ALP23 remains fully charged up to pH 13 within an ether-linked lipid environment.<sup>(10)</sup> Helix translocation, side chain snorkeling and membrane deformation can also serve to stabilize the positive charge, allowing the Arg side chain to engage in favorable interactions at the membrane interface.<sup>(9, 48-49)</sup>

Influence of R14. The unmodified GW<sup>5,19</sup>ALP23 helix already displayed a transmembrane orientation with low levels of dynamic averaging.(31) Incorporating R14 resulted in a 10° increase in tilt, 80° change in helix rotation and mean helix displacement/membrane thinning (observed via coarse grain simulations)(9) that allow the Arg to snorkel and access the membrane interface. The transmembrane orientations for the helices with W<sup>5,19</sup> and W<sup>4,20</sup> are similar, with low dynamic averaging for each, when R14 is present. The respective helix tilt angles differ by about 9° in DLPC and DMPC (Table 3) but by only about 3° in DOPC. The helix azimuthal rotation differs modestly by 25-36° when the Trp sequence context is changed with R14 present (see Table 3, Figure 4). The arginine residue R14 is therefore the primary determinant of the helix tilt and azimuthal rotation, but the interfacial Trp residues – whether W5 and W19, or W4 and W20 – exert secondary influence for fine tuning of the helix tilt and rotation. Residue R14 also lowers the extent of dynamic averaging, dramatically for the highly dynamic GW<sup>4,20</sup>ALP23 helix, and much more modestly for the already low-averaging GW<sup>5,19</sup>ALP23 helix.(25) The rotational slippage in the form of  $\sigma\rho$  for both helices with R14 is remarkably low in all three lipids (< 25°, Table 3), indeed lower than for GW<sup>5,19</sup>ALP23 with arginine absent. Therefore, the single arginine residue governs the overall properties of these transmembrane helices, with the small differences in the tilt and rotation due to the locations of the juxta-terminal Trp residues.

The dominance of arginine R14 over the peptide dynamics would also explain the helix unwinding observed at the C-terminal in R<sup>14</sup>GW<sup>4,20</sup>ALP23. The opposing radial positions of the distal tryptophans, W4 and W20, are responsible for the high dynamic motion exhibited by the host peptide. This arrangement causes the indole side chains to compete with one another for better positions at the lipid/water interface. Furthermore, as the helix cannot solely rely on

adjusting its  $\tau_0$  and  $\rho_0$  to satisfy hydrophobic mismatch, it additionally exhibits increased oscillations about its average  $\rho_0$  to meet the demands of the membrane interior.(12)

Incorporating R14 into  $\text{GW}^{4,20}\text{ALP23}$  introduces an interaction between the Arg side chain and the lipid membrane that is strong enough to drastically limit the rotational averaging about  $\rho_0$ , exemplified by the massive drop in  $\sigma_\rho$  from  $122^\circ$  to  $10^\circ$  in DOPC, essentially locking the transmembrane helix into place. In spite of the arginine dominance, the competition between the two Trp residues remains, such that W20 likely causes additional C-terminal residues to unravel from the core helix (Figure 4), in order to obtain a preferential orientation for the W20 indole ring at the lipid/water interface. While residues A3 and A21 often are observed to unwind, (see figure 3)(29, 32) now additional fraying of residues W20 and A19 is observed when R14 is present. By contrast, residue A3 near the N-terminal now fits to the central helix of  $\text{R}^{14}\text{GW}^{4,20}\text{ALP23}$ , indicating a shifting of the midpoint of the core helix. The N-terminus is likely compensating for the unwinding at the other end of the helix (see figure 10 for a model).

Influence of R12. Placing the Arg residue (R12) at the center of  $\text{GWALP23}$  sequences with varying locations for the outer Trp residues has interesting consequences. The peptide  $\text{R}^{12}\text{W}^{5,19}\text{ALP23}$  produces  $^2\text{H}$  NMR spectra with multiple states for every alanine residue in DOPC bilayers. According to molecular dynamics simulations, it adopts three primary states of which two are transmembrane and one is at the membrane surface.(9) When the tryptophans are moved outward by two residues each,  $\text{R}^{12}\text{W}^{3,21}\text{ALP23}$  has ample room to accommodate R12 between the outer Trp residues.(11) The helix with W3 and W21 is able to remain transmembrane by adopting large tilt angles ( $24\text{-}30^\circ$ ) to accommodate the snorkeling of R12 toward the surface of DOPC, DMPC or DLPC bilayers, without interference from the aromatic side chains.

Introducing a small amount of cholesterol (10 mol %) was enough to drive R<sup>12</sup>GW<sup>5,19</sup>ALP23 completely to the surface of DOPC bilayers.<sup>(10)</sup> Similarly, H12 and K12 both drive GW<sup>5,19</sup>ALP23 to the membrane surface, at low pH when H12 or K12 is positively charged.<sup>(6-7)</sup> Here, R<sup>12</sup>GW<sup>4,20</sup>ALP23 adopts a single overall orientation perpendicular to the DOPC bilayer normal, yet unlike the previous peptides, R<sup>12</sup>GW<sup>4,20</sup>ALP23 is distorted when bound on the membrane surface. The distortion is apparent from (a) the NMR resonance doubling of A9 and (b) the N-terminal residues preceding A9 not fitting to the same quadrupolar wave plot as the rest of the helix on the C-terminal side of A9 (Figures 6-8). The resonance doubling of A9 is likely observed because the helix actually starts to distort at residue A11, next to the central Arg at position 12. Thus, A9 is found, with about equal probability, within both the N-terminal and C-terminal helical segments. While residue A11 gives only one major <sup>2</sup>H NMR signal, additional minor peaks may be evident (Figure 6), although we are unable to assign specific minor peaks. Interestingly, and seemingly by coincidence, the major <sup>2</sup>H  $|\Delta\nu_q|$  value for A11 fits both the N-terminal <sub>310</sub>-helix and the C-terminal  $\alpha$ -helix (Figure 7). While R14 caused unwinding of the R<sup>14</sup>GW<sup>4,20</sup>ALP23 helix at A19 (see above), the larger and more central distortion with R12 likely also is caused by the competing Trp residues W4 and W20, while the Arg again dominates the peptide dynamics. The C-terminal helix exhibits  $\sigma\rho$  of 12°-25°, significantly lower than the parent helix when Arg is absent (Table 4). We note that the CD spectra (Figure 4B) are not particularly sensitive to the helix distortion revealed by the <sup>2</sup>H and <sup>15</sup>N NMR spectra. As noted, it is likely that the R<sup>12</sup>GW<sup>4,20</sup>ALP23 helix on the DOPC membrane surface contains a <sub>310</sub>-helical segment as well as an  $\alpha$ -helical segment. The <sup>2</sup>H quadrupolar splittings of the C-terminal alanines fit only to an  $\alpha$ -helix. Fitting the <sup>2</sup>H quadrupolar splittings of the N-terminal alanines to an  $\alpha$ -helix is not possible, nevertheless, even in combination with the <sup>15</sup>N data (table

4). On the other hand, a tighter  $3_{10}$ -helix predicts a surface bound N-terminal segment with only a  $40^\circ$  difference in azimuthal rotation from the C-terminal helix. The rotational difference and the tighter N-terminal  $3_{10}$ -helix then would allow the W20 side chain to reside at the membrane interface, oriented toward the lipids (see Figure 11), instead of projecting out of the membrane as would have been dictated by an extension of the C-terminal  $\alpha$ -helix. Indeed, the  $^{15}\text{N}$  chemical shifts also discount the possibility of a transmembrane orientation and are instead characteristic of an orientation perpendicular to the bilayer normal.(39, 50) In a  $3_{10}$ -helix, the carbonyl oxygens are more exposed, such that the folding of such a transmembrane structure is unfavorable due to the low dielectric of the bilayer interior.(27) On the membrane surface, nevertheless, a  $3_{10}$ -helix becomes a reasonable motif for adjusting the relative radial locations of the side chains of W4 and W20, such that both of the indole rings can face the membrane interface (Figure 11). We note as well that both the C-terminal  $\alpha$ -helix and N-terminal  $3_{10}$ -helix orientations are similar to the major interfacial state preferred by R<sup>12</sup>GW<sup>5,19</sup>ALP23 when cholesterol is added to the membrane.(10)

The  $^{15}\text{N}$  separated local field experiments are in full support of a surface-bound helix, yet essentially show little sensitivity to the geometric differences between an  $\alpha$ -helix or  $3_{10}$ -helix at this orientation. The insensitivity is largely because the plane perpendicular to the magnetic field/bilayer normal is additionally a reflection plane for the resonance frequencies(50-51) resulting in overlapping PISA wheel arcs over a small range of  $^1\text{H}$ - $^{15}\text{N}$  dipolar couplings and  $^{15}\text{N}$  chemical shifts, which are both further reduced by motional averaging. While this symmetry plane also affects the  $^2\text{H}$  experiments, they instead span a much wider frequency range (0-50 kHz)(10, 52) for surface bound helices and are therefore more sensitive in distinguishing the particular type of helix. The distinction would be easier for a transmembrane oriented peptide,

as  $\alpha$ -helices and  $3_{10}$ -helices aligned on a plane parallel to the magnetic field each produce a distinctive PISA wheel pattern.(39) Indeed there are precedents for an Arg-rich motif containing an  $\alpha$ -helix that kinks into a  $3_{10}$ -helix, for example in the voltage sensing domains of membrane channel proteins.(53-56) A model for such a helix transition may be manifest here.

### **3.6 Conclusions**

Incorporating one single central Arg residue into the highly dynamic GW<sup>4,20</sup>ALP23 helix framework has led to unique consequences. Placing Arg at position 14 arrests the dynamics, reorients the helix and causes the C-terminal residues around W20 to unwind from the helix, probably to optimize the interfacial interactions of residue W20. By contrast, an Arg residue at position 12 brings the entire helix to the surface of DOPC bilayer membranes and distorts the helix so that residues 3-11 form a  $3_{10}$ -helix while residues 9-19 remain  $\alpha$ -helical, with deuterated Ala-9 itself giving two distinct <sup>2</sup>H NMR spectral signals that represent both of the helix motifs.

### **3.7 Acknowledgements**

This work was supported in part by NSF MCB grant 1713242, and by the Arkansas Biosciences Institute. The peptide, NMR and mass spectrometry facilities were supported in part by NIH grant GM103429.

A portion of this work was performed at the National High Magnetic Field Laboratory, which is supported by the National Science Foundation Cooperative Agreement No. DMR-1644779\* and the State of Florida.

UCSF Chimera was developed by the Resource for Biocomputing, Visualization, and Informatics at the University of California, San Francisco, with support from NIH P41-GM103311.



### 3.8 References

1. Li, Q.; Wanderling, S.; Paduch, M.; Medovoy, D.; Singharoy, A.; McGreevy, R.; Villalba-Galea, C.; Hulse, R. E.; Roux, B.; Schulten, K.; Kossiakoff, A.; Perozo, E. 2014. Structural mechanism of voltage-dependent gating in an isolated voltage-sensing domain. *Nature Structural Molecular Biology* 21:244-252.
2. Guo, J.; Zeng, W.; Chen, Q.; Lee, C.; Chen, L.; Yang, Y.; Cang, C.; Ren, D.; Jiang, Y. 2015. Structure of the voltage-gated two-pore channel TPC1 from *Arabidopsis thaliana*. *Nature* 531:196.
3. Killian, J. A.; von Heijne, G. 2000. How proteins adapt to a membrane–water interface. *Trends in Biochemical Sciences* 25:429-434.
4. Mishra, V. K.; Palgunachari, M. N.; Segrest, J. P.; Anantharamaiah, G. M. 1994. Interactions of synthetic peptide analogs of the class A amphipathic helix with lipids. Evidence for the snorkel hypothesis. *J. Biol. Chem* 269:7185-7191.
5. Vostrikov, V. V.; Grant, C. V.; Daily, A. E.; Opella, S. J.; Koeppe, R. E., II. 2008. Comparison of "Polarization Inversion with Spin Exchange at Magic Angle" and "Geometric Analysis of Labeled Alanines" methods for transmembrane helix alignment. *J. Am. Chem. Soc* 130:12584.
6. Gleason, N. J.; Vostrikov, V. V.; Greathouse, D. V.; Koeppe, R. E. 2013. Buried lysine, but not arginine, titrates and alters transmembrane helix tilt. *Proceedings of the National Academy of Sciences* 110:1692-1695.
7. Martfeld, A. N.; Greathouse, D. V.; Koeppe, R. E. 2016. Ionization properties of histidine residues in the lipid bilayer membrane environment. *J. Biol. Chem.* 291:19146-19156.
8. Mortazavi, A.; Rajagopalan, V.; Sparks, K. A.; Greathouse, D. V.; Koeppe, R. E. 2016. Juxta-terminal helix unwinding as a stabilizing factor to modulate the dynamics of transmembrane helices. *Chembiochem* 17:462-465.
9. Vostrikov, V. V.; Hall, B. A.; Greathouse, D. V.; Koeppe, R. E.; Sansom, M. S. P. 2010. Changes in transmembrane helix alignment by arginine residues revealed by solid-state NMR experiments and coarse-grained MD simulations. *J. Am. Chem. Soc.* 132:5803-5811.
10. Thibado, J. K.; Martfeld, A. N.; Greathouse, D. V.; Koeppe, R. E. 2016. Influence of high pH and cholesterol on single arginine-containing transmembrane peptide helices. *Biochemistry* 55:6337-6343.
11. Vostrikov, V. V.; Hall, B. A.; Sansom, M. S. P.; Koeppe, R. E. 2012. Accommodation of a central arginine in a transmembrane peptide by changing the placement of anchor residues. *J. Phys. Chem. B* 116:12980-12990.

12. McKay, M. J.; Martfeld, A. N.; De Angelis, A. A.; Opella, S. J.; Greathouse, D. V.; Koeppe, R. E. 2018. Control of transmembrane helix dynamics by interfacial tryptophan residues. *Biophys. J.* 114:2617-2629.
13. Thomas, R.; Vostrikov, V. V.; Greathouse, D. V.; Koeppe, R. E. 2009. Influence of proline upon the folding and geometry of the WALP19 transmembrane peptide. *Biochemistry* 48:11883-11891.
14. Nevzorov, A. A.; Opella, S. J. 2007. Selective averaging for high-resolution solid-state NMR spectroscopy of aligned samples. *J. Magn. Reson.* 185:59-70.
15. Gor'kov, P. L.; Chekmenev, E. Y.; Li, C. G.; Cotten, M.; Buffy, J. J.; Traaseth, N. J.; Veglia, G.; Brey, W. W. 2007. Using low-E resonators to reduce RF heating in biological samples for static solid-state NMR up to 900 MHz. *J. Magn. Reson.* 185:77-93.
16. Levitt, M. H.; Suter, D.; Ernst, R. R. 1986. Spin dynamics and thermodynamics in solid-state NMR cross polarization. *J. Chem. Phys.* 84:4243-4255.
17. Fung, B.; Khittrin, A.; Ermolaev, K. 2000. An improved broadband decoupling sequence for liquid crystals and solids. *J. Magn. Reson.* 142:97-101.
18. Delaglio, F.; Grzesiek, S.; Vuister, G. W.; Zhu, G.; Pfeifer, J.; Bax, A. 1995. NMRPIPE - a multidimensional spectral processing system based on unix Pipes. *J. Biomol. NMR* 6:277-293.
19. Goddard, T. D.; Kneller, D. G. SPARKY 3. University of California, San Francisco.
20. Wishart, D. S.; Bigam, C. G.; Yao, J.; Abildgaard, F.; Dyson, H. J.; Oldfield, E.; Markley, J. L.; Sykes, B. D. 1995. <sup>1</sup>H, <sup>13</sup>C and <sup>15</sup>N chemical-shift referencing in biomolecular NMR. *J. Biomol. NMR* 6:135-140.
21. van der Wel, P. C. A.; Strandberg, E.; Killian, J. A.; Koeppe, R. E. 2002. Geometry and intrinsic tilt of a tryptophan-anchored transmembrane alpha-helix determined by <sup>2</sup>H NMR. *Biophys. J.* 83:1479-1488.
22. Enkhbayar, P.; Hikichi, K.; Osaki, M.; Kretsinger, R. H.; Matsushima, N. 2006. 3(10)-helices in proteins are parahelices. *Proteins* 64:691-699.
23. Rosendaal, T. B. A., Kuznetsov, A., Nussbaumer, A, Riakiotakis, A., Skorupa, B., Montagne, B., et al. 1998. Blender [computer program]. Version 2.79. Amsterdam: Blender Foundation.
24. Pettersen, E. F. G. T., Huang, C. C., Couch, G. S., Greenblatt, D. M., Meng, E. C, Ferrin, T. E. 2004. UCSF Chimera--a visualization system for exploratory research and analysis. *J Comput Chem.* 25:1605-1612.

25. Vostrikov, V. V.; Grant, C. V.; Opella, S. J.; Koeppe, R. E. 2011. On the combined analysis of  $^2\text{H}$  and  $^{15}\text{N}/^1\text{H}$  solid-state NMR data for determination of transmembrane peptide orientation and dynamics. *Biophys. J.* 101:2939-2947.
26. Strandberg, E.; Esteban-Martin, S.; Salgado, J.; Ulrich, A. S. 2009. Orientation and dynamics of peptides in membranes calculated from  $^2\text{H}$ -NMR data. *Biophys. J.* 96:3223-3232.
27. Page, R. C.; Kim, S.; Cross, T. A. 2008. Transmembrane helix uniformity examined by spectral mapping of torsion angles. *Structure* 16:787-797.
28. Daily, A. E.; Greathouse, D. V.; van der Wel, P. C. A.; Koeppe, R. E. 2008. Helical distortion in tryptophan- and lysine-anchored membrane-spanning  $\alpha$ -helices as a function of hydrophobic mismatch: a solid-state deuterium NMR investigation using the geometric analysis of labeled alanines method. *Biophys. J.* 94:480-491.
29. Afrose, F.; McKay, M. J.; Mortazavi, A.; Suresh Kumar, V.; Greathouse, D. V.; Koeppe, R. E. 2018. Transmembrane helix integrity versus fraying to expose hydrogen bonds at a membrane-water interface. *Biochemistry* 58:633-645.
30. Vostrikov, V. V.; Daily, A. E.; Greathouse, D. V.; Koeppe, R. E. 2010. Charged or aromatic anchor residue dependence of transmembrane peptide tilt. *J. Biol. Chem.* 285:31723-31730.
31. Sparks, K. A.; Gleason, N. J.; Gist, R.; Langston, R.; Greathouse, D. V.; Koeppe, R. E. 2014. Comparisons of interfacial Phe, Tyr, and Trp residues as determinants of orientation and dynamics for GWALP transmembrane peptides. *Biochemistry* 53:3637-3645.
32. McKay, M. J.; Afrose, F.; Koeppe, R. E.; Greathouse, D. V. 2018. Helix formation and stability in membranes. *Biochimica et Biophysica Acta (BBA) - Biomembranes*.
33. van der Wel, P. C. A.; Reed, N. D.; Greathouse, D. V.; Koeppe, R. E. 2007. Orientation and motion of tryptophan interfacial anchors in membrane-spanning peptides. *Biochemistry* 46:7514-7524.
34. Strandberg, E.; Esteban-Martin, S.; Ulrich, A. S.; Salgado, J. 2012. Hydrophobic mismatch of mobile transmembrane helices: Merging theory and experiments. *BBA-Biomembranes* 1818:1242-1249.
35. Vieira-Pires, R. S.; Morais-Cabral, J. H. 2010. 310 helices in channels and other membrane proteins. *The Journal of General Physiology* 136:585-592.
36. Payandeh, J.; Scheuer, T.; Zheng, N.; Catterall, W. A. 2011. The crystal structure of a voltage-gated sodium channel. *Nature* 475:353.

37. Zhang, X.; Ren, W.; DeCaen, P.; Yan, C.; Tao, X.; Tang, L.; Wang, J.; Hasegawa, K.; Kumasaka, T.; He, J.; Wang, J.; Clapham, D. E.; Yan, N. 2012. Crystal structure of an orthologue of the NaChBac voltage-gated sodium channel. *Nature* 486:130.
38. Pauling, L.; Corey, R. B.; Branson, H. R. 1951. The structure of proteins: Two hydrogen-bonded helical configurations of the polypeptide chain. *Proceedings of the National Academy of Sciences* 37:205-211.
39. Kim, S.; Cross, T. A. 2004. 2D solid state NMR spectral simulation of  $^3\text{J}_{\text{H-C}}$ ,  $\alpha$ , and  $\pi$ -helices. *J. Magn. Reson.* 168:187-193.
40. Marassi, F. M.; Ma, C.; Gesell, J. J.; Opella, S. J. 2000. Three-dimensional solid-state NMR spectroscopy is essential for resolution of resonances from in-plane residues in uniformly N-15-labeled helical membrane proteins in oriented lipid bilayers. *J. Magn. Reson.* 144:156-161.
41. Traaseth, N. J.; Buffy, J. J.; Zmoon, J.; Veglia, G. 2006. Structural dynamics and topology of phospholamban in oriented lipid bilayers using multidimensional solid-state NMR. *Biochemistry* 45:13827-13834.
42. Opella, S. J.; Marassi, F. M. 2004. Structure determination of membrane proteins by NMR spectroscopy. *Chem Rev* 104:3587-3606.
43. Fitch, C. A.; Platzer, G.; Okon, M.; Garcia-Moreno, B.; McIntosh, L. P. 2015. Arginine: Its pK(a) value revisited. *Protein Sci* 24:752-761.
44. Dorairaj, S.; Allen, T. W. 2007. On the thermodynamic stability of a charged arginine side chain in a transmembrane helix. *Proc. Natl. Acad. Sci. U. S. A.* 104:4943-4948.
45. Roux, B. 2007. Lonely arginine seeks friendly environment. *J Gen Physiol* 130:233-236.
46. Li, L.; Vorobyov, I.; MacKerell, A. D.; Allen, T. W. 2008. Is arginine charged in a membrane? *Biophys. J.* 94:L11-L13.
47. Harms, M. J.; Schlessman, J. L.; Sue, G. R.; Garcia-Moreno, B. 2011. Arginine residues at internal positions in a protein are always charged. *Proc. Natl. Acad. Sci. U. S. A.* 108:18954-18959.
48. Ulmschneider, J. P.; Smith, J. C.; White, S. H.; Ulmschneider, M. B. 2018. The importance of the membrane interface as the reference state for membrane protein stability. *BBA-Biomembranes* 1860:2539-2548.
49. Freitas, J. A.; Tobias, D. J.; von Heijne, G.; White, S. H. 2005. Interface connections of a transmembrane voltage sensor. *Proc. Natl. Acad. Sci. U. S. A.* 102:15059-15064.

50. Marassi, F. M.; Opella, S. J. 2000. A solid-state NMR index of helical membrane protein structure and topology. *J. Magn. Reson.* 144:150-155.
51. Murray, D. T.; Das, N.; Cross, T. A. 2013. Solid state NMR strategy for characterizing native membrane protein structures. *Accounts Chem Res* 46:2172-2181.
52. Strandberg, E.; Grau-Campistany, A.; Wadhvani, P.; Burck, J.; Rabanal, F.; Ulrich, A. S. 2018. Helix fraying and lipid-dependent structure of a short amphipathic membrane-bound peptide revealed by solid-state NMR. *J. Phys. Chem. B* 122:6236-6250.
53. Long, S. B.; Campbell, E. B.; MacKinnon, R. 2005. Crystal structure of a mammalian voltage-dependent Shaker family K<sup>+</sup> channel. *Science* 309:897-903.
54. Long, S. B.; Tao, X.; Campbell, E. B.; MacKinnon, R. 2007. Atomic structure of a voltage-dependent K<sup>+</sup> channel in a lipid membrane-like environment. *Nature* 450:376-U3.
55. Clayton, G. M.; Altieri, S.; Heginbotham, L.; Unger, V. M.; Morais-Cabral, J. H. 2008. Structure of the transmembrane regions of a bacterial cyclic nucleotide-regulated channel. *Proc. Natl. Acad. Sci. U. S. A.* 105:1511-1515.
56. Schwaiger, C. S.; Bjelkmar, P.; Hess, B.; Lindahl, E. 2011. 3(10)-helix conformation facilitates the transition of a voltage sensor S4 segment toward the down state. *Biophys. J.* 100:1446-1454.
57. Esteban-Martin, S.; Strandberg, E.; Salgado, J.; Ulrich, A. 2010. Solid state NMR analysis of peptides in membranes: Influence of dynamics and labeling scheme. *BBA-Biomembranes* 1798:252-257.

### 3.9 Tables

TABLE 1 Sequences of Arginine Containing GW<sup>4,20</sup>ALP23 and GW<sup>5,19</sup>ALP Peptides

Name	Sequence	Reference
GW <sup>4,20</sup> ALP23	acetyl-GGAW <sup>4</sup> ALALALALALALALAW <sup>20</sup> AGA-amide	(12)
R <sup>12</sup> GW <sup>4,20</sup> ALP23	acetyl-GGAW <sup>4</sup> ALALALAR <u>AL</u> ALALALAW <sup>20</sup> AGA-amide	This work
R <sup>14</sup> GW <sup>4,20</sup> ALP23	acetyl-GGAW <sup>4</sup> ALALALALAR <u>AR</u> ALALALAW <sup>20</sup> AGA-amide	This work
GW <sup>5,19</sup> ALP23	acetyl-GGALW <sup>5</sup> LALALALALALALW <sup>19</sup> LAGA-amide	(5)
R <sup>12</sup> GW <sup>5,19</sup> ALP23	acetyl-GGALW <sup>5</sup> LALALAR <u>AR</u> ALALALW <sup>19</sup> LAGA-amide	(11)
R <sup>14</sup> GW <sup>5,19</sup> ALP23	acetyl-GGALW <sup>5</sup> LALALAR <u>AR</u> ALALALW <sup>19</sup> LAGA-amide	(11)

TABLE 2 *Quadrupolar Splitting Magnitudes ( $|\Delta\nu_q|$ , in kHz) for Labeled Alanine CD<sub>3</sub> Groups in R<sup>14</sup>GW<sup>4,20</sup>ALP23 and R<sup>12</sup>GW<sup>4,20</sup>ALP23<sup>a</sup>*

Lipid(s)	R <sup>14</sup> GW <sup>4,20</sup> ALP23 Alanine CD <sub>3</sub> Position/ $\Delta\nu_q$ (kHz)									
	3	5	7	9	11	13	15	17	19	21
DLPC	30.0	20.2	25.8	0.1	11.2	20.0	13.2	27.0	33.0	24.0
DMPC	29.4	14.2	23.2	2.6	8.8	19.7	12.5	28.0	28.0	24.0
DOPC	30.2	8.2	20.1	7.3	4.1	19.3	10.8	28.1	22.4	14.3
Lipid	R <sup>12</sup> GW <sup>4,20</sup> ALP23 Alanine CD <sub>3</sub> Position/ $\Delta\nu_q$ (kHz)									
	3	5	7	9(a)/(b)	11	13	15	17	19	21
DOPC <sup>b</sup>	18.9	0.5	23.2	27.4/11.4	21.0	0.7	13.2	37.1	25.0	31.0

<sup>a</sup> $\beta = 0^\circ$  sample orientation.

<sup>b</sup>Residue A9 gives two signals in DOPC, designated as 9a (27.4 kHz) and 9b (11.4 kHz).

TABLE 3 GALA and Gaussian Fits Using Ala-CD<sub>3</sub>  $|\Delta v_q|$  magnitudes of Arg Containing GWALP23 Family Peptides<sup>a</sup>

Lipid	Peptide	GALA fit results				Gaussian fit results					Ref.
		$\tau_o$	$\rho_o$	$S_{zz}$	RMSD	$\tau_o$	$\rho_o$	$\sigma\rho$	$\sigma\tau$	RMSD	
DLPC	W <sup>4,20</sup>	6.0°	322°	0.72	0.70	16°	321°	85°	15°	0.49	(12)
	W <sup>5,19</sup>	20.7°	305°	0.71	0.66	23°	304°	33°	5 <sup>ob</sup>	0.70	(12)
	R <sup>14</sup> W <sup>4,20</sup>	21.3°	223°	0.77	0.92	21°	223°	24°	14°	0.74	This
	R <sup>14</sup> W <sup>5,19</sup>	30.0°	259°	0.83	1.58	30°	260°	< 10°	5 <sup>ob</sup>	1.65	(9);This
DMPC	W <sup>4,20</sup>	3.3°	349°	0.71	0.85	5°	347°	51°	20°	0.68	(12)
	W <sup>5,19</sup>	11.7°	311°	0.87	0.90	13°	308°	44°	5 <sup>ob</sup>	1.10	(12)
	R <sup>14</sup> W <sup>4,20</sup>	16.7°	228°	0.85	0.75	17°	228°	12°	6°	0.72	This
	R <sup>14</sup> W <sup>5,19</sup>	25.8°	252°	0.81	1.59	26°	252°	28°	5 <sup>ob</sup>	0.97	(9);This
DOPC	W <sup>4,20</sup>	1.7°	133°	0.81	0.80	9°	129°	122°	5°	0.78	(12)
	W <sup>5,19</sup>	6.0°	323°	0.87	0.60	9°	321°	48°	5 <sup>ob</sup>	0.70	(12)
	R <sup>14</sup> W <sup>4,20</sup>	13.3°	221°	0.90	0.81	14°	220°	9°	2°	0.87	This
	R <sup>14</sup> W <sup>5,19</sup>	16.1°	246°	0.94	1.29	16°	246°	< 10°	5 <sup>ob</sup>	1.20	(9);This

<sup>a</sup> The abbreviations refer to peptides based on the locations of selected aromatic residues, W<sup>4,20</sup> in GW<sup>4,20</sup>ALP23 and W<sup>5,19</sup> in GW<sup>5,19</sup>ALP23, with or without arginine R14, as noted. See also Table 1.

<sup>b</sup>A modified three variable gaussian treatment<sup>31, 57</sup> was used to analyze the six core Ala-CD<sub>3</sub> data points constraining  $\sigma\tau$  to 5°.



TABLE 4  $R^{12}W^{4,20}$  ALP23 Structure, Orientation and Dynamics at the Surface of DOPC Bilayers<sup>a</sup>

$R^{12}W^{4,20}$	C-Terminus					N-Terminus				
	$\tau_0$	$\rho_0$	$\sigma\rho$	$\sigma\rho$	RMSD (kHz)	$\tau_0$	$\rho_0$	$\sigma\rho$	$\sigma\rho$	RMSD (kHz)
$^2\text{H}$	83°	31°	12°	28°	1.28 <sup>b</sup>	No fit.				
$^{15}\text{N}, ^1\text{H}/^{15}\text{N}$	87°	42°	25°	5°	0.69	88°	178°	44°	7°	0.89
Combined	84°	34°	22°	5°	0.86	No fit.				
$3_{10}$ -Helix <sup>c</sup>										
$^2\text{H}$	No fit.					85°	353°	27°	30°	0.66 <sup>d</sup>
$^{15}\text{N}, ^1\text{H}/^{15}\text{N}$	86°	22°	42°	5°	0.66	88°	348°	48°	7°	0.74
Combined	No fit.					85°	349°	29°	27°	1.22

<sup>a</sup> The N-terminal fits were calculated using  $^2\text{H}$  resonances for residues A3, A5, A7, A9b, and A11, or  $^1\text{H}/^{15}\text{N}$  observables for residues A5, L6, A7, L8, A9b. The C-terminal data points included  $^2\text{H}$  quadrupolar splittings for residues A9a, A11, A13, A15, A17, A19, or  $^1\text{H}/^{15}\text{N}$  observables for residues A9a, A13, L14, A15, L16 and A17. The combined fits used the  $^2\text{H}$  quadrupolar splittings together with the indicated  $^1\text{H}/^{15}\text{N}$  observables.

<sup>b</sup> For comparison with the Gaussian fit for the  $^2\text{H}$  data to the C-terminal  $\alpha$ -helix, a semi-static GALA analysis gave  $\tau_0 = 86^\circ$ ,  $\rho_0 = 33^\circ$ ,  $S_{zz}$  of 0.64 and RMSD of 1.25 kHz.

<sup>c</sup> The results suggest that the  $^{15}\text{N}/^1\text{H}$  results could fit either an  $\alpha$ -helix or a similarly oriented  $3_{10}$ -helix for either segment (N-terminal or C-terminal), with in all cases a significant discontinuity (change in azimuthal rotation  $\rho_0$ ) at residue 9. The  $^2\text{H}$  results, by contrast, show distinct preferences of an  $\alpha$ -helix for the C-terminus and a  $3_{10}$ -helix for the N-terminus. The  $^2\text{H}$  quadrupolar splitting is highly sensitive to the local bond orientation.

<sup>d</sup> For comparison, a semi-static GALA analysis gave  $\tau_0 = 86^\circ$ ,  $\rho_0 = 3^\circ$ ,  $S_{zz}$  of 0.51 and RMSD of 0.47 kHz.

### 3.10 Figures

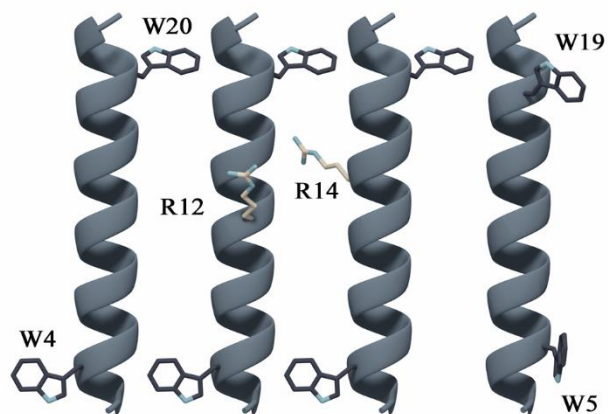


*FIGURE 1 GWALP-like Peptide Models. From left to right:  $GW^{4,20}ALP23$ ,  $R^{12}GW^{4,20}ALP23$ ,  $R^{14}GW^{4,20}ALP23$ ,  $GW^{5,19}ALP23$ . See Table 1 for the amino acid sequences. While not depicted here, the helix terminals tend to fray.*

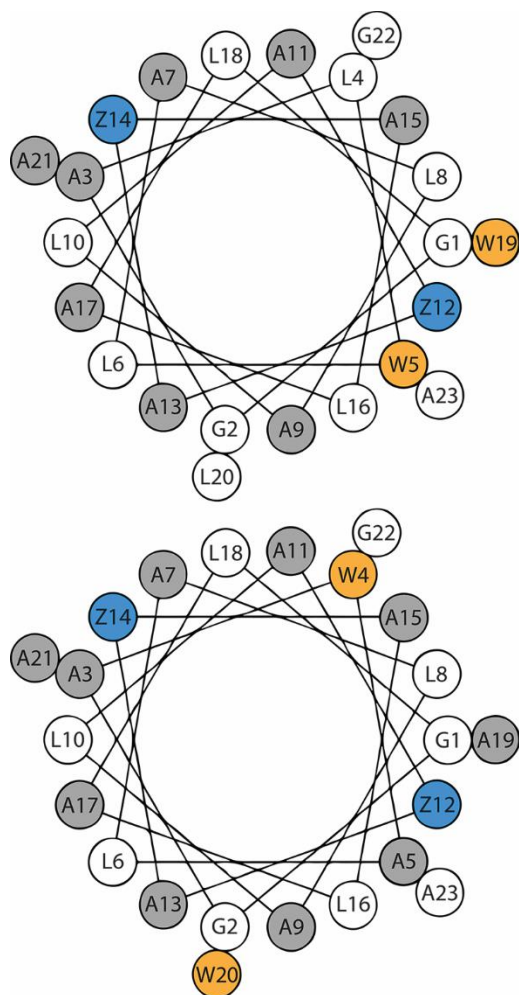


**FIGURE 2** Helical wheel plots for GWALP-like peptides highlighting the Trp (W) locations with respect to residues 12 and 14. Top:  $GW^{5,19}ALP23$ ; bottom:  $GW^{4,20}ALP23$ . Ala residues used for  $^2H$ -labeling are depicted in gray. Trp residues are shown in yellow. Positions Z12 and Z14 (blue) are either Leu or one of them is substituted with Arg.

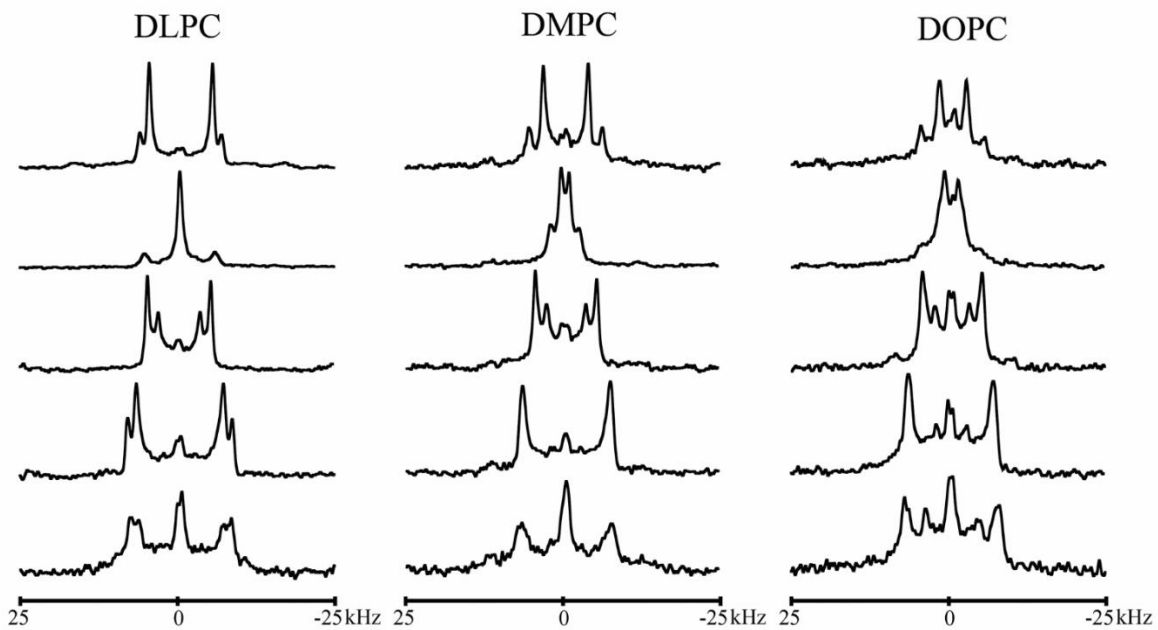


FIGURE 3  $^2\text{H}$  NMR spectra for labeled alanines of  $R^{14}GW^{4,20}ALP23$  in mechanically aligned DLPC, DMPC and DOPC bilayers set at  $\beta = 90^\circ$ , temperature  $50^\circ\text{C}$ . The identities of the pairs of  $^2\text{H}$ -labeled alanines in each sample, from top to bottom, are ( $A5^{100\%}$ ,  $A7^{50\%}$ ); ( $A9^{100\%}$ ,  $A11^{50\%}$ ); ( $A13^{100\%}$ ,  $A15^{50\%}$ ); ( $A17^{100\%}$ ,  $A19^{50\%}$ ); ( $A3^{100\%}$ ,  $A21^{50\%}$ ).

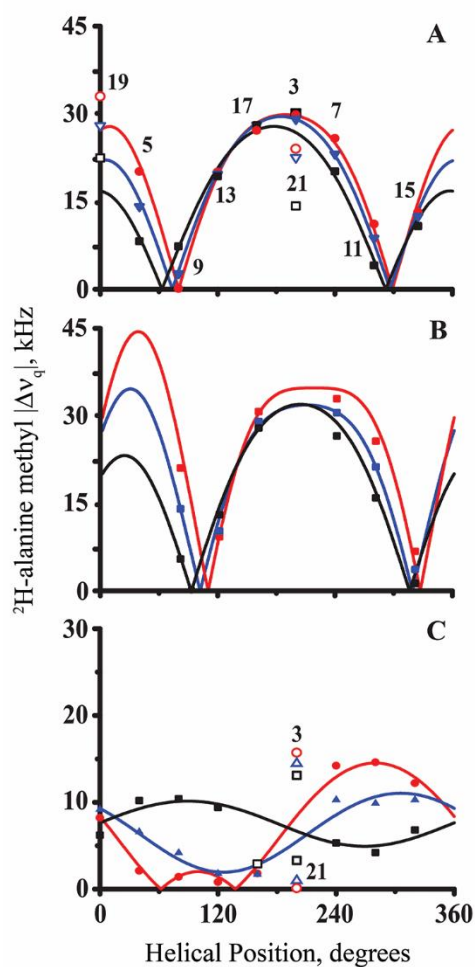


FIGURE 4 GALA quadrupolar wave plots for A)  $R^{14}GW^{4,20}ALP23$ , B)  $R^{14}GW^{5,19}ALP23$  and C)  $GW^{4,20}ALP23$  in DLPC (red), DMPC (blue) and DOPC (black) bilayers. Data points with white filling were omitted from the analysis. The helix orientations corresponding to the quadrupolar waves are listed in Table 3.

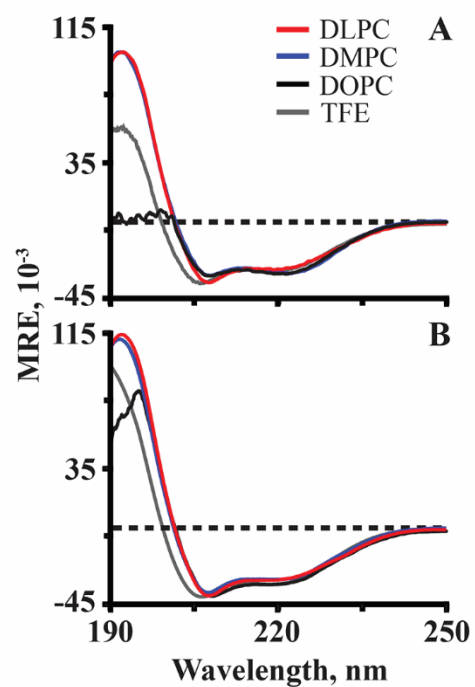


FIGURE 5 Circular dichroism spectra for A)  $R^{14}GW^{4,20}ALP23$  and B)  $R^{12}GW^{4,20}ALP23$  in lipid vesicles. The dotted black lines indicate where the mean residue ellipticity is zero. The DOPC double bond absorbs below 200 nm and is responsible for the distortion shown.

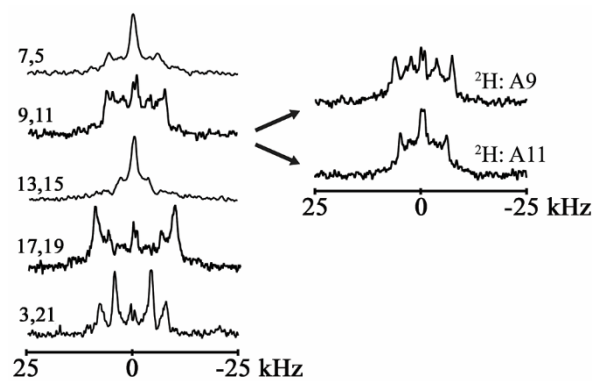


FIGURE 6  $^2\text{H}$  NMR spectra for labeled alanines  $R^{12}GW^{4,20}ALP23$  in mechanically aligned DOPC bilayers.  $\beta = 90^\circ$ .  $50^\circ\text{C}$ . The label positions and % deuteration are from top to bottom: ( $A5^{100\%}$ ,  $A7^{50\%}$ ); ( $A9^{100\%}$ ,  $A11^{50\%}$ ); ( $A13^{100\%}$ ,  $A15^{50\%}$ ); ( $A17^{100\%}$ ,  $A19^{50\%}$ ); ( $A3^{100\%}$ ,  $A21^{50\%}$ ).

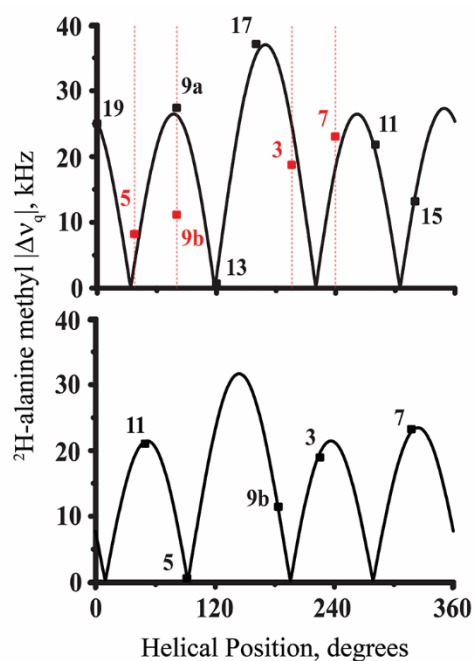
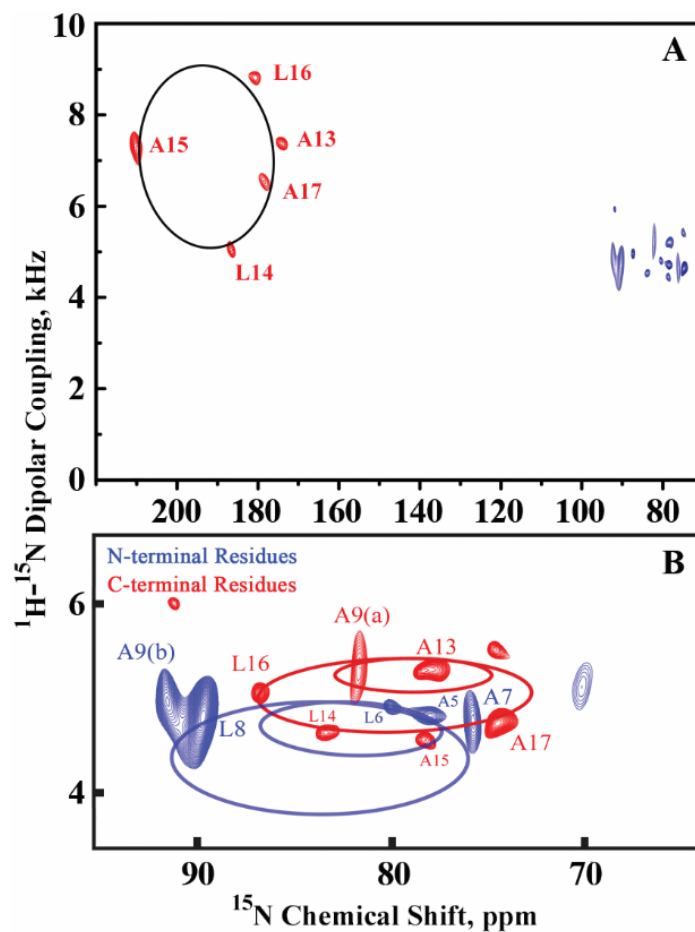


FIGURE 7 GALA quadrupolar wave plots for  $R^{12}GW^{4,20}$  ALP23 DOPC bilayers. A. Wave plot for the C-terminal  $\alpha$ -helix ( $\tau_0$   $86^\circ$ ,  $\rho_0$   $33^\circ$ ), with data points for A9b, A7, A5 and A3 (red) not fitting the curve and omitted in the analysis used to generate the wave plot. B. Wave plot for a  $3_{10}$ -helix for the N-terminal (A3-A11 with A9b).





**FIGURE 8** Separated local field  $^{15}\text{N}$  spectra for a transmembrane helix and a distorted surface helix. **A.** The red peaks arise from resonances for selected  $^{15}\text{N}$  backbone labels on transmembrane KWALP23 in static aligned DLPC bilayers oriented at  $\beta = 0^\circ$ , with the ellipse representing a helix tilted  $19^\circ$  from the bilayer normal. The blue peaks arise from  $^{15}\text{N}$  labels in  $R^{12}\text{GW}^{4,20}\text{ALP23}$ , bound to the surface of DOPC bilayers. **B.** Expansion and highlights for selectively labeled  $R^{12}\text{GW}^{4,20}\text{ALP23}$  peptides in static aligned DOPC bilayers oriented with  $\beta = 0^\circ$ . The PISA wheels shown are fitted to C-terminal residues (red,  $\alpha$ -helix) and N-terminal residues (blue,  $3_{10}$ -helix). See also table 4. The assignments for  $^{15}\text{N}$  backbone labels are shown. Temperature  $50^\circ\text{C}$ .

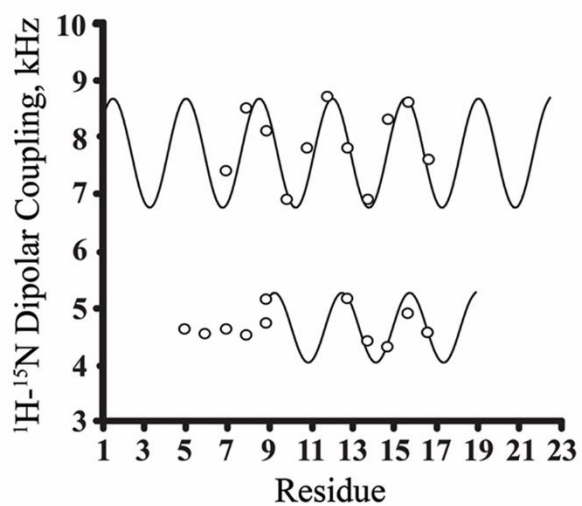
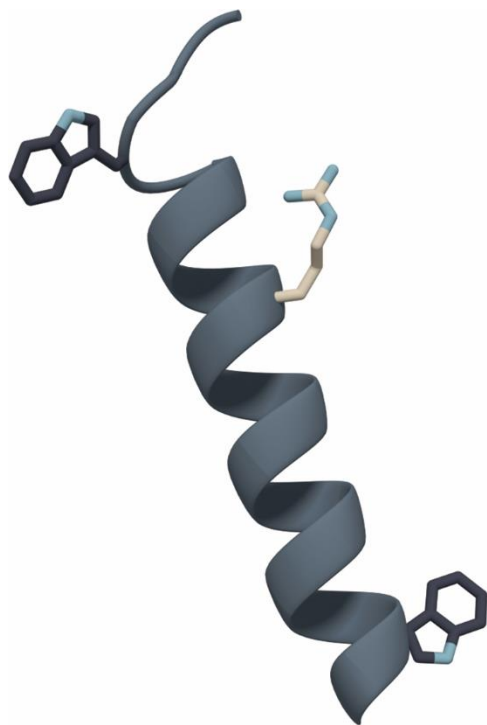
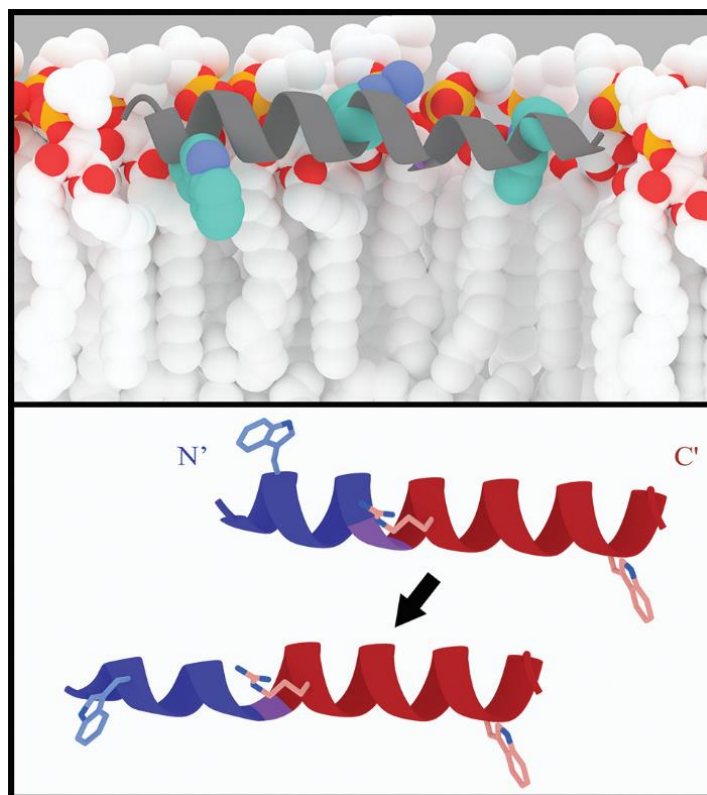


FIGURE 9 Dipolar waves depicting the static  $^1\text{H}$ - $^{15}\text{N}$  dipolar couplings as a function of residue position for transmembrane  $\text{GW}^{5,19}\text{ALP23}$  in DLPC bilayers (top) adapted from <sup>25</sup> and surface bound  $\text{R}^{12}\text{GW}^{4,20}\text{ALP23}$  in DOPC bilayers (bottom).



*Figure 10 3D model of R<sup>14</sup>GW<sup>4.20</sup>ALP23. The C-terminal unwinding begins at residue A19.*



**FIGURE 11** 3D model for  $R^{12}GW^{4,20}ALP23$  of the surface of a DOPC bilayer. Side chain space filling model is shown in the top panel with the predicted helix distortion. In the bottom panel, the upper peptide assumes no distortion and adopts the entire orientation for the C-terminal residues (red) as fit to an  $\alpha$ -helix with average orientation  $\tau_o = 86^\circ$  and azimuthal rotation  $\rho_o = 33^\circ$ . In the peptide below, the N-terminal residues (blue) instead fit a  $3_{10}$ -helix with a similar  $\tau_o = 89^\circ$  but a different  $\rho_o = 353^\circ$ . The discontinuity occurs at residue A9 (purple), which displays two signals in the  $^2H$  NMR spectra (Figures 6-7). The rotational discontinuity and helix variation place both tryptophans W4 and W20 in similar interfacial locations, which the arginine R12 projects outward from the bilayer surface.

### 3.11 Supplemental Figures

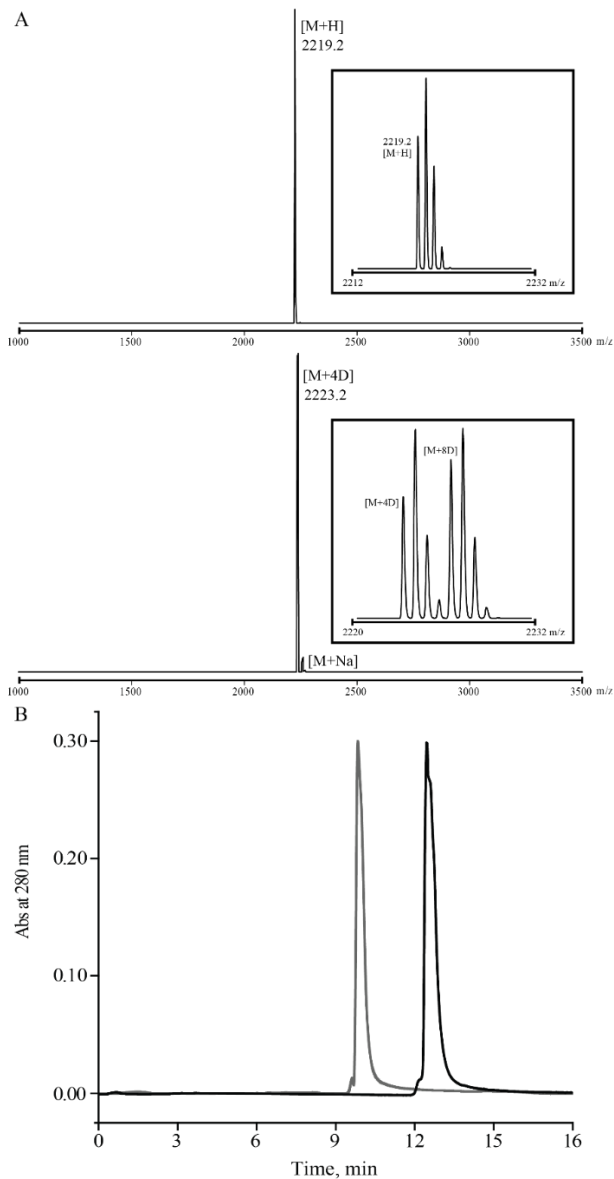


FIGURE S1 A) MALDI-MS spectra of  $R^{14}GW^{4,20}ALP23$  unlabeled (top) and double labeled  $R^{12}GW^{4,20}ALP23$  with Ala- $D_4$  (bottom). Expected  $m/z$  of the  $[M+H]$  ion for both peptides is 2219.2. B) RP-HPLC elution profile to confirm purification of  $R^{12}GW^{4,20}ALP23$  (gray) and  $R^{14}GW^{4,20}ALP23$  (black).

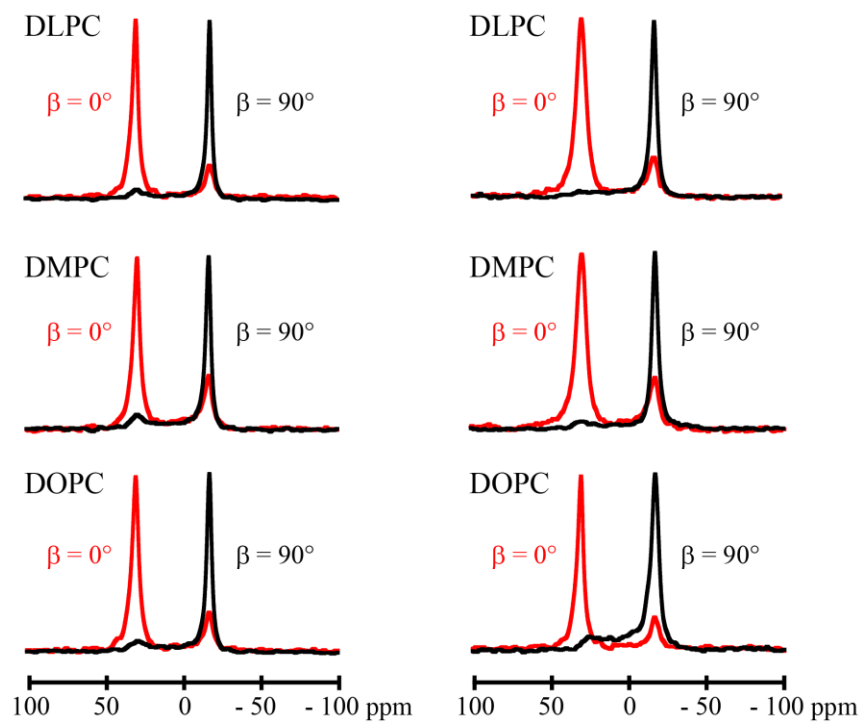


FIGURE S2  $^{31}\text{P}$  NMR spectra with  $^1\text{H}$  broadband decoupling for  $R^{12}\text{GW}^{4,20}\text{ALP23}$  (left) and  $R^{14}\text{GW}^{4,20}\text{ALP23}$  (right) in mechanically aligned DLPC, DMPC and DOPC bilayers; temperature set to  $50^\circ\text{C}$ .

$R^{14}GW^{4,20}ALP23, \beta = 0^\circ$

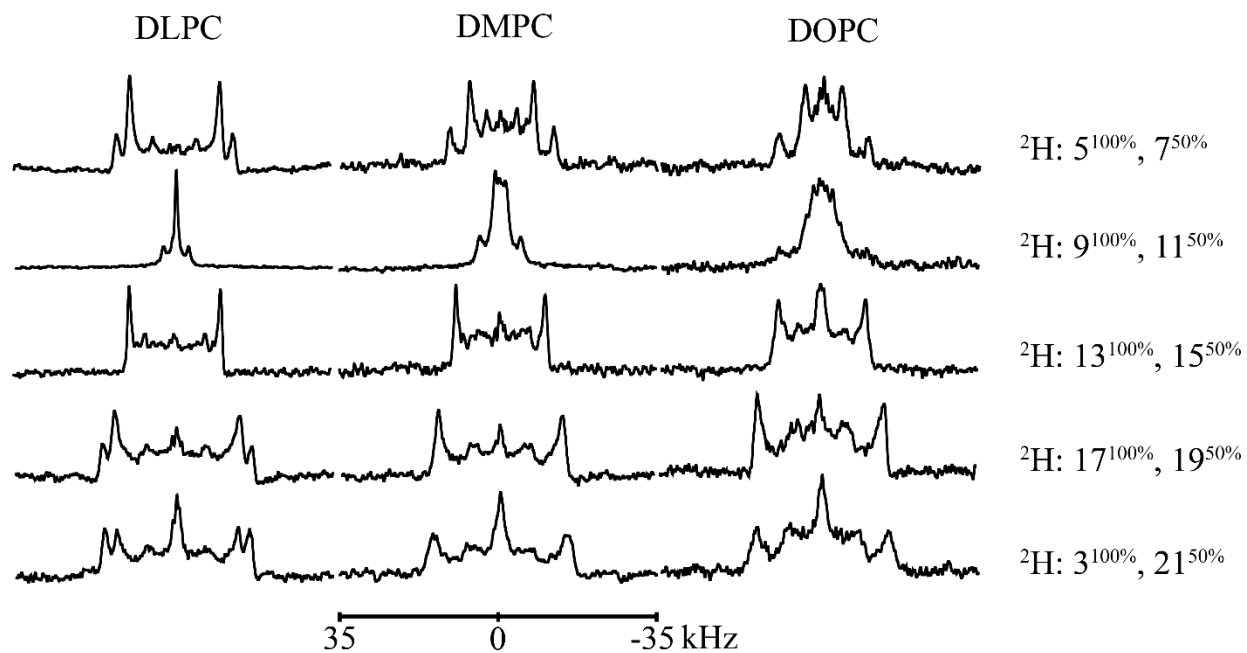
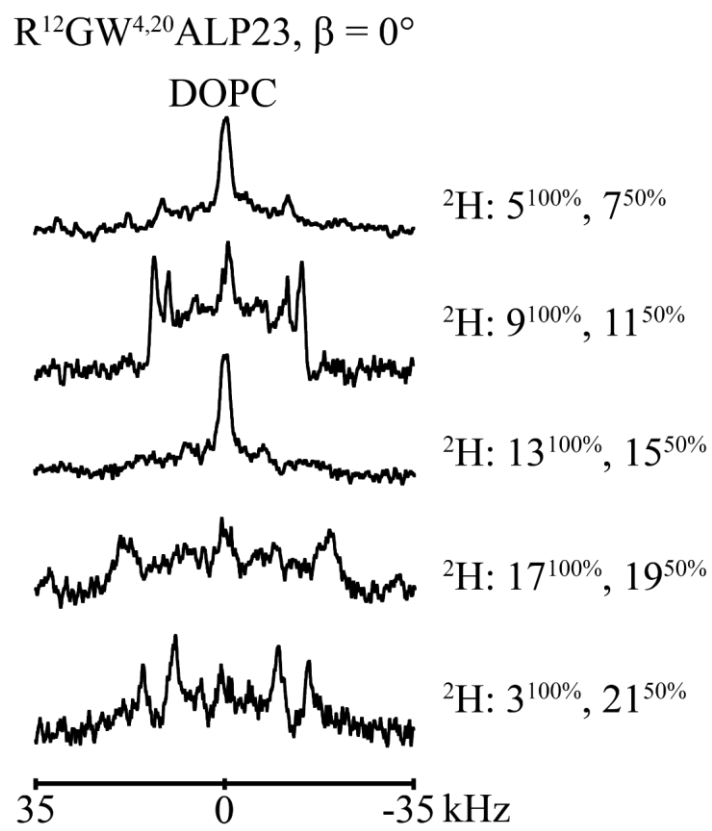


FIGURE S3  $^2H$  NMR spectra for  $R^{14}GW^{4,20}ALP23$  in mechanically aligned DLPC, DMPC and DOPC bilayers set at  $\beta = 0^\circ$  and performed at  $50^\circ C$ .



*FIGURE S4*  $^2H$  NMR spectra for  $R^{12}GW^{4,20}ALP23$  in mechanically aligned DOPC bilayers set at  $\beta = 0^\circ$  and performed at  $50^\circ C$ .



## CHAPTER 4

### A Link Between Flanking Aromatic Residue Competition and Transmembrane Peptide Dynamics

#### 4.1 Abstract

Transmembrane protein dynamics are often difficult to analyze due to the numerous experimental complications associated with these types of proteins. Simple model systems can instead be used to circumvent such obstacles in order to provide information about the basic principles behind protein-lipid interactions. Recently the GW<sup>4,20</sup>ALP23 peptide was reported to undergo significant amounts of motional averaging over <sup>2</sup>H and <sup>15</sup>N NMR observables in model bilayers of different thicknesses. Here two new peptides based on the GW<sup>4,20</sup>ALP23 sequence, lacking charged or polar residues, are characterized in DLPC, DMPC and DOPC bilayers using solid-state <sup>2</sup>H NMR. One, L<sup>5,19</sup>GW<sup>4,20</sup>ALP23 an isomer of the moderately dynamic GW<sup>5,19</sup>ALP23, was made to analyze the importance of terminal leucine residues near the interface and how they affect rotational slippage about the peptide's azimuthal rotation. The same motional averaging profile is observed when compared to the parent sequence. The second peptide, F<sup>4,5</sup>GW<sup>20</sup>ALP23, is found to unwind significantly at the C-terminal portion of the helix in the various lipid bilayers and furthermore undergoes only moderate levels of dynamic motion. Interestingly, the majority of the helix adopts low tilt values in all three lipid bilayers and both solid-state <sup>2</sup>H NMR and CD experiments suggest the helix possibly undergoes oligomerization.

#### 4.2 Introduction

Aromatic amino acids, like Trp, Tyr or Phe, situated at the lipid bilayer interfacial region of transmembrane proteins help stabilize the protein's membrane orientation.(1, 2) Tryptophan's indole ring, for example, can form hydrogen bonds with the polar lipid head groups.(1-4) Single

spanning transmembrane peptides such as GWALP23 have provided valuable insight into how various arrangements of flanking aromatic side chains influence transmembrane peptide behavior and protein-lipid interactions.(5-8) Originally, peptides containing multiple Trp residues such as the WALP family peptides exhibited high dynamic motion about their azimuthal rotation.(9) Cutting down the number of Trp residues to two in GW<sup>5,19</sup>ALP23 resulted in a well behaved peptide system that exhibited low dynamics and a tilt that scaled with bilayer thickness to satisfy hydrophobic matching.(10)

Recently, the tryptophan residues of GW<sup>5,19</sup>ALP23 were moved outward to opposite faces of the helix at positions 4 and 20. It is believed that this new peptide, GW<sup>4,20</sup>ALP23 undergoes excessive motion about its azimuthal rotation in order to compensate for the competition between the two opposing aromatic residues while still satisfying hydrophobic mismatch. In the new framework, additional alanine residues are located on either side of the terminal Trp residues and can be used as additional labeling sites in <sup>2</sup>H solid-state NMR experiments. The inclusion of these alanine residues results in GW<sup>4,20</sup>ALP23 lacking leucine residues at these locations when compared to the moderately dynamic GW<sup>5,19</sup>ALP23. Therefore, to determine how terminal leucine residues affect the peptide dynamics, a modified W4,20 peptide was created as a true isomer of GW<sup>5,19</sup>ALP23, instead containing Leu residues at positions 5 and 19. While only containing six core alanine residues for <sup>2</sup>H solid-state NMR labeling, the L<sup>5,19</sup>GW<sup>4,20</sup>ALP23 peptide is shown to exhibit the same lipid bilayer dependent dynamics as GW<sup>4,20</sup>ALP23 while instead adopting the same lipid-dependent tilt behavior as GW<sup>5,19</sup>ALP23. Phenylalanine (F), which lacks the ability to form hydrogen bonds, has served as a control for investigations into high peptide dynamics caused by competing aromatic residues such as Tyr in Y<sup>4,5</sup>GW<sup>5,19</sup>ALP23.(7) W5 and L4 of GW<sup>5,19</sup>ALP23 were replaced with phenylalanine residues

(F4,5) and the resultant peptide was shown to undergo only moderate amounts of motional averaging and exhibited a behavior similar to that of the parent peptide.(7, 11) The same modification was made in this study to GW<sup>4,20</sup>ALP23 and while similar dynamics were observed, the peptide adopts lower on-average tilt angles accompanied by C-terminal distortion. Both CD and NMR experiments offer evidence of oligomerization.

### 4.3 Materials and Methods

Fmoc-amino acids were purchased from NovaBiochem (San Diego, CA). Commercial L-Ala-d<sub>4</sub> was purchased from Cambridge Isotope labs (Andover, MA) and modified with an Fmoc group as described.(12) All peptides were synthesized via solid-state FastMoc synthesis on a 0.1 mmol scale as previously described. Most peptides were synthesized with two Ala-d<sub>4</sub> labeled residues in either 100% or 50% labeled abundances. Both peptides (L<sup>5,19</sup>GW<sup>4,20</sup>ALP23 and F<sup>4,5</sup>GW<sup>20</sup>ALP23) were purified via reverse-phase HPLC on an octyl silica column (Zorbax Rx-C8, 9.4 × 250 mm, 5 μm particle size; Agilent Technologies, Santa Clara, CA) and a gradient of 92–98% methanol (with 0.1% trifluoroacetic acid) over 40 min. Purification and synthesis were confirmed by MALDI-mass spectrometry and reversed-phase HPLC (see supplemental figure S1).

Circular dichroism (CD) experiments were performed on a Jasco (Easton, MD) J-1500 CD/Fluorescence spectropolarimeter with a 1 mm cell path, 1.0 nm bandwidth, 0.1 mm slit, and a scan speed of 20 nm/min, with averaging of 5 scans. Far UV/CD experiments were conducted to determine the extent of peptide helicity in peptide-lipid samples (62.5 nmol/3.75 μmol; P/L; 1:60) using DLPC, DMPC and DOPC lipid vesicles. Near UV/CD experiments were performed to analyze the perturbations of the Trp and Phe aromatic side chain local environments using

0.665  $\mu\text{M}$  peptide-lipid samples (1:60) in DLPC, DMPC and DOPC vesicles (each sample contained  $\sim 1.5$  mg of peptide).

Steady-state fluorescence experiments were performed on peptide-lipid samples (1:60) prepared by diluting (1/20) with water samples prepared for CD (see above). Experiments were performed using a Jasco (Easton, MD) J-1500 CD/Fluorescence spectropolarimeter. The samples were excited at 280 nm and excitation slit width of 5 nm. Emission spectra were recorded with a 5 nm emission slit width between 300-450 nm, with a with averaging of 5 scans.

Solid-state NMR experiments were performed on mechanically aligned peptide-lipid samples (1:60 mol/mol) prepared as described previously(13) with DLPC, DMPC and DOPC lipids purchased from Avanti Polar Lipids (Alabaster, AL). Samples were hydrated with deuterium depleted water (Cambridge Isotopes) up to a hydration of 45% (w/w). Bilayer alignment was confirmed using  $^{31}\text{P}$  NMR with broadband  $^1\text{H}$  decoupling at both  $\beta = 90^\circ$  and  $\beta = 0^\circ$  macroscopic sample orientations.  $^2\text{H}$  NMR experiments were performed using a 300 MHz Bruker Avance Spectrometer with a solid quadrupolar-echo pulse sequence(14) with a  $3.0 \mu\text{s}$   $90^\circ$  pulse length, a 90 ms recycle delay and 115  $\mu\text{s}$  echo delay. The collected spectra recorded between 0.7 and 1.5 million scans and were processed with 100 Hz line broadening.

The  $^2\text{H}$  Ala-quadrupolar splittings were analyzed using the semi-static GALA method(13) which generates a quadrupolar wave based on the peptide's given orientation with regards to its apparent tilt ( $\tau_0$ ), apparent rotation ( $\rho_0$ ), and an isotropic motion order parameter ( $S_{zz}$ ) as described in detail in Chapter 3. The experimental  $^2\text{H}$  quadrupolar splittings are compared to those calculated by the analysis for each Ala residue in the sequence to determine the peptide's

average orientation with the lowest root mean square deviation (RMSD). The adjustable parameters were varied as follows:  $\tau_0$  ( $0^\circ$ - $90^\circ$  by  $1^\circ$ ),  $\rho_0$  ( $0^\circ$ - $359^\circ$  by  $1^\circ$ ) and  $S_{zz}$  (0.1-1.0 by 0.1).

A Gaussian treatment (based on model 6 from Strandberg et al 2009) was also used to expand on the above semi-static analysis in order to determine the extent of additional dynamic motion about the peptide's average rotation in the form of "rotational slippage" ( $\sigma\rho$ ) and about the peptide's average tilt, "helix wobble" ( $\sigma\tau$ ). This calculation requires four adjustable parameters:  $\tau_0$  ( $0^\circ$ - $90^\circ$ ),  $\rho_0$  ( $0^\circ$ - $359^\circ$ ),  $\sigma\tau$  ( $0^\circ$ - $30^\circ$ ) and  $\sigma\rho$  ( $0^\circ$ - $200^\circ$ ) which were all varied by  $1^\circ$  while holding  $S_{zz}$  constant at 0.88 as an estimate of peptide motion. A modified version of this calculation was also performed holding  $\sigma\tau$  to a low finite value when a limited number of data points were available.(7)

#### 4.4 Results

##### $L^{5,19}GW^{4,20}ALP23$

The  $GW^{4,20}ALP23$  sequence was modified by replacing A5 and A19 with Leu to determine whether the high dynamic motion exhibited by the peptide is governed by the Trp residues or the hydrophobicity of the transmembrane core. Oriented solid-state NMR can be used answer such questions and estimate the average orientation and dynamics of a transmembrane peptide in a lipid bilayer system. The deuterated methyl group quadrupolar splitting range for  $L^{5,19}GW^{4,20}ALP23$  in table 2 is narrow (0.1 kHz to 15 kHz; figure 2, table 2) and resembles that of  $GW^{4,20}ALP23$  (0.1 kHz to 16 kHz), indicating high motional averaging could be present.(15) A moderately dynamic peptide such as  $GW^{5,19}ALP23$  for example produces splittings over a range of 0.1 kHz to 27 kHz.(10)

Comparison of experimental quadrupolar splittings to those calculated for various helix orientations with respect to the magnetic field allows one to determine the peptide's transmembrane behavior. Incorporating the NMR observables into the semi-static GALA calculation predicts low values of  $\tau_0$  ( $< 10^\circ$ ) and varying values of  $\rho_0$  for L<sup>5,19</sup>GW<sup>4,20</sup>ALP23 in all three lipid bilayers (see table 3) with no observed trend for either trait. The isomer, GW<sup>5,19</sup>ALP23 adopts a tilt that decreases as lipid bilayer thickness is increased, while also making minor adjustments about  $\rho_0$ .(10) Lower predicted  $\tau_0$  values and non-static  $\rho_0$  values across all three membranes are typically symptomatic of high motional averaging, usually in the form of rotational slippage ( $\sigma\rho$ ). (6, 7, 15, 16) This necessitates the use of a more aggressive Gaussian treatment which considers these additional oscillations. Due to the limited number of data points in the core sequence, a modified calculation was used constraining  $\sigma\tau$  to a low finite value.(7) As predicted, the  $\sigma\rho$  values are high in DLPC and DOPC ( $80^\circ$  and  $108^\circ$ ; see table 3) and the actual tilt in both lipids is higher than that predicted by the GALA,  $23^\circ$  and  $11^\circ$  respectively. Alternatively, the rotational slippage in DMPC is much lower ( $34^\circ$ ) and the predicted tilt is essentially unchanged between the two calculations. Interestingly, the  $\tau_0$  adopted by L<sup>5,19</sup>GW<sup>4,20</sup>ALP23 in each of the three lipids is almost identical to that of its isomer, GW<sup>5,19</sup>ALP23 (see table 3). The trend in  $\sigma\rho$  however, matches that observed in the dynamic profile of the parent GW<sup>4,20</sup>ALP23 peptide in all three lipid bilayers, even the moderate  $\sigma\rho$  observed in DMPC. Although a  $20^\circ$  drop in  $\sigma\rho$  is observed in the two thicker lipids, these results likely indicate the Trp radial locations are responsible for the dynamic motion while the makeup of the hydrophobic core primarily dictates the tilt (see discussion).

F<sup>4,5</sup>W<sup>20</sup>ALP23

The quadrupolar splitting range for  $F^{4.5}GW^{20}ALP23$  is also small (0.8 kHz to 19.5 kHz; see table 2, figure 4). At least five of the spectra recorded for labeled residues A3/A21 and A15/A17 produce three sets of quadrupolar splittings. In DOPC for example, the two  $CD_3$  labels at A15 and A17 generate  $^2H$  NMR spectrum with three sets of quadrupolar splittings with high signal intensities (figure 5). The larger quadrupolar splitting disappears when either label is removed. Incorporating two populations of single-labeled A15 and A17 peptides (2:1) into the same sample regenerates the third splitting at a much lower intensity. Summation of the two single-label spectra can also regenerate the splitting to roughly the same effect. The additional splittings observed for the various spectra could be resultant of a similar minor state for each label or an unknown interaction occurring within the system.

Far UV/CD spectra indicate the peptide has typical  $\alpha$ -helical structure in both DLPC and DMPC vesicles (figure) with  $\epsilon_{222}$  nm to  $\epsilon_{208}$  nm ellipticity ratios at 0.98 and 1.06 respectively. In DOPC however, the spectrum yields an even higher  $\epsilon_{222}$  nm to  $\epsilon_{208}$  nm ratio of 1.8. Ratios greater than 1.0 are often observed for coiled-coils.(17, 18) The parent framework has  $\epsilon_{222}$  nm to  $\epsilon_{208}$  nm ratios of less than 0.9 in all three lipids (see Chapter 2). Furthermore, the near UV/CD spectrum for the peptide in DOPC shows suppressed peaks at 260 nm and 290 nm when compared to DLPC and DMPC, indicating a significant difference in the local environments of the terminal Phe and Trp residues.

The GALA analysis predicts reasonable  $\tau_0$  values in DLPC and DMPC bilayers ( $17^\circ$  and  $8^\circ$ ) and a  $\sim 30^\circ$  difference in  $\rho_0$ . Interestingly, the apparent tilt is near zero in DOPC (table 3). Typically, a low  $\tau_0$  is usually indicative of high motional averaging caused by an extensive  $\sigma\rho$ . However, despite the low quadrupolar splitting range, the Gaussian analysis is surprisingly in agreement

with the semi-static GALA method and only moderate amounts of rotational slippage are predicted compared to both  $\text{GW}^{4,20}\text{ALP23}$  and  $\text{L}^{5,19}\text{GW}^{4,20}\text{ALP23}$ . The dynamics of  $\text{F}^{4,5}\text{GW}^{20}\text{ALP23}$  are instead more akin to those of  $\text{GW}^{5,19}\text{ALP23}$  (table 3). In all three lipid bilayers, C-terminal residues after A15 do not fit to the quadrupolar wave plot. Past experiments have shown that residues off these curves are not a part of the core helix.(11, 19) Therefore at least seven C-terminal residues, including W20, are not part of the core helix in  $\text{F}^{4,5}\text{GW}^{20}\text{ALP23}$ .

#### 4.5 Discussion

The original WALP peptides contained two flanking Trp residues at either terminus and underwent high degrees of motional averaging about their average rotation.(9) Side chain competition between the neighboring Trp residues is likely the primary factor, although with four Trp residues at various radial locations about the helix it is impossible to attribute the high dynamics to a single Trp pair. Removing a Trp residue at either helix end resulted in the formation of the  $\text{GW}^{5,19}\text{ALP23}$  framework. This peptide adopts a well-defined tilt in lipid bilayers and expresses only moderate levels of dynamic averaging.(10, 15) Moving the Trp residues outward to opposing radial locations about the helix in  $\text{GW}^{4,20}\text{ALP23}$  reintroduced high dynamic motion about the helix azimuthal rotation.(15) Side chain competition due to the radial locations of the Trp residues was once again suggested to be the primary cause of the observed motional averaging. The new sequence, however, was not a complete isomer of the  $\text{W}^{5,19}$  peptide. In particular, the tryptophans at positions 4 and 20 lacked adjacent leucine residues and it was unknown if their absence had any impact on the observed dynamics.

$\text{L}^{5,19}\text{GW}^{4,20}\text{ALP23}$



Here, a complete isomer of GW<sup>5,19</sup>ALP23 using the W4,20 framework was characterized. L<sup>5,19</sup>GW<sup>4,20</sup>ALP23 undergoes high degrees of rotational slippage ( $\sigma\rho$ ) in both DLPC and DOPC bilayers with low/moderate amounts in DMPC. This follows the same pattern as the dynamic profile of the parent GW<sup>4,20</sup>ALP23 helix, however a 20° drop in  $\sigma\rho$  is observed in the two thicker lipids when the two additional Leu residues are present in the core sequence. The lower  $\sigma\rho$  is likely due to the longer leucine side chain which may be less “slippery” compared to alanine. Regardless, even with this difference in  $\sigma\rho$ , it seems the radial distribution of the flanking Trp residues is still primarily responsible for the dynamics observed, once again supporting side chain competition between these two residues. The major impact altering the core sequence had was in forcing the peptide to adjust its tilt to compensate for hydrophobic mismatch. This causes the helix to adopt almost identical tilt angles to that of its isomer, GW<sup>5,19</sup>ALP23, in each lipid bilayer.

#### F<sup>4,5</sup>GW<sup>20</sup>ALP23

Previous studies that replaced W5 and L4 of GW<sup>5,19</sup>ALP23 with F5 and F4 did not determine any significant difference in the peptide dynamics or orientation when comparing both peptides (see Table 3).(7) Both peptides maintain a similar, static rotation and analogous tilt angles that scale with lipid bilayer thickness. Importantly, the extent of dynamic motion is moderate whether W5 is present or not. Side chain competition between two Phe residues is not an issue as neither group is capable of hydrogen bond formation, and presumably, the two side chain phenyl rings can adopt favorable positions when simply placed near the interface.(7)

Here, we are interested in characterizing the dynamics of the GW<sup>4,20</sup>ALP23 framework when W4 and A5 are removed and replaced with F4 and F5. Indeed, the removal of W4 decreases the rotational slippage to less than 50° in all three lipids. Interestingly, the C-terminal residues from

A17 outward (including W20) are not a part of the core helix. No helix distortion was observed previously with W19 present, so the question remains: why is the distortion observed here in this sequence with residue W20? One possibility is the presence of the Leu residues surrounding W19 stabilize the helix, whereas the Ala residues surrounding W20 may make the helix more susceptible to breakage. The lower dynamics of F<sup>4,5</sup>GW<sup>20</sup>ALP23 do not seem to play any part in causing the distortion as the parent GW<sup>4,20</sup>ALP23 sequence also distorts at residue A17 in DOPC bilayers while undergoing a rotational slippage of 122° (Table 3, Figure 3). In DMPC bilayers, both F<sup>4,5</sup> peptides share a similar tilt with the major orientation difference being the azimuthal rotation (Table 3). W20 may be situated at an unfavorable location due to the average rotation of the helix (see Figure 7). Deformation of the helix at the C-terminus would allow W20 to adopt a more desirable orientation at the interface.

Oligomerization is a possibility for F<sup>4,5</sup>GW<sup>20</sup>ALP23. In DOPC bilayers, F<sup>4,5</sup>GW<sup>20</sup>ALP23 is almost parallel to the bilayer normal. Helix distortion discussed above could potentially help the peptide to avoid hydrophobic mismatch, however; this near-zero tilt angle is highly irregular for single spanning transmembrane domains. The CD spectra show both the potential for a coiled-coil motif in all three lipids with the highest probability in DOPC. Furthermore, the additional quadrupolar splittings observed in the various NMR spectra could be due to some type of interaction between two or more helices. Similar <sup>2</sup>H NMR spectral features have been observed while varying the temperature in experiments with ErbB-2 transmembrane peptides in oriented bilayers, and the same phenomenon could be occurring here with F<sup>4,5</sup>GW<sup>20</sup>ALP23.(20)

#### **4.6 Conclusions**

The primary factor in causing the unique pattern of dynamic motion for the GW<sup>4,20</sup>ALP23 framework in various lipid bilayers has now been confirmed as the side chain competition

between the flanking tryptophan residues. Modifying the hydrophobicity of the core sequence using L<sup>5,19</sup>GW<sup>4,20</sup>ALP23 leads to a slight decrease in dynamics, but mainly forces the peptide to adjust its tilt in lipid bilayers. The replacement of W4 with F4,5 also removes the side chain competition and decreases the dynamics. It also causes the peptide to partially distort at the C-terminus and undergo possible oligomerization.

#### 4.8 Acknowledgements

This work was supported in part by NSF MCB grant 1713242, and by the Arkansas Biosciences Institute. The peptide, NMR and mass spectrometry facilities were supported in part by NIH grant GM103429.

#### 4.7 References

1. Killian, J., and G. von Heijne. 2000. How proteins adapt to a membrane-water interface. *Trends in Biochemical Sciences* 25(9):429-434.
2. Yau, W. M., W. C. Wimley, K. Gawrisch, and S. H. White. 1998. The preference of tryptophan for membrane interfaces. *Biochemistry* 37(42):14713-14718.
3. Sun, H., D. Greathouse, O. Andersen, and R. Koeppe. 2008. The preference of tryptophan for membrane interfaces - Insights from n-methylation of tryptophans in gramicidin channels. *Journal of Biological Chemistry* 283(32):22233-22243.
4. Beaven, A., A. Sodt, R. Pastor, R. Koeppe, O. Andersen, and W. Im. 2017. Characterizing residue-bilayer interactions using gramicidin a as a scaffold and tryptophan substitutions as probes. *Journal of Chemical Theory and Computation* 13(10):5054-5064.
5. van der Wel, P., N. Reed, D. Greathouse, and R. Koeppe. 2007. Orientation and motion of tryptophan interfacial anchors in membrane-spanning peptides. *Biochemistry* 46(25):7514-7524.
6. Gleason, N. J., V. V. Vostrikov, D. V. Greathouse, C. V. Grant, S. J. Opella, and R. E. Koeppe. 2012. Tyrosine replacing Tryptophan as an anchor in GWALP peptides. *Biochemistry* 51(10):2044-2053.

7. Sparks, K. A., N. J. Gleason, R. Gist, R. Langston, D. V. Greathouse, and R. E. Koeppe. 2014. Comparisons of interfacial Phe, Tyr, and Trp residues as determinants of orientation and dynamics for GWALP transmembrane peptides. *Biochemistry* 53(22):3637-3645.
8. Vostrikov, V. V., and R. E. Koeppe. 2011. Response of GWALP Transmembrane peptides to changes in the tryptophan anchor positions. *Biochemistry* 50(35):7522-7535.
9. Strandberg, E., S. Esteban-Martin, A. Ulrich, and J. Salgado. 2012. Hydrophobic mismatch of mobile transmembrane helices: Merging theory and experiments. *Biochimica Et Biophysica Acta-Biomembranes* 1818(5):1242-1249.
10. Vostrikov, V. V., C. V. Grant, A. E. Daily, S. J. Opella, and R. E. Koeppe, II. 2008. Comparison of "Polarization Inversion with Spin Exchange at Magic Angle" and "Geometric Analysis of Labeled Alanines" methods for transmembrane helix alignment. *Journal of the American Chemical Society* 130(38):12584.
11. Afrose, F., M. McKay, A. Mortazavi, V. Kumar, D. Greathouse, and R. Koeppe. 2019. Transmembrane helix integrity versus fraying to expose hydrogen bonds at a membrane-water interface. *Biochemistry* 58(6):633-645.
12. Martfeld, A., D. Greathouse, and R. Koeppe. 2016. Ionization properties of histidine residues in the lipid bilayer membrane environment. *Journal of Biological Chemistry* 291(36):19146-19156.
13. van der Wel, P. C. A., E. Strandberg, J. A. Killian, and R. E. Koeppe. 2002. Geometry and intrinsic tilt of a tryptophan-anchored transmembrane alpha-helix determined by H-2 NMR. *Biophysical Journal* 83(3):1479-1488.
14. Davis, J. H., K. R. Jeffrey, M. Bloom, M. I. Valic, and T. P. Higgs. 1976. Quadrupolar echo deuteron magnetic-resonance spectroscopy in ordered hydrocarbon chains. *Chemical Physics Letters* 42(2):390-394.
15. McKay, M., A. Martfeld, A. De Angelis, S. Opella, D. Greathouse, and R. Koeppe. 2018. Control of transmembrane helix dynamics by interfacial tryptophan residues. *Biophysical Journal* 114(11):2617-2629.
16. Vostrikov, V. V., C. V. Grant, S. J. Opella, and R. E. Koeppe. 2011. On the combined analysis of H-2 and N-15/H-1 solid-state NMR data for determination of transmembrane peptide orientation and dynamics. *Biophysical Journal* 101(12):2939-2947.
17. Lau, S., A. Taneja, and R. Hodges. 1984. Synthesis of a model protein of defined secondary and quaternary structure - effect of chain-length on the stabilization and formation of 2-stranded alpha-helical coiled-coils. *Journal of Biological Chemistry* 259(21):3253-3261.

18. Crooks, R., T. Rao, and J. Mason. 2011. Truncation, randomization, and selection generation of a reduced length C-JUN antagonist that retains high interaction stability. *Journal of Biological Chemistry* 286(34):29470-29479.
19. Mortazavi, A., V. Rajagopalan, K. A. Sparks, D. V. Greathouse, and R. E. Koeppe. 2016. Juxta-terminal helix unwinding as a stabilizing factor to modulate the dynamics of transmembrane helices. *Chembiochem* 17(6):462-465.
20. Sharpe, S., K. Barber, and C. Grant. 2002. Evidence of a tendency to self-association of the transmembrane domain of ErbB-2 in fluid phospholipid bilayers. *Biochemistry* 41(7):2341-2352.

## 4.9 Tables

*TABLE 1 Sequences of GWALP23 Family Peptides*

Name	Sequence	Reference
GW <sup>4,20</sup> ALP23	acetyl-GGAW <sup>4</sup> ALALALALALALALAW <sup>20</sup> AGA-amide	(15)
GW <sup>5,19</sup> ALP23	acetyl-GGALW <sup>5</sup> LALALALALALALW <sup>19</sup> LAGA-amide	(10)
L <sup>5,19</sup> GW <sup>4,20</sup> ALP23	acetyl-GGAW <sup>4</sup> L <sup>5</sup> LALALALALALALL <sup>19</sup> W <sup>20</sup> AGA-amide	This work
F <sup>4,5</sup> GW <sup>20</sup> ALP23	acetyl-GGAF <sup>4</sup> F <sup>5</sup> LALALALALALALAW <sup>20</sup> AGA-amide	This work
F <sup>4,5</sup> GW <sup>19</sup> ALP23	acetyl-GGA F <sup>4</sup> F <sup>5</sup> LALALALALALALW <sup>19</sup> LAGA-amide	(7)

TABLE 2 *Quadrupolar Splittings ( $|\Delta\nu_q|$ , in kHz) for Deuterated Alanine Methyl Groups in  $L^{5,19}GW^{4,20}ALP23$  and  $F^{4,5}GW^{20}ALP23^a$*

Lipid(s)	$L^{5,19}GW^{4,20}ALP23$								
	3	7	9	11	13	15	17	21	
DLPC	11.3	6.3	2.1	2.5	6.4	2.2	7.6	0.6	
DMPC	13.2	7.6	6.4	0.2	10.9	3.8	8.8	2.2	
DOPC	13.0	4.2	11.2	3.2	9.8	7.6	5.8	3.8	
Lipid	$F^{4,5}GW^{20}ALP23$								
	3	7	9	11	13	15	17	19	21
DLPC	9.2	2.2	11.4	9.1	17.2	12.0	19.4	16.4	5.4
DMPC	4.4	9.2	6.2	2.5	13.1	3.4	13.4	14.1	7.1
DOPC	0.8	6.4	11.6	6.2	9.8	9.1	3.4	10.1	3.4

$^a\beta = 0^\circ$  sample orientation.

TABLE 3 GALA and Gaussian Analyses Using Ala-CD<sub>3</sub>  $|\Delta v_q|$  magnitudes of GW<sup>4,20</sup>ALP23 Peptides<sup>a</sup>

Lipid	Peptide	GALA				Gaussian					Ref.
		$\tau_o$	$\rho_o$	$S_{zz}$	RMSD	$\tau_o$	$\rho_o$	$\sigma\rho$	$\sigma\tau$	RMSD	
DLPC	W <sup>4,20</sup>	6.0°	322°	0.72	0.70	16°	321°	85°	15°	0.49	(15)
	W <sup>5,19</sup>	20.7°	305°	0.71	0.66	23°	304°	33°	5° <sup>b</sup>	0.70	(15)
	L <sup>5,19</sup> W <sup>4,20</sup>	10.7°	225°	0.31	0.32	23°	224°	80°	5° <sup>b</sup>	0.57	This
	F <sup>4,5</sup> W <sup>20</sup>	16.7°	180°	0.48	0.80	18°	180°	30°	5° <sup>b</sup>	0.30	This
	F <sup>4,5</sup> W <sup>19</sup>	21.3°	317°	0.67	0.50	18°	314°	< 5°	15°	0.50	(11)
DMPC	W <sup>4,20</sup>	3.3°	349°	0.71	0.85	5°	347°	51°	20°	0.68	(15)
	W <sup>5,19</sup>	11.7°	311°	0.87	0.90	13°	308°	44°	5° <sup>b</sup>	1.10	(15)
	L <sup>5,19</sup> W <sup>4,20</sup>	9.0°	204°	0.45	1.31	11°	205°	34°	5° <sup>b</sup>	0.89	This
	F <sup>4,5</sup> W <sup>20</sup>	8.3°	212°	0.64	0.35	10°	213°	< 30°	5° <sup>b</sup>	1.03	This
	F <sup>4,5</sup> W <sup>19</sup>	11.3°	331°	0.80	1.3	-	-	-	-	-	(11)
DOPC	W <sup>4,20</sup>	1.7°	133°	0.81	0.80	9°	129°	122°	5°	0.78	(15)
	W <sup>5,19</sup>	6.0°	323°	0.87	0.60	9°	321°	48°	5° <sup>b</sup>	0.70	(15)
	L <sup>5,19</sup> W <sup>4,20</sup>	2.7°	99°	0.80	0.72	11°	98°	108°	5° <sup>b</sup>	0.76	This
	F <sup>4,5</sup> W <sup>20</sup>	1.7°	95°	0.95	0.42	3.0°	88°	47°	5° <sup>b</sup>	1.18	This
	F <sup>4,5</sup> W <sup>19</sup>	6.0°	323°	0.80	0.90	10°	329°	54°	9°	1.60	(11)

<sup>a</sup> The abbreviations refer to peptides based on the locations of selected aromatic residues, W<sup>4,20</sup> in GW<sup>4,20</sup>ALP23 and W<sup>5,19</sup> in GW<sup>5,19</sup>ALP23. See also Table 1.

<sup>b</sup> A modified three variable gaussian treatment was used to analyze the six core Ala-CD<sub>3</sub> data points constraining  $\sigma\tau$  to 5°.



#### 4.10 Figures

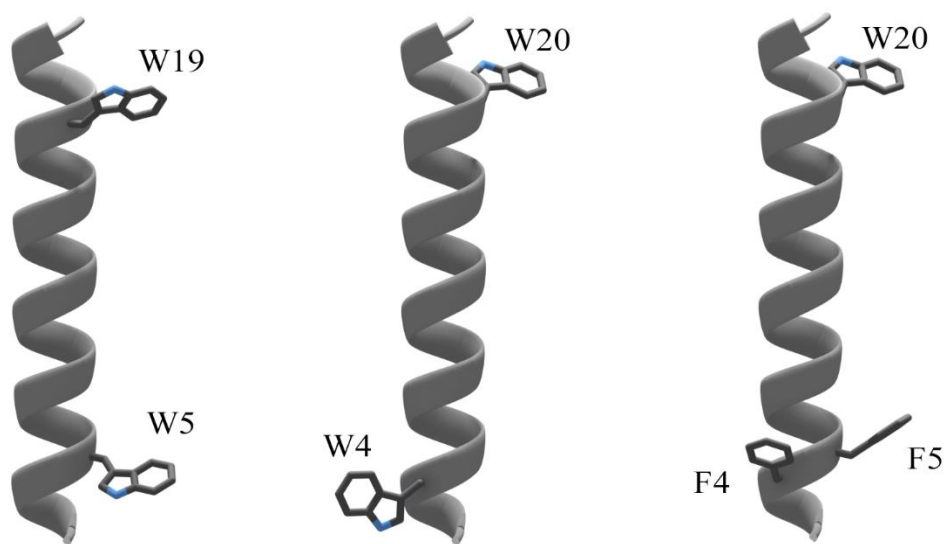


*FIGURE 1 From left to right, 3D models of  $GW^{5,19}ALP23$ ,  $GW^{4,20}ALP23$  and  $F^{4,5}GW^{20}ALP23$ . See also table 1 for sequences.*

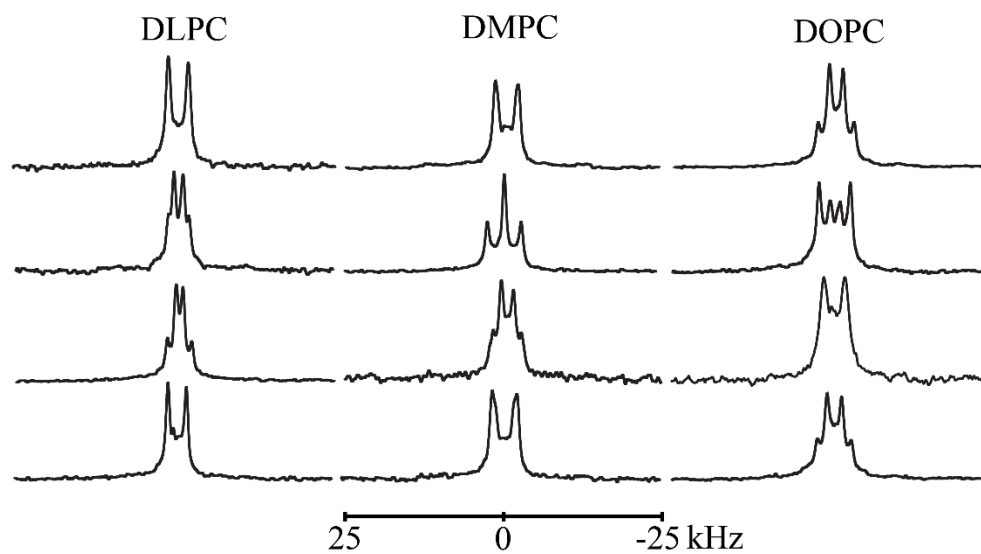
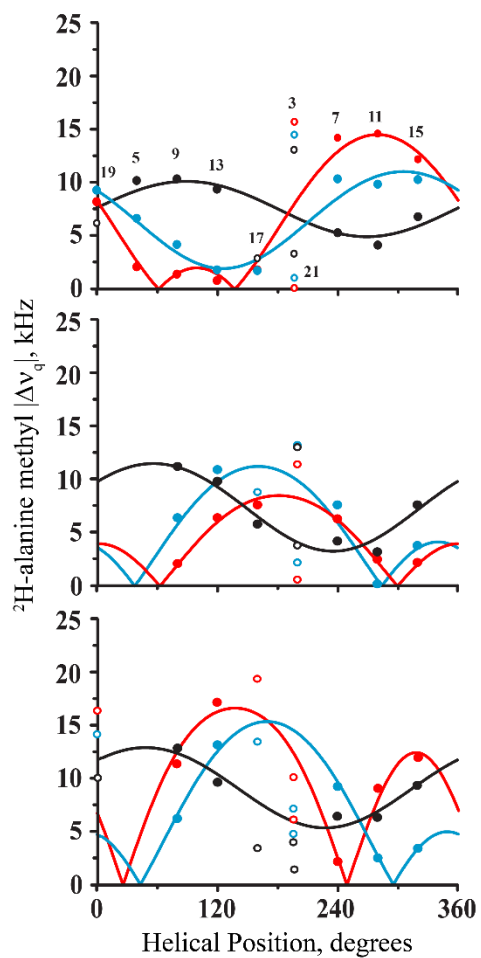


FIGURE 2  $^2\text{H}$  NMR spectra of  $L^{5.19}GW^{4.20}ALP23$  acquired at  $\beta = 90$ , with temperature set at 50 °C. From top to bottom,  $^2\text{H}$  labeled alanines and abundances are:  $A7^{100\%}$ ,  $A9^{50\%}$ ;  $A11^{100\%}$ ,  $A13^{50\%}$ ;  $A15^{100\%}$ ,  $A17^{50\%}$ ;  $A3^{100\%}$ ,  $A21^{50\%}$ .



*FIGURE 3* Semi-static analysis quadrupolar wave plots for  $GW^{4,20}ALP23$  (top),  $L^{5,19}GW^{4,20}ALP23$  (middle) and  $F^{4,5}GW^{20}ALP23$  (bottom) in DLPC (red), DMPC (blue), and DOPC (black). White filled dots represent residues which were not included in the analysis to obtain the average orientation.

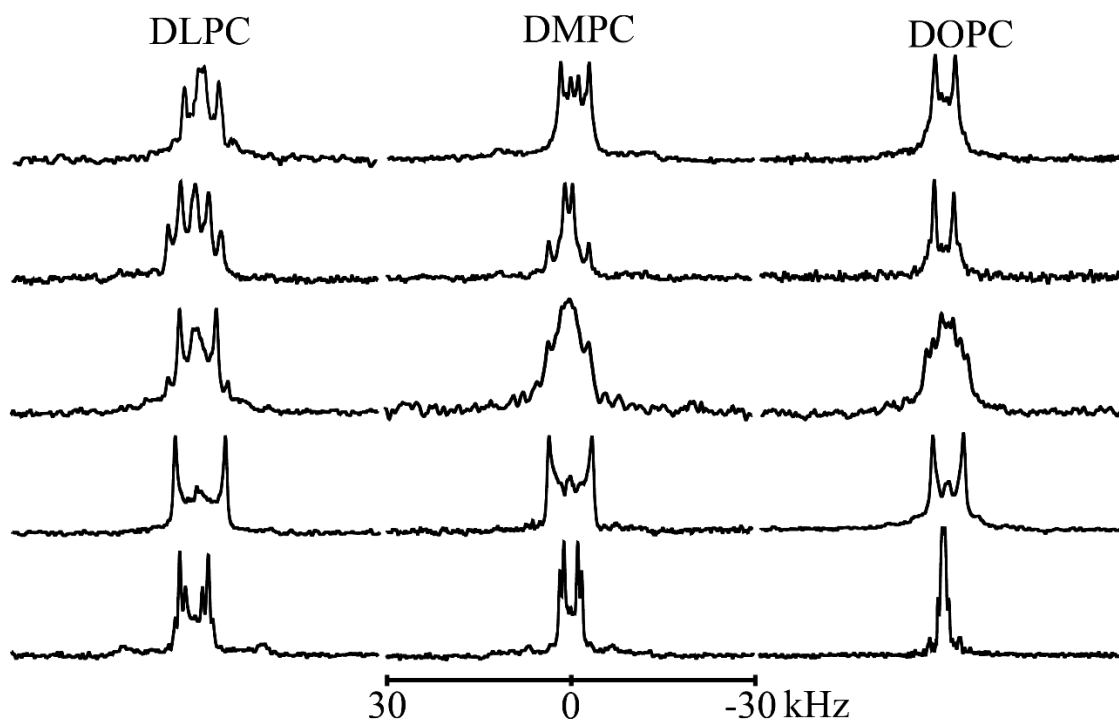


FIGURE 4  $^2\text{H}$  NMR spectra of  $F^{4.5}GW^{20}ALP23$  acquired at  $\beta = 90^\circ$ , with temperature set at  $50^\circ\text{C}$ . From top to bottom,  $^2\text{H}$  labeled alanines and abundances are:  $A7^{100\%}$ ,  $A9^{50\%}$ ;  $A11^{100\%}$ ,  $A13^{50\%}$ ;  $A15^{100\%}$ ,  $A17^{50\%}$ ;  $A3^{100\%}$ ,  $A21^{50\%}$ .

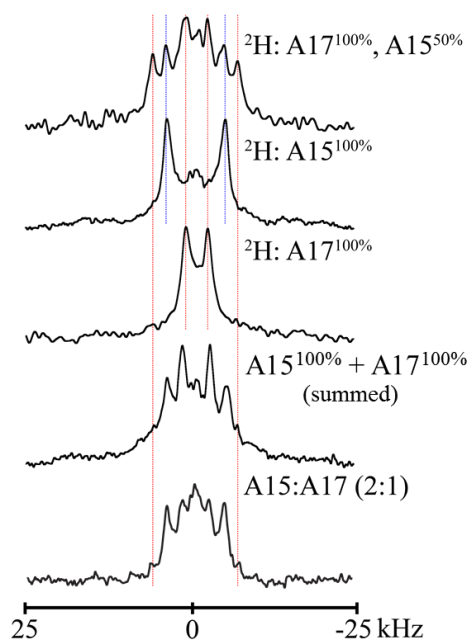


FIGURE 5  $^2\text{H}$  NMR spectra of  $F^{4,5}\text{GW}^{20}\text{ALP}23$  acquired at  $\beta = 90^\circ$ , with temperature set at  $50^\circ\text{C}$ . (A) Spectrum of peptide containing both A17 and A15  $^2\text{H}$  labels shown at top. (B,C) Peptide with single label at either positions A15 or A17 are below. (D) The summed single label spectra using Bruker TopSpin. € Sample containing two peptide populations labeled at either A15 or A17 in a 2:1 ratio at overall peptide:lipid ratio of 1:60.

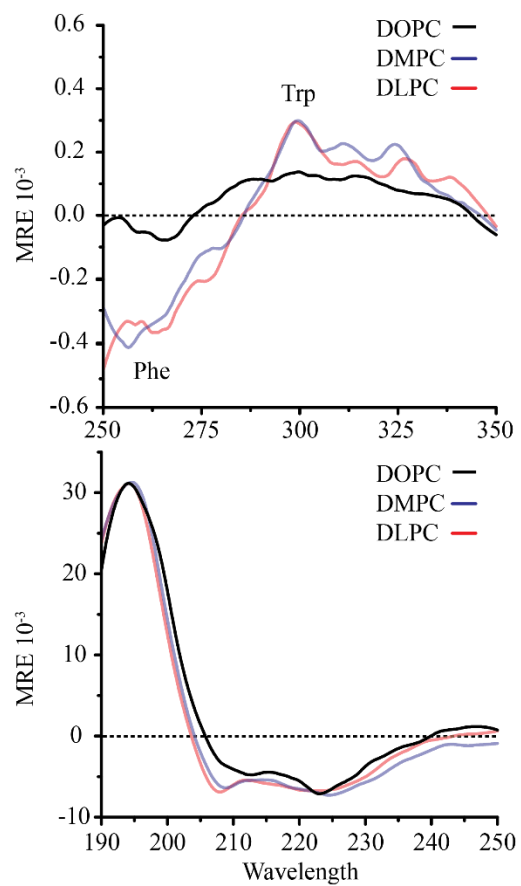


FIGURE 6 Near and far UV-circular dichroism spectra for  $F^{4.5}GW^{20}ALP23$  in DLPC, DMPC, and DOPC lipid vesicles (1:60 peptide/lipid).

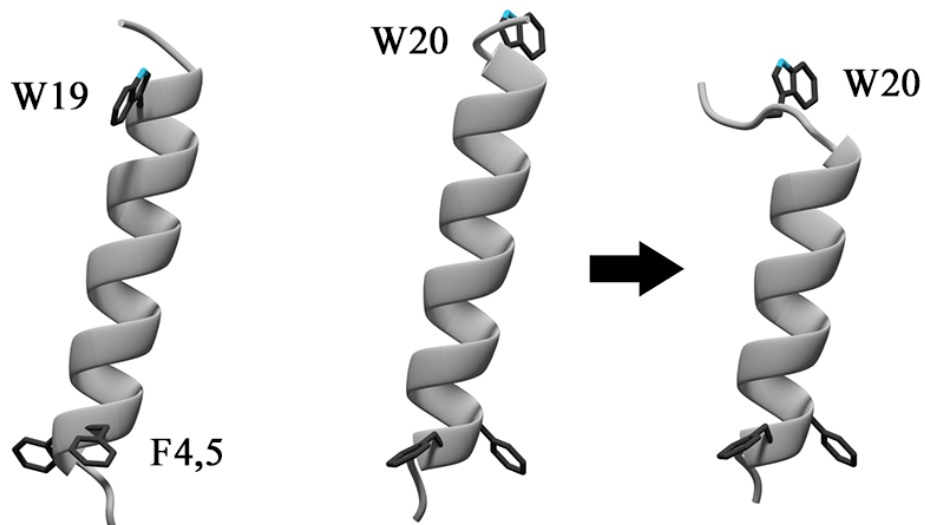
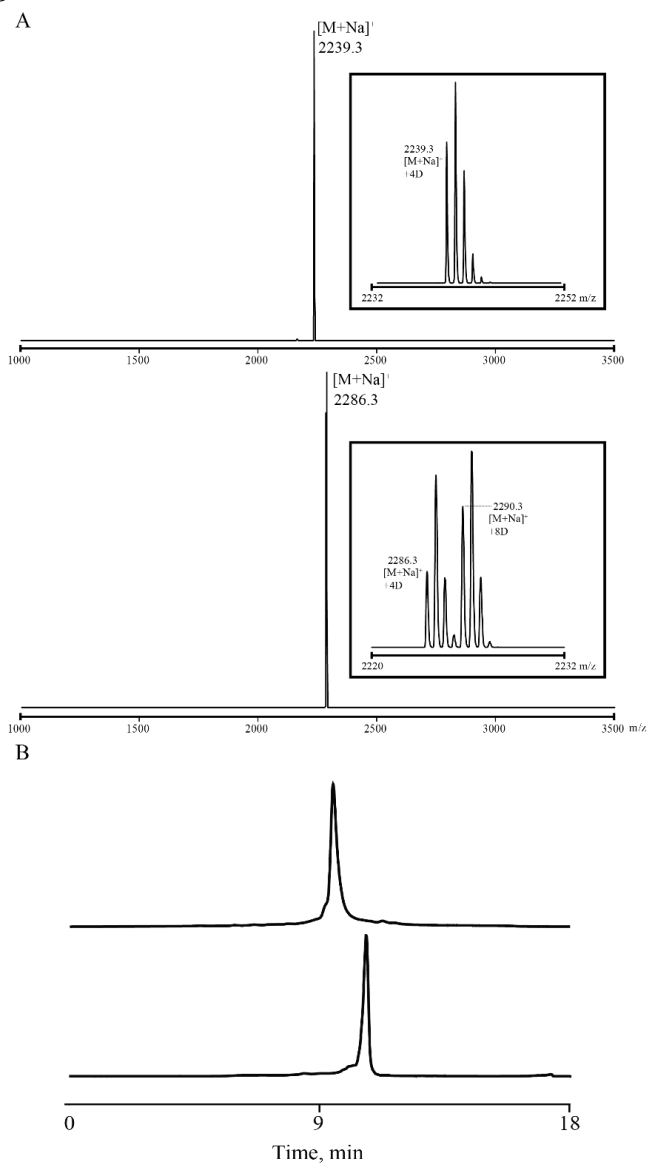


FIGURE 7 3D models of F<sup>4,5</sup>GW<sup>19</sup>ALP23 (left) and F<sup>4,5</sup>GW<sup>20</sup>ALP23 (right) with either undistorted or distorted conformations at orientations predicted in DMPC bilayers (see Table 3).

## 4.11 Supplemental Figures



**FIGURE S1** (A) MALDI MS spectra for  $F^{4,5}GW^{20}ALP23$  with Ala- $D_4$  (Top) and  $L^{5,19}GW^{4,20}ALP23$  with two Ala- $D_4$  (bottom). Expected  $m/z$  for  $[M+H]^+$  ions are 2213.45 and 2260.79 respectively. (B) Analytical HPLC profile spectra for purified  $F^{4,5}GW^{20}ALP23$  (Top) and  $L^{5,19}GW^{4,20}ALP23$  (bottom).



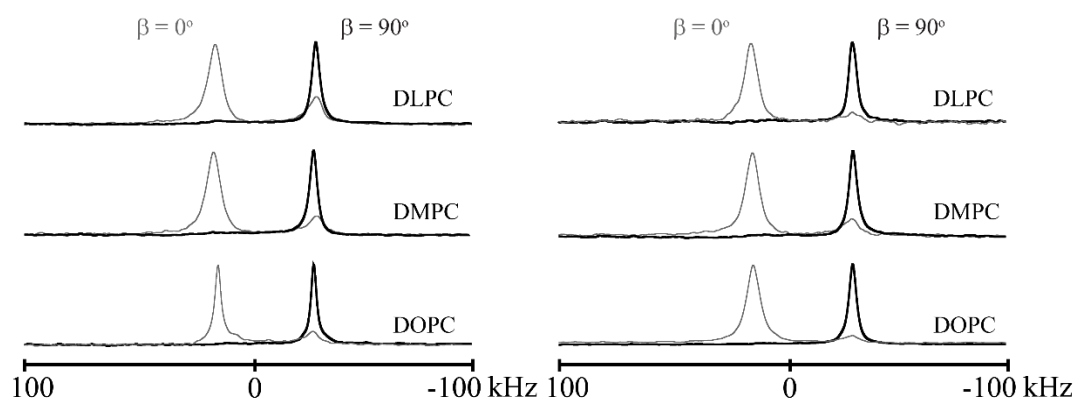


FIGURE S2  $^{31}\text{P}$  NMR spectra with  $^1\text{H}$  broadband decoupling for  $F_{4,5}\text{GW}^{20}\text{ALP23}$  (left) and  $L_{5,19}\text{GW}^{4,20}\text{ALP23}$  (right) in mechanically aligned DLPC, DMPC and DOPC bilayers; temperature set to  $50^\circ\text{C}$ .

$L^{5,19}GW^{4,20}ALP23, \beta = 0^\circ$

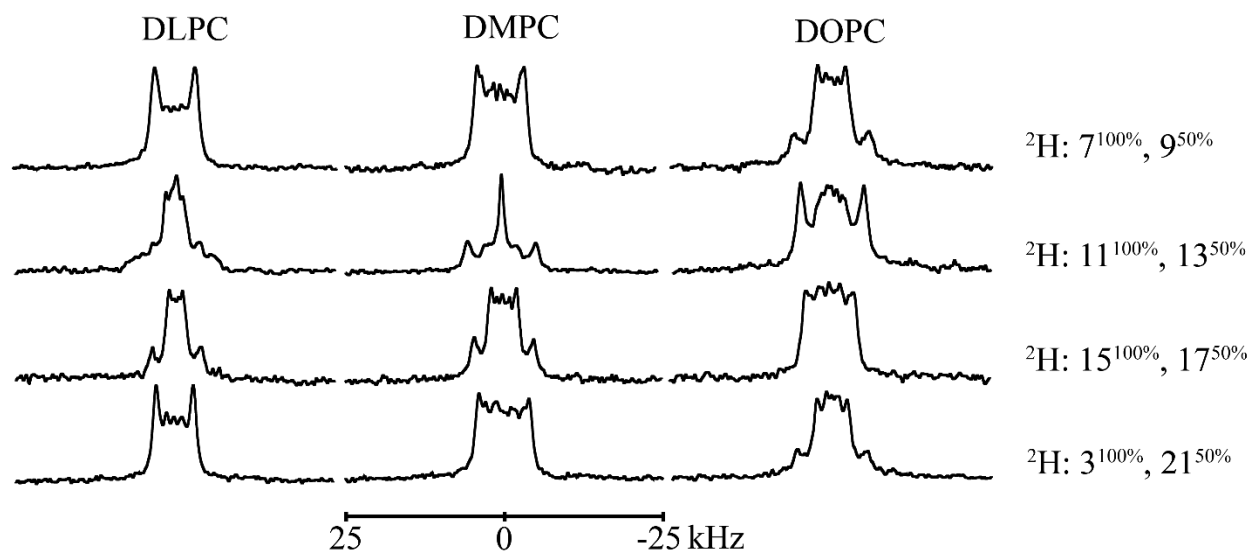


FIGURE S3  $^2H$  NMR spectra for  $L^{5,19}GW^{4,20}ALP23$  in mechanically aligned DLPC, DMPC and DOPC bilayers set at  $\beta = 0^\circ$  and performed at  $50^\circ C$ .

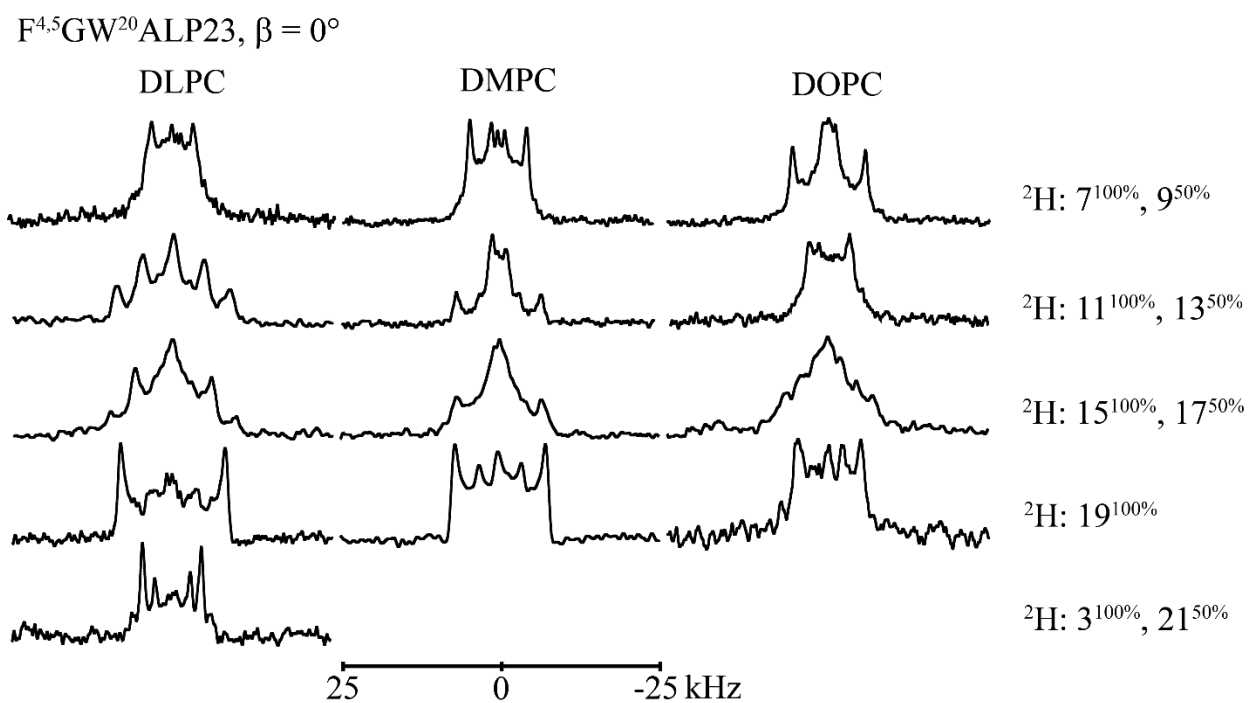


FIGURE S4  $^2H$  NMR spectra for  $F^{4.5}GW^{20}ALP23$  in mechanically aligned DLPC, DMPC and DOPC bilayers set at  $\beta = 0^\circ$  and performed at  $50^\circ C$ .

## CHAPTER 5

### Titration of Glutamic Acid at the Lipid Bilayer Interface

#### 5.1 Abstract

Simple model transmembrane peptides and solid-state  $^2\text{H}$  NMR can be used together in order to deduce the titration points of ionizable residues at various depths within lipid bilayers. The  $\text{GW}^{5,19}\text{ALP23}$  (acetyl-GGALW<sup>5</sup>(LA)<sub>6</sub>LW<sup>19</sup>LAGA-amide) peptide framework was modified to include a Glu(E) residue at position 4 in order to determine the pKa of the carboxylic acid side chain at the membrane interface. Solid-state  $^2\text{H}$  NMR was used to monitor the changes in deuterated Ala-methyl quadrupolar splittings of residue Ala3 as the pH was increased. Changes in the measured quadrupolar splitting of Ala3 can be attributed to the charged state of the neighboring Glu4. Titration curves were established for Glu4 in DLPC, DMPC and DOPC lipid bilayers. A lipid dependence was observed as the calculated pKa of Glu4 increases with lipid acyl chain length (4.8 up to 11.0) as the ionizable side chain loses access to water. These results provide important insights into the wide range of pKa values calculated for the Glu side chain within proteins and at various depths of the lipid bilayer.

#### 5.2 Introduction

A lipid bilayer membrane consists of a low dielectric hydrophobic core surrounded by polar lipid head groups and the high dielectric content of both the outer and inner cellular spaces. While the membrane interior would appear to be inhospitable to charges, membrane proteins will sometimes contain titratable residues within this region. Furthermore, their presence is usually important for the biological function of the protein. The side chain protonation state of residues like Arg, His, Lys, Glu and Asp is dependent on numerous local electrostatic environmental factors such as lipid hydrophobic effects, hydrogen bonding, membrane fluidity and solvent

accessibility.(1-3) The charged state of such residues will have consequences on the helix orientation, dynamics and structure. Arg residues for example are found throughout the voltage sensing domains of numerous channel proteins(4, 5) and have been observed to cause helix distortions even within simple model peptides (see Chapter 3). Glu can be found in the interior of certain membrane proteins and when charged can alter protein folding.(6)

Selectively deuterated transmembrane peptides can be analyzed with oriented solid-state NMR to determine the titration point of such residues at various depths within lipid bilayers. The model GW<sup>5,19</sup>ALP23 sequence (acetyl-GGALW(LA)<sub>6</sub>LWLAGA-amide) adopts a well-defined tilt within lipid bilayers and has been used to determine the pKa of residues such as His, Tyr, Arg and Lys.(7-9) Varying degrees of success have been achieved while characterizing the protonation state of Glu, made difficult by the indifferent response of the helix to ionization state of the carboxylate side chain.(10)

Here the titration point of the Glu side chain is probed at the membrane interface of DLPC, DMPC and DOPC bilayers, again using the GW<sup>5,19</sup>ALP23 sequence. Residue L4 of the parent sequence was mutated to Glu and the pKa was determined via observing pH-dependent changes in the neighboring A3 deuterated methyl group quadrupolar splitting (Figure 1). Titration points were determined in DLPC, DMPC and DOPC bilayers and were also dependent on lipid bilayer thickness despite the interfacial location of the Glu residue.

### **5.3 Materials and Methods**

N-Fmoc-amino acids with additional protecting groups were purchased from NovaBiochem (San Diego, CA). Deuterated alanine was purchased from Cambridge Isotope Laboratories (Tewksbury, MA) and modified with an Fmoc group as described previously.(11) Successful

synthesis was confirmed with  $^1\text{H}$  NMR. Lipids were purchased from Avanti Polar Lipids (Alabaster, Alabama). Solid-phase FastMoc® peptide synthesis was performed to make  $^2\text{H}$ -labeled  $\text{E}^4\text{GW}^{5,19}\text{ALP23}$  peptides on a 0.1 mmol scale using an Applied Biosciences 433A peptide synthesizer (Foster City, CA). Peptides were purified using reverse-phase HPLC with a gradient of 88-92% MeOH over 13 min using an octyl silica column (Zorbax Rx-C8,  $9.4 \times 250$  mm,  $5 \mu\text{m}$  particle size; Agilent Technologies, Santa Clara, CA). Peptide purity and molar mass were confirmed by HPLC and MALDI-MS (see supplemental Figure S1).

Mechanically oriented solid-state NMR samples were prepared as previously described (12) consisting of peptides in (DLPC, DMPC or DOPC) lipid bilayers at a 1:60 peptide:lipid molar ratio and a final hydration of 45% (w/w) with 10 mM glycine, citrate, 4-(cyclohexylamino)-1-butanefulfonate or phosphate buffer in deuterium-depleted water (Cambridge Isotope Laboratories) at pH values between 3.0 and 13.0. Bilayer alignment at both  $\beta = 90^\circ$  and  $\beta = 0^\circ$  sample orientations was confirmed with  $^{31}\text{P}$  NMR spectroscopy on a Bruker Avance 300 MHz spectrometer with  $^1\text{H}$  broadband decoupling and 128 scans. Static solid-state  $^2\text{H}$  NMR experiments were performed with a quadrupolar echo pulse sequence(13) at  $50^\circ\text{C}$  using a Bruker Avance 300 MHz spectrometer at a Larmor frequency of 46.08 MHz over both sample ( $\beta = 90^\circ$  and  $\beta = 0^\circ$ ) orientations. The pulse sequence included a pulse time of  $3.2 \mu\text{s}$ , an echo delay of  $115 \mu\text{s}$ , and a recycle delay of 90 ms. Each  $^2\text{H}$  NMR experiment acquired between 0.9 and 1.5 million scans. Fourier transformation was applied using an exponential weighting function with 150 Hz line broadening.

## 5.4 Results

Solid-state NMR can be used to monitor the changes in the quadrupolar splitting of Ala3 in E<sup>4</sup>GW<sup>5,19</sup>ALP23 to determining the titration point of the Glu4 side chain. Importantly, the sequence contains no other ionizable residues and therefore any observed changes in the NMR experiments are directly related to the charged state of the Glu4 side chain. The methyl <sup>2</sup>H quadrupolar splitting of Ala3 decreased from 15.5 kHz to 12.4 kHz in DLPC bilayers and from 16.1 kHz to 13.6 kHz in DMPC within the pH range of 3.0 to 8.0, and increased from 16.8 kHz in DOPC up to 20.1 kHz in the pH range of 8.0 to 13.0 (see Table 2, Figure 2). The less flexible *i* + 2 residue, W5 was mutated to Ala-CD<sub>3</sub> and upon increasing the pH, no difference in the quadrupolar splitting is observed over the pH range of 3.0 to 8.0 in DLPC bilayers, indicating the core transmembrane helix is less sensitive to the ionized state of the Glu side chain (Figure S3).

Three titration curves were obtained for the Ala3 quadrupolar splitting in each lipid bilayer. Previous studies have shown that there is not titration observed for the parent peptide framework as no ionizable residues are included within the sequence.<sup>(7)</sup> The midpoint and thereby predicted pKa of the Glu4 side chain is 4.8 in DLPC, 6.3 in DMPC and 11.0 in DOPC (Figure 3). The increase in pKa coinciding with lipid bilayer thickness likely indicates a lipid dependence on the titration point of the Glu4 side chain at the membrane interface. The high pKa predicted in DOPC offers support for previous experiments that predicted higher titration points when side chain is buried deeper into the lipid bilayer and has less access to water (see discussion).<sup>(10)</sup>

## 5.5 Discussion

GW<sup>5,19</sup>ALP23 has served as a useful model peptide framework for determining the titration points of numerous residues within lipid bilayers.<sup>(7, 10)</sup> Monitoring the changes in the

deuterated methyl quadrupolar splittings of Ala residues that neighbor titratable side chains has proven to be an effective way of predicting the pKa.(7) The titration of Glu at various depths of lipid bilayers using these methods has proven to be difficult as the helix orientation is indifferent to the charged state of the side chain.(10) Analyzing Glu4 at the membrane interface offers certain advantages over positions within the helix core. For example, there is the added flexibility of the neighboring terminal residue Ala3 which is normally frayed and not part of the core  $\alpha$ -helix.(14, 15) The buried Glu side chain would prefer a local environment that favors its charge state. As Glu4 adjusts its average orientation based on its ionized state, any consequential change in the orientation of Ala3 can be observed with the high sensitivity of  $^2\text{H}$  NMR. Accordingly, the methyl quadrupolar splitting of Ala3 changed in each lipid bilayer. The methyl quadrupolar splitting of the other neighboring residue, Ala5, did not change in response to pH variation in the thinnest bilayer which indicates the core helix does not show an orientational dependence to the charged state of the interfacial Glu4 side chain. Unwinding studies have shown that within the GW<sup>5,19</sup>ALP23 sequence, residue 5 is normally a part of the core helix whereas residues 4 and lower fray.(14, 15) Therefore, Glu4 side chain is likely able to adjust its orientation to stabilize its charged state without affecting the core  $\alpha$ -helix.

The titration curves show an increase in pKa for Glu4 side chain as bilayer thickness also increases. Therefore, the side chain carboxylic acid titration shows a lipid dependence at the membrane interface. Within the thinnest bilayer, the glutamic acid side chain has a similar but slightly higher pKa than in soluble small model proteins or solution which is on average 4.3 to 4.5.(1) The side chain pKa accordingly increases with bilayer thickness as the carboxylic acid becomes less able to efficiently gain access to water.



The high titration point of Glu4 in DOPC at pH 11.0 is not unreasonable and finds support from experiments with transmembrane model peptides and actual membrane proteins. For example, previous studies on Glu located at various depths within the core sequence of GW<sup>5,19</sup>ALP23 (positions 14 and 16) found helix structural changes at higher pH values (pH 12 to 13) while the core helix orientation largely remained uninfluenced by the charged state of the Glu side chain.<sup>(10)</sup> Furthermore, while the pKa of exposed Glu residues in soluble proteins are closer to 4.3, the pKa of transmembrane Glu286 in *Rhodobacter sphaeroides* cytochrome c oxidase is raised to 9.4 which has been both experimentally calculated<sup>(16)</sup> and reproduced with continuum electrostatic calculations.<sup>(17)</sup> The lipid dependence of the Glu4 pKa at the bilayer interface observed in experiments here provides insight into how buried ionizable residues can have such a wide range of pKa's based on the conditions of their local microenvironments.

## 5.6 Conclusions

The GW<sup>5,19</sup>ALP23 framework was used to successfully determine the titration point of glutamic acid at the membrane interface. The glutamic acid side chain pKa shows a lipid dependence based on the thickness of the bilayer. In the thinnest bilayer, the pKa is similar to its solution pKa. Upon increasing the lipid acyl chain length, the titration point occurs at higher pH values (up to pH 11.0) likely as a result of decreased access to water.

## 5.7 Acknowledgements

This work was supported in part by NSF MCB grant 1713242, and by the Arkansas Biosciences Institute. The peptide, NMR and mass spectrometry facilities were supported in part by NIH grant GM103429.

## 5.8 References

1. Kuhlman, B., D. Luisi, P. Young, and D. Raleigh. 1999. pK(a) values and the pH dependent stability of the N-terminal domain of L9 as probes of electrostatic interactions in the denatured state. Differentiation between local and nonlocal interactions. *Biochemistry* 38(15):4896-4903.
2. Forsyth, W., J. Antosiewicz, and A. Robertson. 2002. Empirical relationships between protein structure and carboxyl pK(a) values in proteins. *Proteins-Structure Function and Bioinformatics* 48(2):388-403.
3. Silva, A., X. Kong, and R. Hider. 2009. Determination of the pKa value of the hydroxyl group in the alpha-hydroxycarboxylates citrate, malate and lactate by <sup>13</sup>C NMR: implications for metal coordination in biological systems. *Biometals* 22(5):771-778.
4. Clayton, G., S. Altieri, L. Heginbotham, V. Unger, and J. Morais-Cabral. 2008. Structure of the transmembrane regions of a bacterial cyclic nucleotide-regulated channel. *Proceedings of the National Academy of Sciences of the United States of America* 105(5):1511-1515.
5. Schwaiger, C., P. Bjelkmar, B. Hess, and E. Lindahl. 2011. 3(10)-Helix Conformation facilitates the transition of a voltage sensor S4 segment toward the down state. *Biophysical Journal* 100(6):1446-1454.
6. Legg-E'Silva, D., I. Achilonu, S. Fanucchi, S. Stoychev, M. Fernandes, and H. Dirr. 2012. Role of Arginine 29 and Glutamic Acid 81 Interactions in the conformational stability of human chloride intracellular channel 1. *Biochemistry* 51(40):7854-7862.
7. Martfeld, A., D. Greathouse, and R. Koeppe. 2016. Ionization properties of histidine residues in the lipid bilayer membrane environment. *Journal of Biological Chemistry* 291(36):19146-19156.
8. Thibado, J. K., A. N. Martfeld, D. V. Greathouse, and R. E. Koeppe. 2016. Influence of high pH and cholesterol on single arginine-containing transmembrane peptide helices. *Biochemistry* 55(45):6337-6343.
9. Gleason, N., V. Vostrikov, D. Greathouse, and R. Koeppe. 2013. Buried lysine, but not arginine, titrates and alters transmembrane helix tilt. *Proceedings of the National Academy of Sciences of the United States of America* 110(5):1692-1695.
10. Rajagopalan, V., D. Greathouse, and R. Koeppe. 2017. Influence of glutamic acid residues and pH on the properties of transmembrane helices. *Biochimica Et Biophysica Acta-Biomembranes* 1859(3):484-492.

11. Gleason, N. J., V. V. Vostrikov, D. V. Greathouse, C. V. Grant, S. J. Opella, and R. E. Koeppe. 2012. Tyrosine replacing tryptophan as an anchor in GWALP peptides. *Biochemistry* 51(10):2044-2053.
12. van der Wel, P. C. A., E. Strandberg, J. A. Killian, and R. E. Koeppe. 2002. Geometry and intrinsic tilt of a tryptophan-anchored transmembrane alpha-helix determined by H-2 NMR. *Biophysical Journal* 83(3):1479-1488.
13. Davis, J. H., K. R. Jeffrey, M. Bloom, M. I. Valic, and T. P. Higgs. 1976. Quadrupolar echo deuteron magnetic-resonance spectroscopy in ordered hydrocarbon chains. *Chemical Physics Letters* 42(2):390-394.
14. Afrose, F., M. McKay, A. Mortazavi, V. Kumar, D. Greathouse, and R. Koeppe. 2019. Transmembrane helix integrity versus fraying to expose hydrogen bonds at a membrane-water interface. *Biochemistry* 58(6):633-645.
15. Mortazavi, A., V. Rajagopalan, K. A. Sparks, D. V. Greathouse, and R. E. Koeppe. 2016. Juxta-terminal helix unwinding as a stabilizing factor to modulate the dynamics of transmembrane helices. *Chembiochem* 17(6):462-465.
16. Namslauer, A., A. Aagaard, A. Katsonouri, and P. Brzezinski. 2003. Intramolecular proton-transfer reactions in a membrane-bound proton pump: The effect of pH on the peroxy to ferryl transition in cytochrome c oxidase. *Biochemistry* 42(6):1488-1498.
17. Popovic, D., and A. Stuchebrukhov. 2006. Two conformational states of Glu242 and pK(a)s in bovine cytochrome c oxidase. *Photochemical & Photobiological Sciences* 5(6):611-620.

## 5.9 Tables

TABLE 1 Sequences of  $GW^{5,19}ALP23$ ,  $E^4GW^{5,19}ALP23$  and  $E^4A^5GW^{19}ALP$  Peptides

Name	Sequence
$GW^{5,19}ALP23$	acetyl-GGALW <sup>5</sup> LALALALALALALW <sup>19</sup> LAGA-amide
$E^4GW^{5,19}ALP23$	acetyl-GG <u>A</u> EW <sup>5</sup> LALALALALALALW <sup>19</sup> LAGA-amide
$E^4A^5GW^{19}ALP23$	acetyl-GGAE <u>A</u> <sup>5</sup> LALALALALALALW <sup>19</sup> LAGA-amide

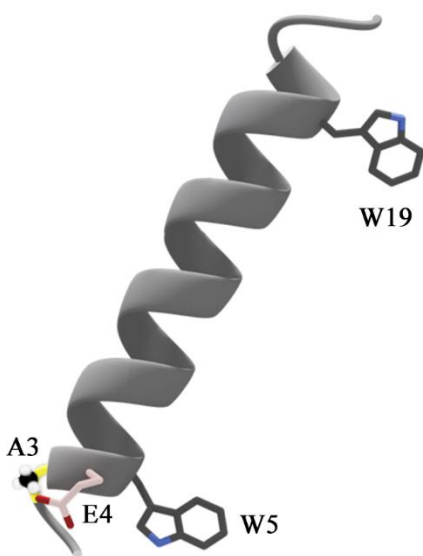
*\*Underlined residues were labeled with Ala-D<sub>3</sub>*

TABLE 2 Quadrupolar Splitting Magnitudes ( $|\Delta\nu_q|$ , in kHz) for Labeled Alanine  $CD_3$  Group of Ala3 in  $E^4GW^{5,19}ALP23^a$

Lipid(s)	pH / $\Delta\nu_q$ (kHz)						
	3.0	4.6	5.0	6.0	8.0	11.0	13.0
DLPC	15.5	14.2	13.3	13.4	12.4	--	--
DMPC	16.1	16.4	16.4	15.6	13.6	--	--
DOPC	16.8	--	16.8	--	16.8	19.0	20.1

$^a\beta = 0^\circ$  sample orientation.

## 5.10 Figures



*FIGURE 1 3D Model of E<sup>4</sup>GW<sup>5,19</sup>ALP23. Deuterium labeled residue A3 is highlighted in yellow.*

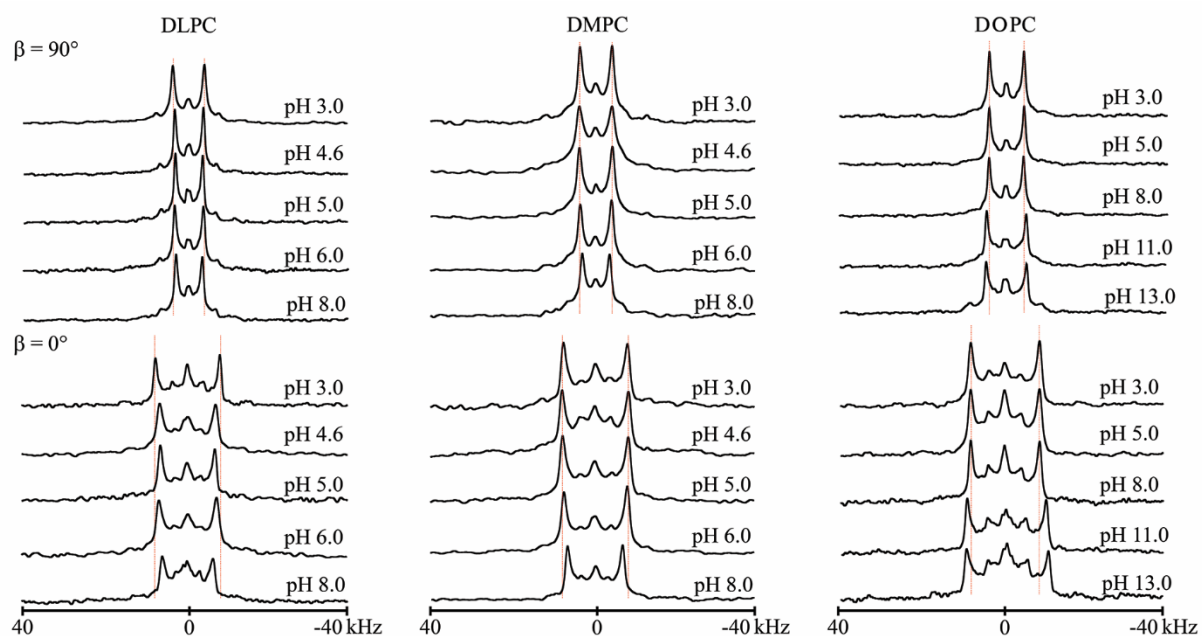
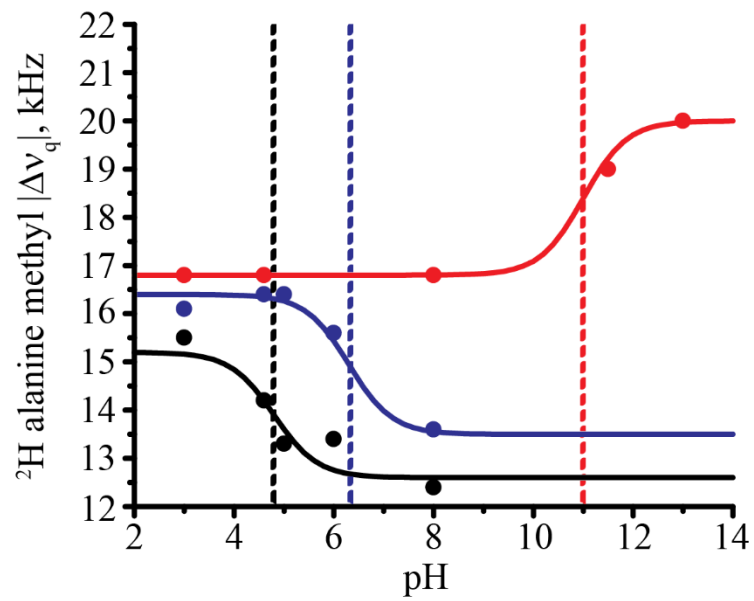


FIGURE 2  $^2\text{H}$  NMR spectra for labeled Ala3 of  $E^4GW^{5,19}ALP23$  in mechanically aligned DLPC, DMPC and DOPC bilayers set at  $\beta = 90^\circ$  and  $\beta = 0^\circ$ , temperature  $50^\circ\text{C}$  and sample pH as indicated.



*FIGURE 3 Titration curves monitoring the  $\text{CD}_3$  quadrupolar splitting of Ala3 in  $E^4\text{GW}^{5,19}\text{ALP23}$  within oriented DLPC (Black), DMPC (Blue) and DOPC (Red) bilayers. Dotted lines represent midpoints at pH values of 4.8 (DLPC), 6.3 (DMPC) and 11.0 (DOPC).*



## 5.11 Supplemental Figures

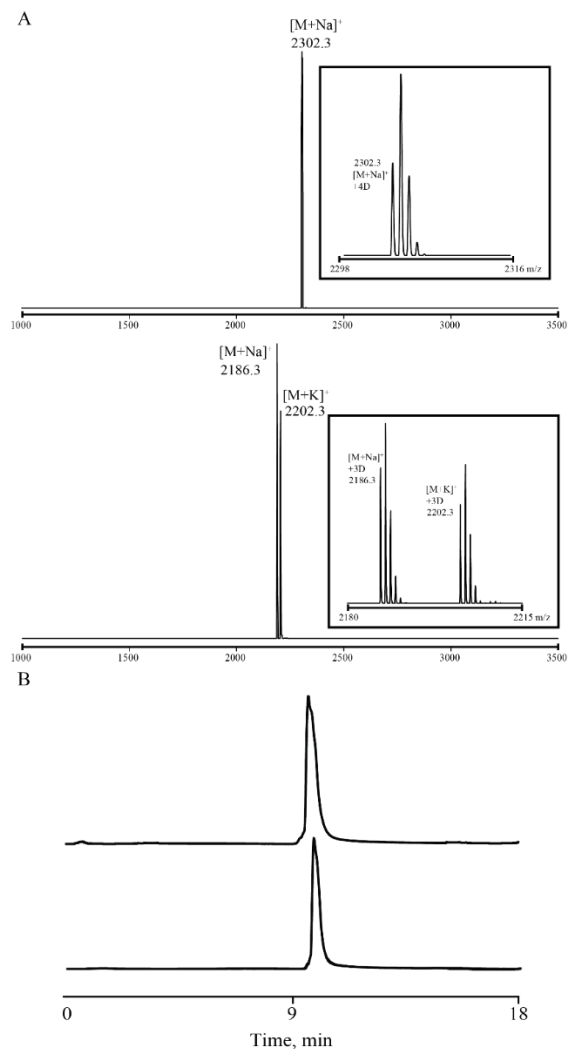


FIGURE S1 (A) MALDI MS spectra for  $E^4GW^{5,19}ALP23$  with Ala-D<sub>4</sub> (Top) and  $E^4A^5GW^{19}ALP23$  with Ala-D<sub>3</sub> (bottom). Expected  $m/z$  for  $[M+H]^+$  ions are 2276.75 and 2161.69 respectively. (B) Analytical HPLC profile spectra for purified  $E^4GW^{5,19}ALP23$  (Top) and  $E^4A^5GW^{19}ALP23$  (bottom).

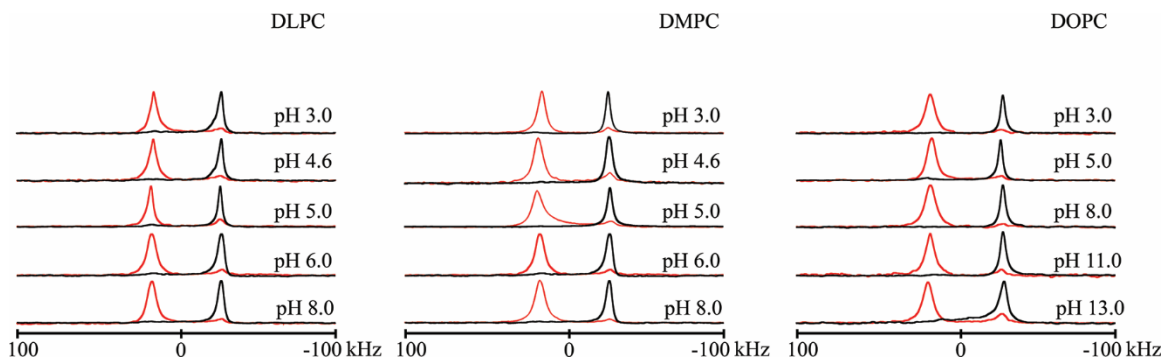
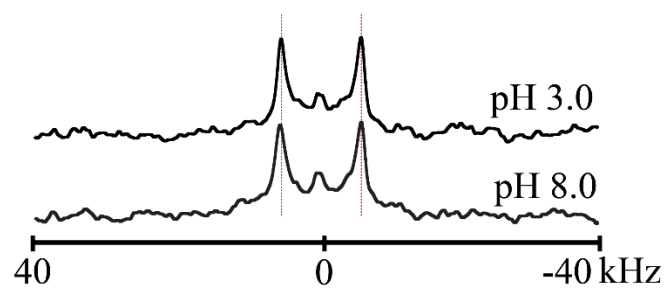


FIGURE S2  $^{31}\text{P}$  NMR Spectra of  $E^4\text{GW}^{5,19}\text{ALP23}$  in DLPC, DMPC and DOPC bilayers at indicated pH values set at  $\beta = 90^\circ$  (red) and  $\beta = 0^\circ$  (black), temperature  $23^\circ\text{C}$ .



*FIGURE S3*  $^2\text{H}$  NMR spectra for labeled Ala5 of  $\text{E}^4\text{A}^5\text{GW}^{19}\text{ALP23}$  in mechanically aligned DLPC bilayers set at  $\beta = 90^\circ$ , temperature  $50^\circ\text{C}$  and sample pH as indicated.

## Chapter 6

### Conclusions

Model transmembrane peptides can help us to understand how protein-lipid interactions influence protein structure, folding and function on the fundamental level. The radial locations of interfacial tryptophan residues about the  $\alpha$ -helix have proven to govern the extent of dynamic motion within the host transmembrane peptide as seen with the highly dynamic GW<sup>4,20</sup>ALP23 framework (Chapter 2). Introducing a charged arginine residue into such a dynamic model system not only arrests the high dynamics, but also induces structural distortions at the helix termini as the tension caused by the aromatic side chain competition remains and needs to be relieved. As shown with the surface bound R<sup>12</sup>GW<sup>4,20</sup>ALP23 peptide, new secondary structures such as a 3<sub>10</sub>-helix can form which is a strikingly similar phenomenon found in the voltage sensing helices of channel proteins (Chapter 3).

Modifying the hydrophobicity of the GW<sup>4,20</sup>ALP23 core sequence dynamic peptide failed to significantly affect the extent of dynamic motion, instead only affecting the peptide's average tilt. Removing one of the flanking tryptophans and replacing it with two non-hydrogen bond forming phenylalanine residues lowered the dynamics significantly and also caused structural distortion at the remaining interfacial Trp residue. Both sets of experiments were able to finally prove the high dynamics are caused by the radial Trp locations (Chapter 4).

Finally, the interfacial pKa of glutamic acid was determined to have a lipid dependence based on the bilayer thickness. The titration point in the thinnest bilayer is similar to its solution pKa while in the thickest bilayer, the carboxylic acid side chain isn't deprotonated until a significantly higher pH is reached (Chapter 5). Altogether, studies such as these are meant to

answer fundamental questions that can ultimately further advance our understanding of the complex relationship shared between membrane proteins and lipids in which they reside.

## Appendix I

### Current List of Additional Publications

#### Published Peer Review:

Fahmida Afrose, **Matthew J. McKay\***, Armin Mortazavi, Vasupradha Suresh Kumar, Denise V. Greathouse, Roger E. Koeppe II. 2019. Transmembrane helix integrity versus fraying to expose hydrogen bonds at a membrane–water interface. *Biochemistry* 58(6):633-645.

Karli Lipinski, **Matthew J. McKay\***, Fahmida Afrose, Ashley N. Martfeld, Denise V. Greathouse, Roger E. Koeppe II. 2019. Influence of lipid saturation, hydrophobic length and cholesterol on double-arginine-containing helical peptides in bilayer membranes. *ChemBioChem*. In Press. [10.1002/cbic.201900282]

**Matthew J. McKay\***, Fahmida Afrose, Denise V. Greathouse, Roger E. Koeppe. 2018. Helix formation and stability in membranes. *BBA Biomembranes* 1860(10):2108-2117.